Development of metal modified brookite TiO_2 used for organic compound pollutants degradation

Jul. 28th, 2022

Kyushu Institute of Technology

Graduate School of Engineering

Major: Engineering; Graduate School of Engineering

195F8002 Yu Cao

Contents

Section 1. Introduction of Organic compound photocatalytic degradation 1

1.1 Background 3

1.2 Principle of organic compounds degradation 5

1.3 Modification of TiO_2 7

1.3.1 Adjusting light adsorption 10

1.3.1.1 Self-doping 10

1.3.1.2 Elements doping and grafting 12

1.3.1.3 Dye-sensitization 15

1.3.1.4 Localized surface plasmon resonance (LSPR) over noble metal 18

1.3.2 Promoting of electron-hole pairs separation 19

1.3.2.1 Self-doping 20

1.3.2.2 Elements doping 22

1.3.2.3 Noble metal modification 24

1.3.2.4 Heterojunction 25

1.4 Summary 28

Reference 28

Section 2. Fe(III)-Pt(II) Oxide-Co-Sensitized Brookite TiO_2 Nanorods for Photocatalytic Degradation of Acetaldehyde under Visible Light 43

Abstract 45

Keywords 45

2.1 Introduction 45

2.2 Experiment 48

2.2.1 Preparation of pure brookite TiO_2 48

2.2.2 Preparation of Fe(III)-sensitized brookite TiO_2 48

2.2.3 Preparation of Pt(0)-sensitized brookite TiO_2 48

2.2.4 Preparation of Pt(IV) or Pt(II)-sensitized brookite TiO_2 49

2.2.5 Preparation of Fe(III)-Pt(II)-co-sensitized brookite TiO_2 49

2.2.6 Characterization 50

2.2.7 Photocatalytic activity tests 50
2.2.9 Double-beam photoacoustic spectroscopic (DB-PAS) measurement 51
2.2.10 DFT calculations 51
2.2.11 Apparent Quantum Efficiency (AQE) calculations:[38, 39] 52
2.3 Results and Discussion 52
2.3.1 Surface and Structural Properties 52
2.3.2 Surface Affinities of Brookite TiO_2 for Fe^{2+}, Fe^{3+} and Pt^{4+} Cations 65
2.3.3 Proposed Formation Mechanism of Fe(III)- Pt(II)/TiO_2 Nanorods 67
2.3.4 Optical Properties 68
2.3.5 Photocatalytic Activities of Fe(III) and Pt-sensitized TiO_2 and Fe(III)-Pt(II)-oxide-co-sensitized TiO_2 nanorods 70
2.3.6 Photocatalytic Activities of Pt(0) and Pt(II) and Pt(IV) Sensitizer-modified Brookite TiO_2 Nanorods 74
2.3.7 Importance of Fe(III) Oxide Sensitizer Outer Layer for Enhancing the Photocatalytic Activity and Stability of Pt(II)/TiO_2 79
2.3.8 Direct Visualization of Electron Transfer in Fe/Pt-sensitized TiO_2 Nanorods under Visible Light Irradiation using *in situ* DB-PAS 80
2.3.9 Proposed Mechanisms of Photocatalytic Acetaldehyde Degradation over Pt(II)/TiO_2 and Fe(III)-Pt(II)/TiO_2 under Visible Light 82
2.4 Conclusions 84
References 85
Section 3. H_2 and CH_4 production from Acetic acid reforming over metal loaded brookite TiO_2 in Ar atmosphere 93
Abstract 95
Key words 95
3.1 Introduction 95
3.2 Experiment 97
3.2.1 Preparation of metal loaded TiO_2 97
3.2.2 Characterization 98
3.2.3 Photocatalytic activity tests 98
3.3 Results and Discussion 98
3.3.1 Surface and Structure properties 98

3.3.2 Optical properties 101
3.3.3 The importance and optimal amount of Pt modification 102
3.4 Conclusion 111
Reference 111
Section 4. Higher efficiency of Acetic acid reforming over Pt0/TiO_2 in the condition of CO_3^{2-} cations 117
Abstract 119
Keyword 119
4.1 Introduction 119
4.2 Experiment 121
4.2.1 Preparation of metal loaded TiO_2 121
4.2.2 Characterization 121
4.2.3 Photocatalytic activity tests 122
4.3 Results and Discussion 122
4.3.1 Acetic acid reforming in Ar and CO_2 atmosphere 122
4.3.2 Mechanism of acetic acid reforming in different gas atmosphere 130
4.4 Conclusion 135
Reference 135
Section 5. Outlook for the future of work 141
Acknowledgements 142

Section 1. Introduction of Organic compound photocatalytic degradation

1.1 Background

It was reported that 71% earth surface is water. However, only 2.5% of earth water is fresh water. Among them, only 0.007% of earth water is accessible.[1] Nowadays, 1.1 billion people all of the world are living in the condition with shortage and unclean water. [2] Thus, the fresh water is become a kind of scarce resource, which is necessary for agriculture, industrial production and people's daily life. Besides, people spend about 80% of their time indoors in daily life.[3] The indoor pollutants come from cooking, secondhand smoke, cleaning, consumer products, home furnishings and building materials and so on, affects indoor air quality and has a vital impact on people's health.[4-7] The organic compounds contained in the waste water and air, is thought to be the main reason causing many diseases, such as cancer, respiratory disease, sick building syndrome and so on. [8-10] Generally speaking, the organic pollutants from the waste and air pollutants, are a huge potential threat to people's health. The problem of organic pollutants is becoming more and more serious for our society. It is necessary to develop some new technologies for removing the organic compounds.

Many methods were tried to solve these organic compounds. The specific process flow is divided into destructive and non-destructive treatment of organic pollutants. Among non-destructive VOCs removal pathway, adsorption, absorption, condensation and membrane separation were extensively explored and reported.[11-14] (1) Adsorption is a traditional and mature technique used for separation of high-level concentration organic compounds in mixed phases. Many materials, such as graphene, activated carbon, mesoporous silica materials and so on, were developed[15-18]. Benefit from low-cost, high-efficiency and et al, the method of adsorption is now widely used in our daily life. However, the problem, which come comes with subsequent treatment of waste adsorbent materials and high maintenance cost., will be produced as well. (2) Condensation can convert VOCs into liquids at lower temperatures or higher pressures, allowing for the recovery of volatile organic compounds in large quantities[19]. However, only valuable VOCs are usually considered to be treated at high concentrations due to

the high cost of condensation treatment. At the same time, the disposal of waste coolant during the condensation process is also another problem. [14, 20] (3) Membrane separation technology is one of the emerging VOCs removal technologies. However, the high cost, poor stability, and low flux of membranes hinder their wide industrial application[21]. (4) As a kind of destructive treatment of organic pollutants catalytic oxidation technology with thermal treatment can catalytic-thermally decompose the organic compounds to CO_2 and H_2O and is another effective method for organic compounds removal. For example, formaldehyde reacts with oxygen (O_2) over noble metals producing CO_2 and H_2O vapor.[22] However, since the catalytic reaction needs to be carried out at high temperature, the energy consumption of catalytic degradation of organic compounds is a big problem. (5) For the plasma catalytic method, the molecules, particles, atoms and free radicals are excited to have high chemical activities for the decomposition of VOCs, but the reactions are difficult to control in normal conditions and the reaction rates are usually slow.[23, 24] (6) Some novel methods such as absorption bio-degradation were developed to solve the problem as well. They still exist some disadvantages, for example production of secondary pollution, high post-processing costs and so on.[25] Currently this technique is not widely applied for the indoor air cleaning. As a result, alternative, cost effective technologies are in high demand.

Photocatalysis method for organic compounds removal should be a promising method. It can use free and clean solar energy for promoting the photocatalytic reaction. In the photocatalytic process, the excitation of a semiconductor material (for example, TiO_2) by photo-irradiation with energy equal to or higher than the semiconductor's band gap (for TiO_2, the energy of light should be above 3.2 eV) induces the electrons transferring from valence to the conduction band. So as to form the electron-hole pairs. [26, 27] The excited electrons can reduce dissolved oxygen to generate superoxide radical ions $\bullet O_2^-$, which are also another kind of oxidative species. And it can further react with H_2O to form $\bullet OH$ radical. In addition, the formed holes are strong oxidants, which

can oxidize the adsorbed H_2O into •OH radical. The •OH radical is a powerful, non-selective chemical oxidant and thought to be the main active group for organic compounds photocatalytic degradation through radical addition, hydrogen extraction, electron transfer, and radical binding.

Many materials such as TiO_2, C_3N_4, WO_3, SnO_2 and $BiVO_4$, has been developed for photocatalytic degradation of organic compounds.[28-31] However, it also has many problems. Limited by the narrow light absorption range and the fast carrier recombination rate of photocatalysts, the photocatalytic activity and efficiency is not very high, which is not good for wide use.

In this section, we summarize the modification methods on TiO_2 for improving the light absorbance range and promote the charge separation, including self-doping, elements doping, metal grafting, noble metal modification, dye-sensitization and heterojunction. As a result, the organic compounds can be efficiently removed over TiO_2 after modification.

1.2 Principle of organic compounds degradation

The mechanism of organic compounds degradation in the condition of O_2 atmosphere is shown in the Fig. 1-1.[32] Under photoirradiation, electrons are excited from valence band to the conduction band of photocatalyst. A hole (h^+), which is a kind of strong oxidizing agent, is left in the latter.[33, 34] Therefore, electron and hole pairs (e^-/h^+) are generated. These pairs can be generated in femtoseconds (fs). Subsequently, photoexcited carriers can be trapped in picoseconds (ps) (shallow wells) or nanoseconds (ns) (deep wells). Holes and electrons can recombine in tens of nanoseconds.[35-37] During the period of electron excitation, a O_2 molecule captures one electron to form superoxide radical (•O_2-). At the same time, a H_2O molecule is oxidized by photoproduced holes to form hydroxyl radical (•OH). It is well known that •O_2- and •OH radical has strong oxidation ability and can directly oxidize organic compounds to be H_2O, CO_2 and some other by-products.[38]

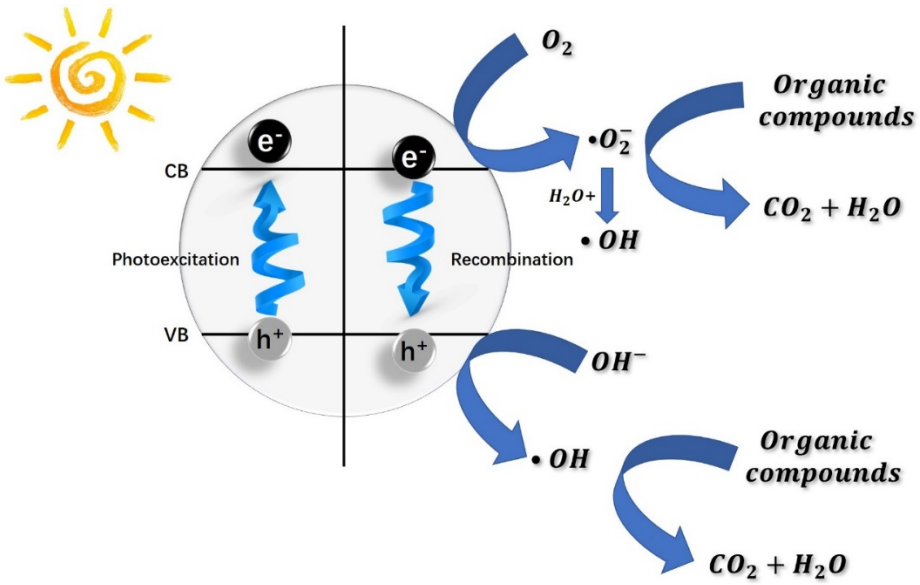

Fig. 1-1 Basic principle of photocatalytic degradation for removal of VOCs.

Organic compounds reforming should be an economic method for organic compounds removing. By this reaction, some complex, uncollectible and useless organic compounds can be reformed to single, enriched and useful energy components, such as methane, ethane and so on. The mechanism of organic compounds photocatalytic transformation is shown in the Fig. 1-2.[39] Under light irradiation, positive holes and electrons are generated in the VB and CB of TiO_2 as presented in Equation (1). These holes can either form hydroxyl radicals (Equation (2)) and then oxidize organic compounds to oxidation products ($R^\bullet$ radcal) (Equation (5)). Besides, the holes can also react directly with organic molecules to form oxidation products ($R^\bullet$ radcal) (Equation (4)). The electrons can reduce H^+ to •H radical. Finally, the produced $H^\bullet$ and $R^\bullet$ combine with each other to form reforming products (Equations (6)-(7)).[40]

$$hv + TiO_2 \rightarrow h_{vb}^+ + e_{CB}^- \quad (1)$$

$$H_2O_{absorbed} + h_{vb}^+ \rightarrow H^+ + OH^\bullet \quad (2)$$

$$H^+ + e_{CB}^- \rightarrow H^\bullet \quad (3)$$

$$Organic\ compounds + h_{vb}^+ \rightarrow Oxidation\ products\ (R^\bullet) \quad (4)$$

$$Organic\ compounds + OH^\bullet \rightarrow Oxidation\ products\ (R^\bullet) \quad (5)$$

$$H^\bullet + H^\bullet \rightarrow H_2 \quad (6)$$

$$Oxidation\ products\ (R^\bullet) + H^\bullet (or\ R^\bullet) \rightarrow Reforming\ products \quad (7)$$

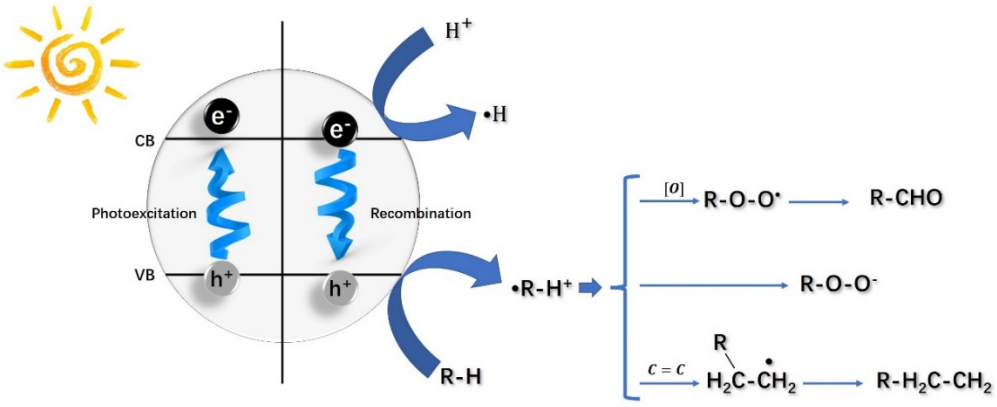

Fig. 1-2 Mechanism of organic compounds photocatalytic reforming.

1.3 Modification of TiO_2

TiO_2 is a non-toxic, accessible, shape-controlled and relatively cheap photocatalyst. TiO_2 exists in three crystalline structures: anatase, rutile and brookite phases and has been widely used in the field of photocatalytic decomposition of organic pollutants.

For anatase and brookite TiO_2, the minimum band gap energy required for exciting electrons from VB to CB is about 3.2 eV, corresponding to the absorption of a 380 nm wavelength photon. Therefore, TiO_2 photoactivation occurs in $\lambda < 380$ nm, near the UV region. For rutile TiO_2, the band gap is about 3.0 eV, corresponding to the absorbance of 400 nm light (visible light).

Zhang et al. investigated the mechanism of •OH radical generation in anatase and rutile photocatalysts using two different probe molecules (coumarin and coumarin-3-carboxylic acid).[41] As shown in the Fig. 1-3, on the surface of anatase, photoproduced holes are trapped at the surface oxygen of TiO_2 to form the group of Ti-O•, a deprotonated form of •OH.[42] After combining with H_2O, a •OH radical is released. Then the Ti-O structure returns to its original state. Compared with anatase TiO_2, rutile TiO_2 produced fewer •OH radicals (Fig. 1-3B). For rutile type TiO_2, the stability of surface trapped holes may be different due to the tighter crystal structure than anatase type. As can be seen in the Fig. 3B, on the surface of rutile TiO_2, the bridging oxygen,

peroxide Ti (**Ti-O-O-Ti**), formed by the combination of two trapped holes acts as a catalyst to generate •OH radicals from water.[43] The formation of bridging oxygen decrease the amount of active site on the surface of TiO_2 and thus inhibits the formation of •OH radical. Generally speaking, •OH radicals were provided to play a key role in the photocatalytic decomposition of VOCs. Compared with anatase TiO_2, the poor generation ability of OH radicals for rutile TiO_2 limits its application in photocatalytic VOCs degradation.

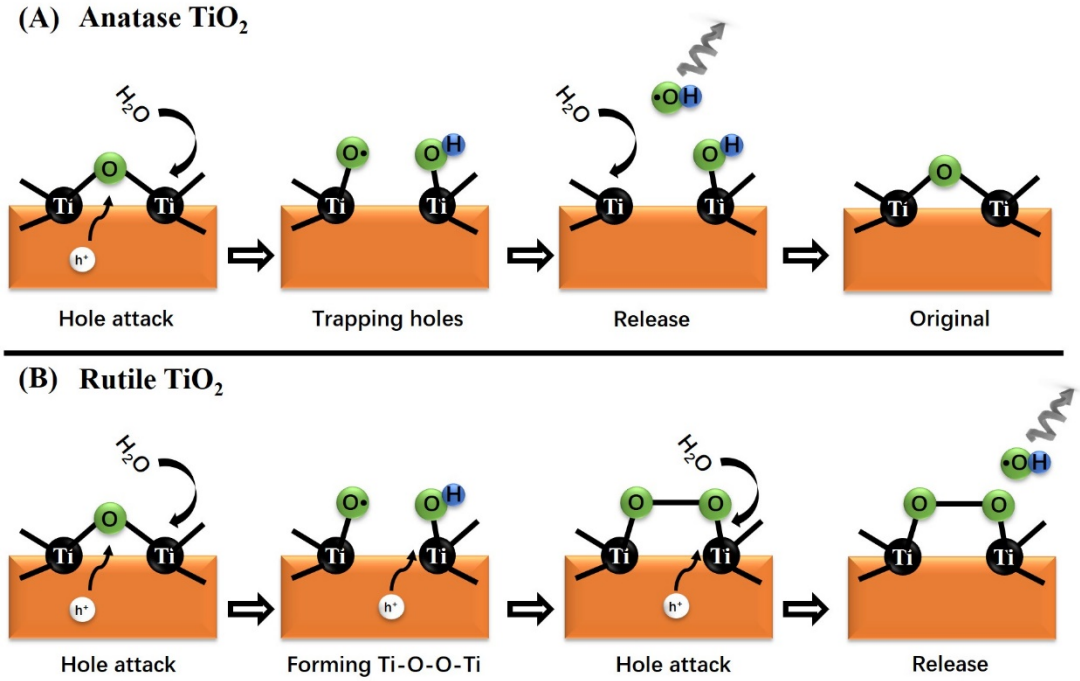

Fig. 1-3 Scheme showing the mechanism of OH radical production with **(A)** anatase and **(B)** rutile.

Recombination of photogenerated charge carriers will shorten the lifetime of photogenerated electrons and holes and reduce the overall quantum efficiency, which thus is the major limitation in the usage of semiconductor photocatalysis.[44] When recombination occurs, the short lifetime of photoproduced electrons and holes means there is no enough time for oxidation and reduction reaction. Most photocatalytic studies have focused on the anatase and rutile phases of TiO_2 due to their relatively high thermal stability and ease of preparation.[45, 46] However, according to the research of A. Yamakata et al, brookite TiO_2 powders have moderate depth of the electron-trap that

can promote both of photocatalytic oxidations and reductions.[47] As can be seen in Fig. 1-4, theoretically, electron trapping at powder defects reduces electron reactivity but delays electron-hole pair recombination, thereby extending the lifetime of holes. The depth on rutile is too deep for electron-induced reduction, and the depth on anatase is too shallow to prolong the lifetime of the holes. For brookite TiO_2, electrons are trapped at moderate depths, which can effectively promote photocatalytic reduction and oxidation. Although brookite TiO_2 is not as commonly used as that of anatase or rutile TiO_2 owing to its metastability, brookite TiO_2 has shown high photocatalytic activities for the degradation of various recalcitrant pollutants.[47, 48] W.-K. Li et al. found the exposed {210} facet of brookite TiO_2 is more reactive than the {101} facet of anatase TiO_2, which is thus beneficial for improving photocatalytic reactions.[49] Brookite TiO_2 also showed higher surface affinity for O_2 adsorption than anatase TiO_2 in oxygen reduction reaction to produce H_2O_2.[50] Moreover, brookite TiO_2 was demonstrated to oxidize propanone to CO_2 and H_2O much faster than anatase TiO_2. Brookite TiO_2 also exhibited higher areal photocatalytic activity for RhB degradation than rutile TiO_2 and anatase TiO_2.[51, 52] These observations suggest brookite TiO_2 is a promising photoconversion material for solving environmental issues.

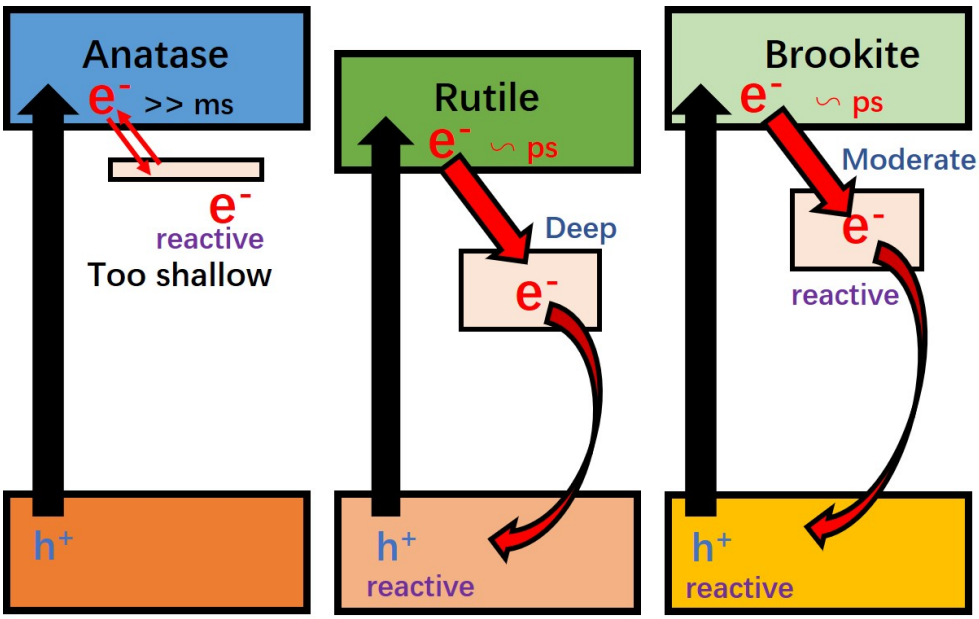

Fig. 1-4 Band energy of electron-trapping level in anatase, rutile and brookite.

1.3.1 Adjusting light adsorption

Due to the wide band gap of TiO_2, it can only be irradiated by ultraviolet light. It is well known that the intensity of visible light accounts for the largest proportion of total solar energy (as shown in the Fig. 1-5). Ultraviolet light makes up only a fraction of sunlight.[53] As mentioned above, although rutile TiO_2 can utilize some visible light, the poor ability to produce •OH radicals result in weaker photocatalytic activity of organic pollutants degradation compared with anatase and brookite TiO_2. However, due to the wide energy bands of anatase TiO_2 and brookiteTiO_2 (about 3.2 eV), these two photocatalysts can only absorb ultraviolet light. Therefore, it is necessary to modify TiO_2 to enhance its photocatalytic activity under visible light.

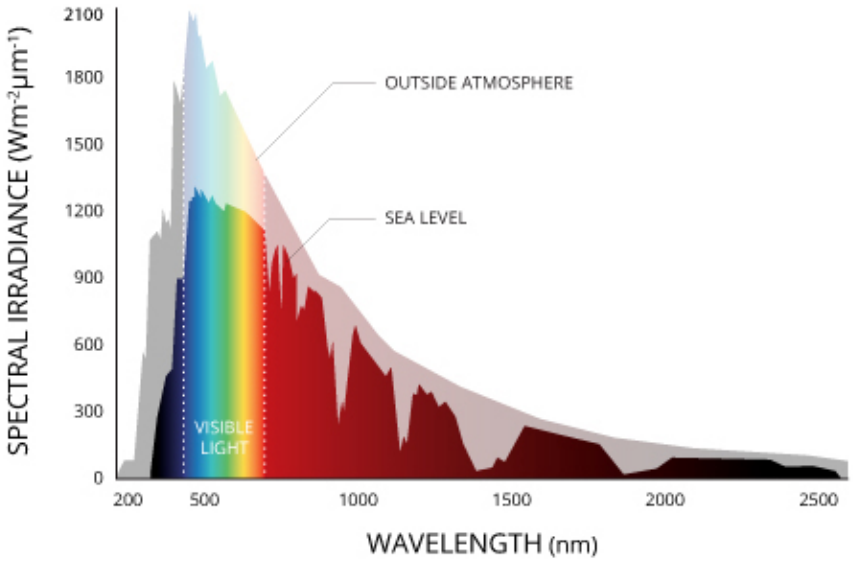

Fig. 1-5 the spectral irradiance of solar light.

1.3.1.1 Self-doping

Surface structure engineering has proven to be a promising strategy to modulate the photocatalytic properties. Without inducing other kinds of elements, oxygen vacancies (or Ti^{3+} defects) created by surface defect engineering is thought to be a promising method to extend the absorbance of TiO_2 from the UV to the visible region, leading to a high visible light catalytic activity.

A black TiO_2, an oxygen vacancy-rich TiO_2, was prepared by H_2 heat-treatment reduction method by Chen et al in 2011.[54] It has good visible light absorption

properties due to the formation of new energy band levels produced from oxygen vacancies. The lowest value of band gap is 1.54 eV, which can make TiO_2 exhibit visible light absorbance even in the near-infrared region. Yu et al reported that titanium hydride and peroxide were employed as Ti source and oxidant for preparing self-hydroxylated TiO_2 by hydrothermal synthesis. The resultant oxygen-detect TiO_2 shows better photocatalytic performance in H_2 evolution, which was 4.6 times superior to that of P25.[55]

The mechanism of absorbance red-shift of TiO_2 caused by defects is shown in the Fig 6. The white TiO_2 nanocrystals displayed typical valence band density of states (DOS) characteristics of TiO_2, with the edge of the maximum energy at about 1.26 eV. The conduction band minimum appears around -2.04 eV. The band gap of the optical absorption spectrum of white TiO_2 is about 3.30 eV. For black TiO_2 nanocrystals, the maximum energy of the valence band is blue-shifted to the vacuum level at around -0.92 eV. At the same time, there is no obvious change for the conduction band of the black TiO_2 nanocrystals. The visible light absorbance in black TiO_2could be due to the narrower electron transport paths (band gap is around 1.54 eV) in which the electrons transfer from valence band edge to these band tail states.[54, 56]

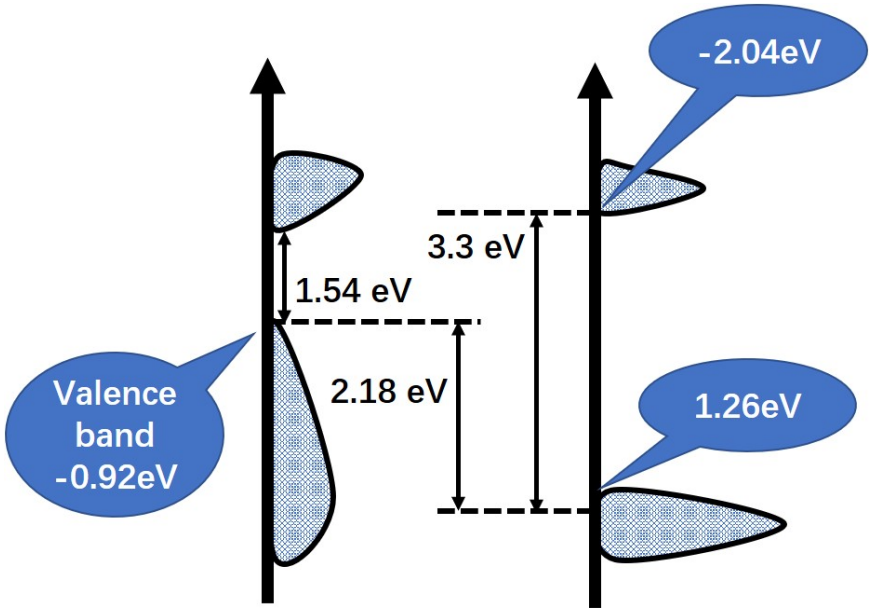

Fig. 1-6 Schematic illustration of the density of states (DOS) of disorder-engineered black TiO_2 nanocrystals, as compared to that of unmodified TiO_2 nanocrystals.

1.3.1.2 Elements doping and grafting

Although self-doping of TiO_2 has shown an improvement in visible light activity, it is very hard to maintain the stabilization of the defects and to control the O_2 vacancies generated through hydrogenation.[57] Doping of metal or non-metal elements onto TiO_2 to narrow the band gap of TiO_2 has become a popular research topic.[58]

Firstly, N-doping is taken as an example. As shown in the Fig. 1-7, with N atoms inducing into the TiO_2 lattice, a slightly higher energy level than oxygen, N 2p, is generated.[59] The generated mid-gap energy level allows the photogenerated electrons inspire from the mid-gap energy level, whereas electrons in the valence band of TiO_2 could not be excited by the visible light. Then, the excited electron from the intermediate gap level transfers to the conduction band. At the same time, a hole leaves at the intermediate gap level. Therefore, the non-metallic species can response to visible light irradiation and generate hydroxyl radicals(•OH radical) for organic compounds degradation, which is a strong oxidant.[60-62]

Furthermore, non-metallic doped TiO_2 prepared with different dopants such as S, C, P, F, B, etc. follow a similar mechanism. The only difference is that the intermediate bandgap energy of the doping is at a different energy level, resulting in different absorption wavelengths in the spectrum. It is worth noting that non-metallic doping of TiO_2 can increase the density of the catalyst and generate oxygen vacancies, which also lead to a red shift in absorption.[63, 64] Table 1-1 shows the synthesis methods and application of some normal non-metal elements doping TiO_2.

Table 1-1. Synthesis methods and Application of Non-metal elements doped onto TiO_2.[65-71]

Sample name	Doping element	Method	Source of energy	Organic compound	degradation	Degradation Time
N-TiO_2	N	Annealing	Visible light	MB	100	4.00
C,N,S-TiO_2	C,N,S	Annealing	Visible light	MC-LR	78	2.00

Sample name	Doping element	Method	Source of energy	Organic compound	degradation	Degradation Time
F-TiO_2	F	Sol-gel method	Sunlight	RhB	100	2.00
C-TiO_2	C	Sol-gel method	Visible light	Atrazine	93.4	3.00
P-TiO_2	P	Sol-gel method	Visible light	MO	83.5	2.00
P-TiO2/CNT	P	Hydrothermal synthesis	Visible light	MO	92.5	4.00
N-TiO_2/CNT	N	Hydrothermal synthesis	Visible light	Ibuprofen	86.0	2.50

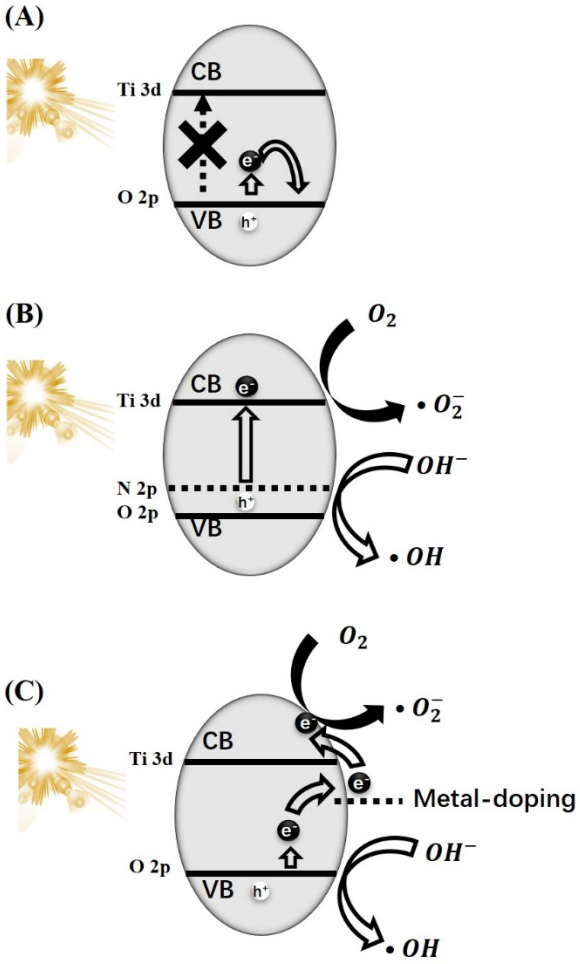

Fig. 1-7 Possible photoreaction mechanism of: (A) pure TiO_2 and (B) N-doping TiO_2 and (C) metal-doping TiO_2 under visible light irradiation.

The photoactivity of metal-doped TiO_2 can be explained by a new energy level

introduced into the band gap of TiO_2, which is near by the CB or VB of TiO_2 (Fig. 1-7C). Unlike non-metal-doped TiO_2, an electron is excited from the energy level of non-metal elements to the CB of TiO_2. The photoexcited electrons is excited from VB of TiO_2 to the middle gap energy level of metal elements, and then migrate to the CB of TiO_2, where they migrate toward the surface of the catalyst for reduction reactions.[72, 73] The holes remained at the VB of TiO_2, and then participate in the oxidation reaction. Table 1-2 shows different kinds of metal elements doping used for degradation organic compounds under visible light.

Table 1-2. The application of transformation metal modified/doping TiO_2.[74-83]

Elements	Method	Light source	Application
Fe(III) /TiO_2	impregnation	Visible light(400~530nm)	2-propanol degradation
Cu(II) /TiO_2	impregnation	Visible light(400~580nm)	2-propanol degradation
Ce(III) /TiO_2	impregnation	monochromic light (460 nm)	2-propanol degradation
Ru(III) /TiO_2	impregnation	Visible light (400~600nm) and UV light (300~450nm)	Acetone degradation
Cr ion/TiO_2	ion implantation	Visible light (>450nm)	NO oxidation
Mn/TiO_2	sol–gel technique	Visible light (>400nm)	methylene blue (MB) degradation
Co ion/TiO_2	Hydrothermal synthesis	Visible light (>400nm)	Acetaldehyde degradation
Pt ion/TiO_2	sol-gel method	Visible light (>420nm)	DCA, 4-CP, and TCA degradation
PbO/TiO_2	chemical vapor deposition	UV-vis	stearic acid degradation
Y_2O_3 modified-TiO_2	one pot/hydrothermal method	Solar light	4-CP solution degradation and reduction of dichromate solution

For improving visible light responsive ability of pure TiO_2, except metal-doping, transition metal grafting should be a possible strategy. As shown in the Fig. 1-8, unlike

metal elements doping, the modified elements on surface are not into embedded the bulk of TiO_2. Hashimoto et al. designed and prepared Cu(II) and Fe(III)-grafted TiO_2 photocatalysts for the efficient decomposition of 2-propanol from acetone to CO_2 under visible light induction.[84, 85] In this case, visible-light activation was caused by the interfacial charge transfer from the valence band of TiO_2 to transition metal. The transition metal ion transforms into its reduced state (for example, Cu(II) to Cu(I)) after capturing electrons, and then participate in the reduction reaction with oxygen adsorbed on the surface of TiO_2. The shortened electron transport distance may be the reason why the entire photocatalyst can absorb visible light.

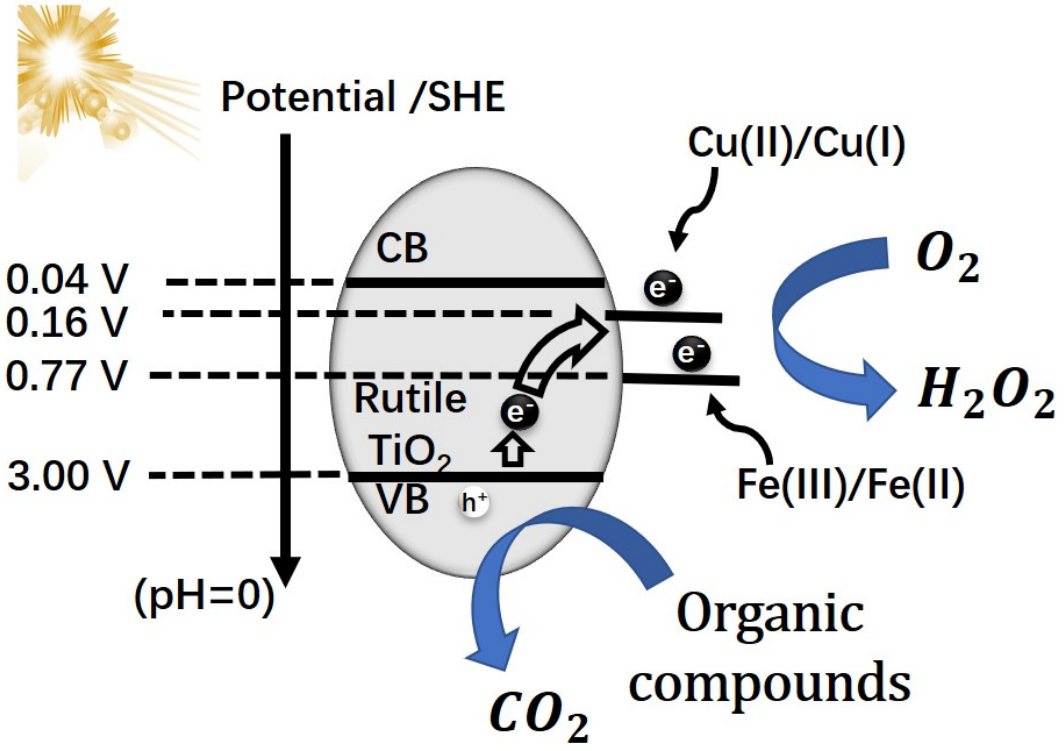

Fig. 1-8 The Schematic diagram illustrating the possible photocatalytic mechanism of Cu (II) or Fe(III) modified TiO_2 involving interfacial electron transfer and multielectron oxygen reduction.

1.3.1.3 Dye-sensitization

Photosensitization is widely used to extend the photo-response of TiO_2 to the visible region. The principle of dye-modification on TiO_2 is shown in Fig. 1-9C. As a strong interaction can be formed between dyes containing catechol moieties and metal oxides,

the dye molecular can connect with Ti^{4+} and adsorbed at the Brønsted acid sites of TiO_2.[86]

Some applications of dye-sensitization are shown in the Table 1-3. With modifying different dye, the photocatalytic degradation of organic compounds and photocatalytic selective oxidation will be performed, respectively. Fig. 1-9A shows the mechanism of dye-induced photocatalytic organic compounds degradation under visible light. The visible light excites the sensitizer molecules adsorbed on TiO_2, then injecting electrons to the CB of TiO_2. The CB acts as a mediator for transferring electrons from the sensitizer to the surface of TiO_2. At the same time, the VB of TiO_2 remains in an unfired state. Finally, the oxidized dye molecule (dye+) can interact with the pollutant (phenol) to return back to its ground state.[87-89]

Fig. 1-9B shows the process of photocatalytic selective oxidation over dye-sensitized TiO_2 (in the Fig. 1-9B is ARS). Under visible light irradiation, the dye adsorbed on the surface of TiO_2 will be excited to its excited state dye^*. After injecting electrons to the CB of TiO_2, the excited state dye^* changes to be dye radical cations, $\bullet dye^+$. Benzyl alcohol captures $\bullet dye^+$ to benzyl alcohol radical and H^+. At the same time, the $\bullet dye^+$ radical restores to its ground state. The valence band does not participate in the photocatalytic reaction process completely. Next, conduction band electrons reduce O_2 to superoxide radicals. Superoxide- interacts with benzyl alcohol radicals to generate benzaldehyde products and HOO^-. The interaction of H^+ and HOO^- lead to the generation of H_2O_2.

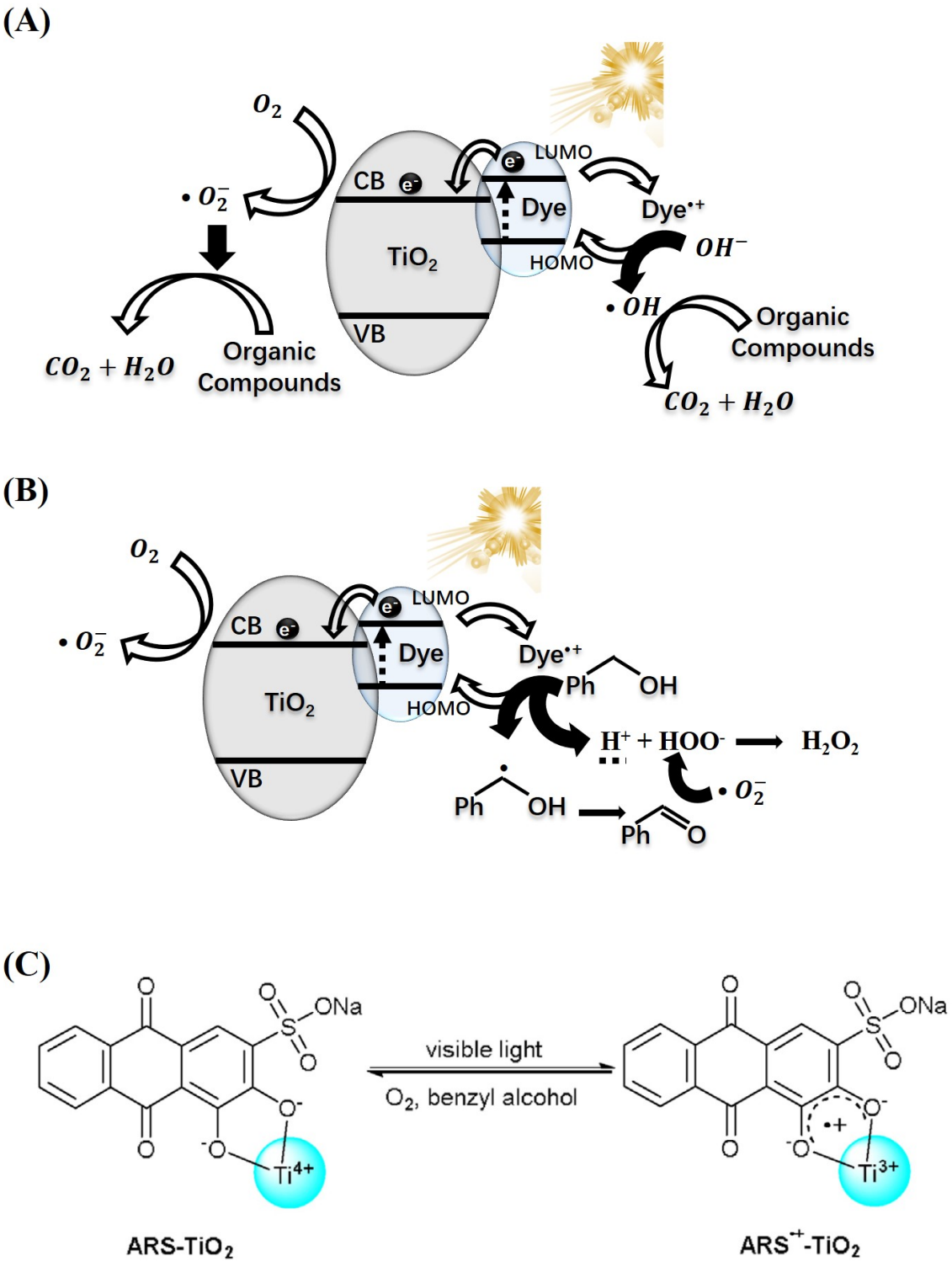

Fig. 1-9 The photocatalytic mechanism of **(A)** organic compounds degradation and **(B)** organic compounds (benzyl alcohol) selective oxidation over Dye-sensitized TiO_2 under visible light. **(C)** The adsorption and visible light-induced electron transfer between ARS and TiO_2.

Table 3 The application of Dye-sensitized TiO_2 under visible light.[89-92]

	Photocatalyst	Dye	Application	Light source
Photocatalytic degradation	P25	Eosin Y	Phenol	Solar light
	P25	Sudan black B	phenolic compounds	Visible light (Mercury lamp)
	P25/ZnO	TEMPO	Alcohol	Visible light(LED)
Selective Oxidation	P25	RuIIL3	CCl_4	Visible light (λ>420nm)
	Noble metal loaded/P25	RuIIL3	Per-chlorinated Compounds	Visible light (λ>420nm)

1.3.1.4 Localized surface plasmon resonance (LSPR) over noble metal

The LSPR effect of the noble metal nanoparticles can enhance the absorption of light, then promoting the local electric field and the excitation of active electrons and holes. Au and Ag are the most popular materials for plasmonic photocatalysis. The visible light responsive ability of photocatalysts can be effectively enhanced with Ag or Au sensitization.[93, 94] Other noble metals such as Pt, Pd and Rh have also been investigated but are not very common[93, 95].

Plasmonic photocatalysis has recently facilitated the rapid progress in enhancing photocatalytic efficiency under visible light irradiation, increasing the prospect of using sunlight for environmental and energy applications such as wastewater treatment, water splitting and carbon dioxide reduction.[96]

The mechanism of photoexcitation and visible light response induced by LSPR is shown in the Fig. 1-10. After excitation, LSPR decays into hot electrons and holes through Landau damping, creating highly energetic charge carriers.[97] Noble metal NPs acted as electron donors for titania injects electrons into the CB of TiO_2 under visible

light. CB of TiO_2, used as an electron transport intermediate, diffuses the electrons to surface of TiO_2, which then react will the O_2 adsorbed on TiO_2. During the period, the VB of TiO_2 remain the ground state.

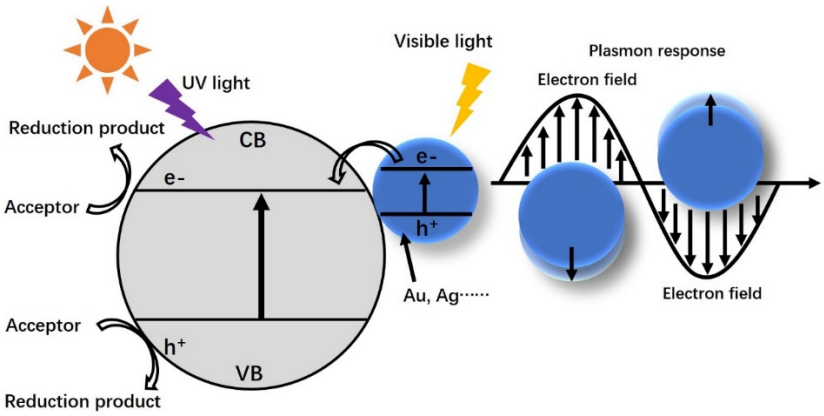

Fig. 1-10 Mechanism of photoexcitation by LSPR under visible light.

1.3.2 Promoting of electron-hole pairs separation

The organic compounds photocatalytic degradation replies on the stable separation of electron-hole pairs. As can be seen in the Fig. 1-11, under suitable wavelength of incident light, electrons will be excited from VB of photocatalyst to CB. Recombination of these charge carriers can compete with both charge separation and interfacial charge transfer.[98] Fast electron-holes recombination will shorten the life time of electrons and holes for reduction reaction and oxidation. Prolonging the life time of photoproduced electrons and holes is important for improving the photocatalytic activity.

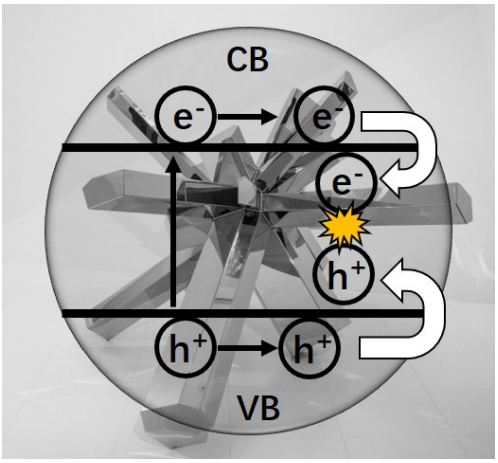

Fig. 1-11. The mechanism of photoproduced electron-hole pairs recombination

1.3.2.1 Self-doping

In section 1.3.1.1, we have discussed that the photo-response of TiO_2 was extended from the UV region to the visible region by oxygen vacancies and/or Ti^{3+} defects generated by surface defect engineering, resulting in high visible photocatalytic activity.

From the Fig. 1-12B, after inducing oxygen vacancy into the lattice of TiO_2, the photocatalytic activity of H_2 production increases a lot. According to Fig. 1-12A, after quenching in air, the PL strength is greatly improved, indicating the reduction of electron lifetime and the enhancement of carrier recombination. This evidence proves that Ti^{3+} ions with oxygen vacancies can improve the conductivity of TiO_2 and enhance the charge transfer and charge transfer of TiO_2. Surface oxygen vacancies may be responsible for enhancing the photocatalytic activity because they can enhance hole trapping (as shown in the Fig. 1-12D), thereby promoting the separation of photoexcited electrons and holes.[99]

However, the influence of self-doping for improving charge separation is not absolute and still controversial. Y. Nam et al estimated the influence of oxygen vacancy location on charge carriers in reduced TiO_2. As shown in the Fig. 1-12C, the oxygen vacancy in reduced TiO_2 is divided into four forms, tip, facet, edge and inside. According to the theoretical studies, the effect of oxygen vacancies on carrier behavior is related to the position of oxygen vacancies in TiO_2. The inside-oxygen vacancy and tip-oxygen vacancy can suppress the charge recombination due to the strong location of electron and holes. In contrast, the oxygen vacancy located at facet and edge may increase the charge recombination due to the greater nonadiabatic coupling and additional charge recombination channels. The mechanism of charge recombination is shown in the Fig. 1-13. According to the Fig. 1-13A, for triplet ground state systems (TGS, inside-oxygen vacancy and tip-oxygen vacancy), electrons and holes tend to relax step by step and finally are trapped at the oxygen defects. However, from the Fig. 1-13B, in the case of singlet ground state (SGS, facet-oxygen defect), the electron will recombine with hole rapidly. Table. 1-4 shows the recombination time and transition energy of TGS and SGS system. TGS system has much longer recombination time and

bigger transition energy than SGS system, indicating stronger capture and separation capability of carriers.[100]

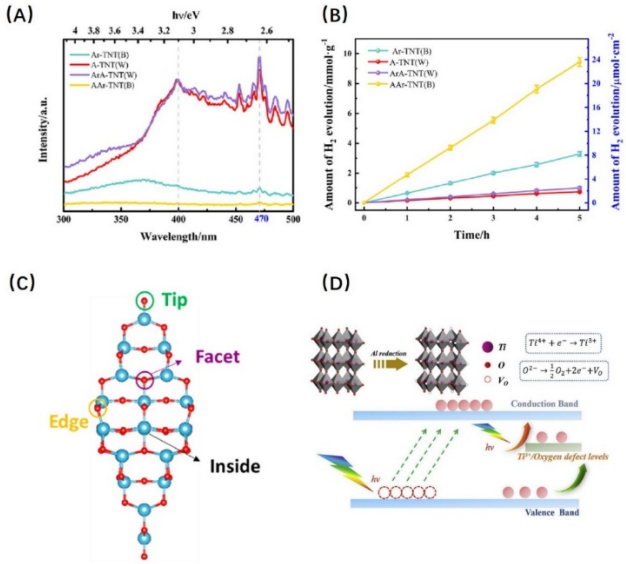

Fig. 1-12. (A) PL spectra of four types of photocatalyst prepared using different annealing condition. **(B)** Comparison of hydrogen evolution rate of four types of photocatalyst prepared using different annealing condition. **(C)** Schematic of different oxygen vacancy domains (left) and four representative structures for the reduced TiO_2 NPs with a single oxygen vacancy at various sites. **(D)** Formation mechanism of Ti^{3+}/oxygen vacancies in B-TiO_2NTAs lattice structure and their energy band.

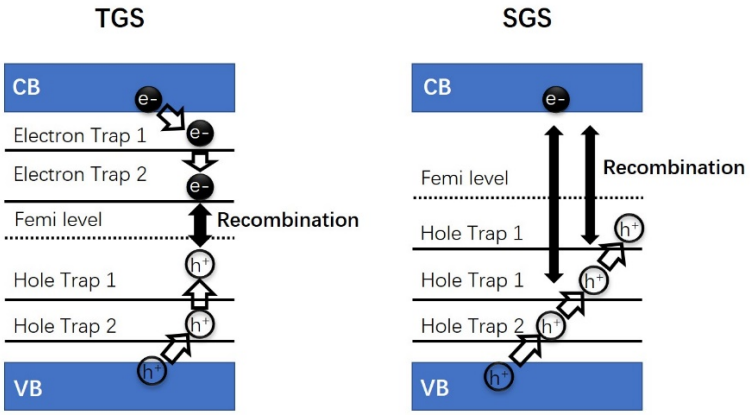

Fig. 1-13 Electronic energy levels involved in the charge carrier trapping and recombination dynamics for (a) triplet ground state (TGS) NPs and (b) singlet ground state (SGS) NPs. HT, ET, ER, and RC refer to hole trapping, electron trapping, electron relaxation, and recombination, respectively.

Table. 1-4 Recombination time and average energy differences of key orbitals (T: trip-oxygen defect, I: inside-oxygen defect, F: facet-oxygen defect)

Defect		Recombination time (ps)	Transition energy (eV)
Original		160.46	1.82
TGS	T1-1	631.79	1.36
	I3-1	678.47	1.68
	I3-2	2045.22	1.60
	I3-4	1228.56	1.65
SGS	F3-10	29.83	0.40
	F2-1	33.24	0.06
	F2-3	43.55	0.54

1.3.2.2 Elements doping

Elements-doping in the lattice of semiconductor photocatalyst to construct new energy bands can not only enhance the ability of visible light absorption (narrowing the band gap), but also improve the efficiency of electron-hole pairs separation.

When the doped non-metallic atoms (B, C, N, S, F, P) are similar in size to oxygen atoms (±15%), these non-metallic elements may replace the oxygen atoms in the lattice, thereby forming oxygen vacancies.

The equation (8) and (9) show the oxygen vacancy formation energy in bulk anatase TiO_2 and N-doped anatase TiO_2, respectively. A large decrease in the formation energy of an oxygen vacancy (from 4.2 to 0.6 eV) can be found. The situation of rutile TiO_2 is shown in the equation (10) and (11).[101] After N doping, the formation energy of oxygen vacancies also decreases obviously (from 10 eV to 6.4 eV). Thus, it is reasonable for oxygen vacancies production after nitrogen doping. Furthermore, as can be seen in the Fig. 1-14(A), Y, Yang et al selectively doped F^- ion onto the {001} facet of anatase TiO_2. [102] By the technology of XPS and EPR, the oxygen vacancies (shown in the Fig. 1-14(B) and (C)) were detected remarkedly. It is also proved that non-metal elemtents doping can efficiently substitute oxygen in the lattice of TiO_2 and produce oxygen vacancies. As described in chapter 1.3.2.1, some oxygen vacancies leading to the formation of suitable electron-trapping energy layers may be responsible for the

promotion of photogenerated electron-hole separation.[103] The existence of these electron-capturing energy level prevents the direct recombination of electrons with holes, thereby prolonging the electron lifetime and improving the separation efficiency of electron-hole carriers

$$TiO_2 \longrightarrow TiO_{2-x} + xV_O + {}^1/_2\, xO_2 \qquad \Delta E=4.2\ eV \qquad (8)$$

$$TiO_{2-2x}N_{2x} \longrightarrow TiO_{2-3x}N_{2x} + xV_O + {}^1/_2\, xO_2 \qquad \Delta E=0.6\ eV \qquad (9)$$

$$TiO_2 + xN_2 \longrightarrow TiO_{2-2x}N_{2x} + xO_2 \qquad \Delta E=10\ eV \qquad (10)$$

$$TiO_{2-x} + xN_2 \longrightarrow TiO_{2-3x}N_{2x} + xO_2 \qquad \Delta E=6.4\ eV \qquad (11)$$

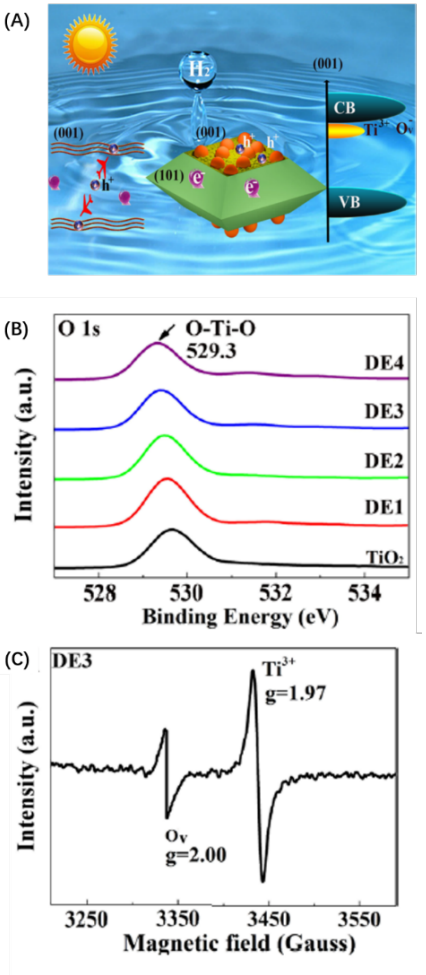

Fig. 1-14 (A) the schematic diagram of F^- ion site-selectively doping on the {001} facets of anatase TiO2. **(B)** the XPS spectra of O 1s in anatase TiO_2 after F^- ion doping. **(C)** the EPR spectrum of 6.9% F^- ion doping TiO_2 nanosheets.

1.3.2.3 Noble metal modification

The LSPR can drastically enhance the light absorption for weakly light-absorbing materials. At the same time, noble metal modification can also promote the electron-hole pairs separation obviously.

As shown in the Fig. 1-15B, in the absence of the Au nanoparticle, the charge carriers recombination easily happens. Fig. 18A shows the photoexcited charges transfer process of plasmonic photocatalysis. The principle of noble metal loading to improve the separation efficiency of photogenerated carriers can be briefly described as the creation of a space-charge region between TiO_2 nanoparticle and loaded the noble metal nanoparticles surface. Here, Au is used as the example. Under UV light photoirradiation, the photoproduced electrons on TiO_2 nanoparticle comes in contact with an Au nanoparticle. At the same time, the photogenerated holes on Au are in contact with the surface of TiO_2. The electrons diffusing from the TiO_2 to the TiO_2-Au interface are then quenched with the holes diffused from the Au to the TiO_2-Au interface, forming a depleted region, name as space-charge region. In the equilibrium state, an equal amount of electrons are trapped in the adjacent Au surface. This builds up an unidirectional electrical field from the TiO_2 side toward the Au side (as indicated by E in Fig. 1-15(A)), preventing charge carriers from moving in the opposite direction. When an electron-hole pair is excited in or near the space-charge region by an incident UV photon, the internal electrical field forces the electron to move to the Au region and the hole to the TiO_2 region, preventing their recombination. The electrons and holes are then captured by the acceptors and donors in the solution, respectively, and initiate further redox reactions.[96]

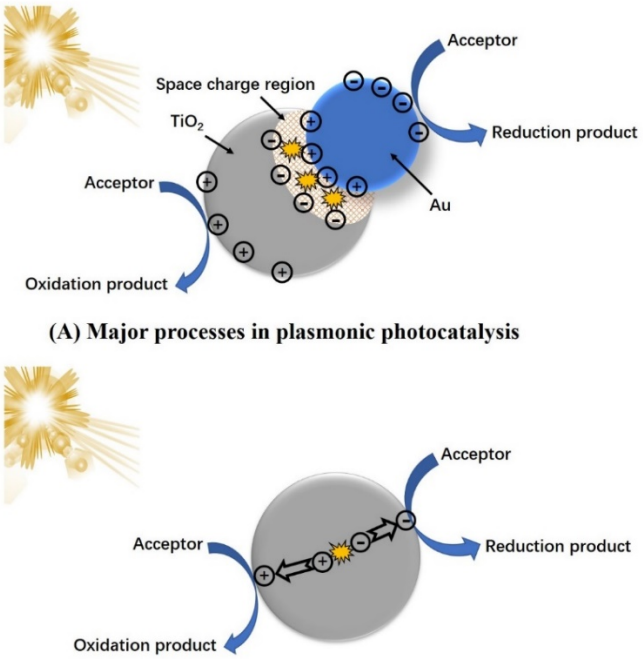

Fig. 1-15 The photoexcited charges transfer process of **(A)** plasmonic photocatalysis and **(B)** common photocatalysis (TiO_2 with oxygen defects).

1.3.2.4 Heterojunction

To overcome the serious drawbacks of fast charge recombination, developing heterojunctions between semiconductors is a most widely used strategy. According to the position of CB and VB of two semiconductors, the heterojunctions are divided into straddling gap (type I), staggered gap (type II) or broken gap (type III) as seen in the Fig. 1-16.[104]

In the Type I heterojunction, photo-production electrons and holes had different transfer pathways (as can be seen in the Fig.1-16A), which can suppress the charge recombination. Moreover, the rate of electrons and holes transfer to the reduction and oxidation site is different, which reduced the recombination of electrons and holes as well.[104, 105]

The energy band of type III heterojunction structure is shown in the Fig. 1-16B.[106] Under visible light photoirradiation, the electrons will be excited from VB of semiconductors (TiO_2 and In_2S_3) to CB of them. According to CB and VB of the 3

semiconductors (the E_{CB} of HPW, TiO_2 and In_2S_3 is 0.22 V, 0.25 V and 0.78 V vs. NHE, and the E_{VB} of HPW, TiO_2 and In_2S_3 is 3.70 V, 2.95 V and 1.18 V vs. NHE, respectively), the photo-excited electrons jump from CB of TiO_2 to CB of HPW and further move to VB of In_2S_3. Finally, the electrons are accumulated at the CB of In_2S_3. At the same time, the photogenerated holes are respectively generated on VB of TiO_2 and In_2S_3, respectively. [107, 108] The electrons at the CB of In_2S_3 react with the oxygen adsorbed on In_2S_3 to form $\bullet O_2^-$, while the holes on the VB of TiO_2 will oxidize H_2O to produce •OH. It is worth noting that the TiO_2 based type III heterojunctions are presented less, because it is difficult to construct type III heterojunctions between TiO_2 and other semiconductors for their unmatched band gap position. Up to now, only TiO_2/C_3N_4, TiO_2/WO_3, TiO_2-Ag-Cu_2O, CdS-Ag-TiO_2 and anatase/rutile TiO_2 are proposed.[109-113]

The enhanced photocatalytic activity of TiO_2-based heterostructure materials is usually discussed based on the electron-hole separation by type II heterojunctions, which are divided into p-n heterojunctions and non-p-n heterojunctions (Fig. 1-16C and D). [114-116] The p-n is a junction between two semiconductors, one doped with a donor (n-type) and another one doped with an acceptor (p-type).[117] In the p-n heterojunction, the large Fermi level difference in two semiconductors provides a very strong internal electric field for efficient charge transfer and separation. Furthermore, at the interface of the two semiconductors, a built-in electric field is formed due to band bending, which can also enhance the separation of photogenerated electron-hole pairs. Thus, engineering the junction between semiconductors is essential for improving charge separation and transfer efficiency, and then photocatalytic activity.

In addition to the p-n type heterostructure, there are also other non-p–n type heterojunction systems, where the most suitable for photocatalytic applications is the staggered bandgap type (Fig. 1-16D). In this type, the semiconductors A and B with matching band potentials are tightly bonded to construct the efficient heterostructure. When the CB level of semiconductor-B is lower than that of semiconductor-A, electrons in the CB of semiconductor-A can be transferred to that of semiconductor-B

under visible light irradiation. If the VB level of semiconductor-B is lower than that of semiconductor-A, holes in the VB of semiconductor-B can be transferred to that of semiconductor-A. As a result, the separation and migration of photogenerated carriers can be promoted by the internal field, so less of a barrier exists. Therefore, the probability of electron-hole recombination can be reduced.

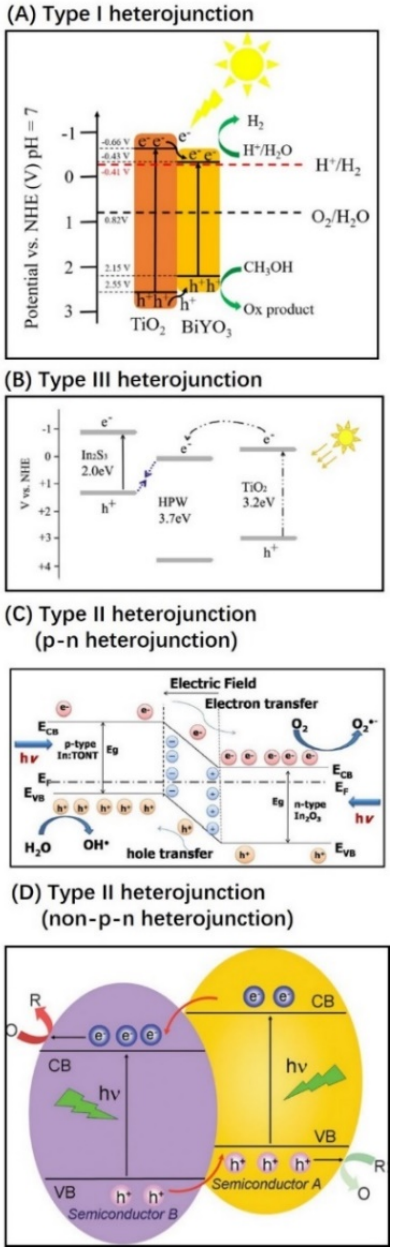

Fig. 1-16 The energy band structure of **(A)** Type I heterojunction, **(B)** Type III heterojunction **(C)** Type II heterojunction (p-n heterojunction) and **(D)** Type II heterojunction (non-p-n heterojunction).

1.4 Summary

In summary, TiO_2 as a kind of traditional photocatalyst has huge potential in removing of organic compounds. However, owing to the wide band gap and fast charge recombination, the photocatalytic efficiency of pure TiO_2 is hindered under visible light. TiO_2 consists of 3 kinds of phases (rutile, anatase and brookite). And different phases have different photocatalytic activity. Compared with rutile, anatase has higher efficiency in •OH radical, which is thought to be a strong oxidizing group. Compared with rutile and anatase, brookite TiO_2 has suitable depth of energy level of electron-trapping, which means more efficient charge separation. For increasing the visible light absorbance and charge separation, modification on the basis of TiO_2, such as elements doping, dye-sensitization, noble metal loading and so on, is a possible way.

Furthermore, it is worth noting that, in addition to the optical properties of the photocatalyst itself, the specific surface area of the photocatalyst and the influence of the environment such as pH, temperature, gas atmosphere, etc., also have a non-negligible effect on the photocatalytic reaction. In future, in wide using photocatalyst for removing organic compounds, all factors should be fully considered.

Reference

[1] L. Petersen, M. Heynen, F. Pellicciotti, Freshwater Resources: Past, Present, Future, International Encyclopedia of Geography2019, pp. 1-12.

[2] P. Rajasulochana, V. Preethy, Comparison on efficiency of various techniques in treatment of waste and sewage water – A comprehensive review, Resource-Efficient Technologies, 2 (2016) 175-184.

[3] Z.N. Tong, Discussion on the health problems of indoor living, IOP Conference Series: Earth and Environmental Science, 186 (2018).

[4] Rosana M. Alberici, W.F. Jardim, Photocatalytic destruction of VOCs in the gas-phase

using titanium dioxide, Applied Catalysis B: Environmental, 14 (1997) 55-68.

[5] X. Zhang, J. Cao, J. Wei, Y. Zhang, Improved C-history method for rapidly and accurately measuring the characteristic parameters of formaldehyde/VOCs emitted from building materials, Building and Environment, 143 (2018) 570-578.

[6] M. Meisutovic-Akhtarieva, T. Prasauskas, D. Ciuzas, E. Krugly, K. Keraityte, D. Martuzevicius, V. Kauneliene, Impacts of exhaled aerosol from the usage of the tobacco heating system to indoor air quality: A chamber study, Chemosphere, 223 (2019) 474-482.

[7] M. Salaspuro, Key role of local acetaldehyde in upper GI tract carcinogenesis, Best Pract Res Clin Gastroenterol, 31 (2017) 491-499.

[8] D. Baderna, S. Maggioni, E. Boriani, S. Gemma, M. Molteni, A. Lombardo, A. Colombo, S. Bordonali, G. Rotella, M. Lodi, E. Benfenati, A combined approach to investigate the toxicity of an industrial landfill's leachate: chemical analyses, risk assessment and in vitro assays, Environ Res, 111 (2011) 603-613.

[9] M. Barba, A. Mazza, C. Guerriero, M. Di Maio, F. Romeo, P. Maranta, I.R. Marino, M.G. Paggi, A. Giordano, Wasting lives: the effects of toxic waste exposure on health. The case of Campania, Southern Italy, Cancer Biol Ther, 12 (2011) 106-111.

[10] L. Koshy, E. Paris, S. Ling, T. Jones, K. Berube, Bioreactivity of leachate from municipal solid waste landfills - assessment of toxicity, Sci Total Environ, 384 (2007) 171-181.

[11] Russell F. Dunn, M.M. El-Halwagi, Optimal design of multicomponent VOC condensation systems, Journal of Hazardous Materials, (1994) 187-206.

[12] Y.-S. Son, Decomposition of VOCs and odorous compounds by radiolysis: A critical review, Chemical Engineering Journal, 316 (2017) 609-622.

[13] F. Heymes, P. Manno-Demoustier, F. Charbit, J.L. Fanlo, P. Moulin, A new efficient absorption liquid to treat exhaust air loaded with toluene, Chemical Engineering Journal, 115 (2006) 225-231.

[14] Y. Liu, X. Feng, D. Lawless, Separation of gasoline vapor from nitrogen by hollow fiber composite membranes for VOC emission control, Journal of Membrane Science, 271 (2006) 114-124.

[15] E. Dumont, G. Darracq, A. Couvert, C. Couriol, A. Amrane, D. Thomas, Y. Andrès, P. Le Cloirec, VOC absorption in a countercurrent packed-bed column using water/silicone oil mixtures: Influence of silicone oil volume fraction, Chemical Engineering Journal, 168 (2011) 241-248.

[16] Y.-h. Li, F.-m. Chang, B. Huang, Y.-p. Song, H.-y. Zhao, K.-j. Wang, Activated carbon preparation from pyrolysis char of sewage sludge and its adsorption performance for organic compounds in sewage, Fuel, 266 (2020).

[17] M.M. Paixão, M.T.G. Vianna, M. Marques, Graphene and graphene nanocomposites for the removal of aromatic organic compounds from the water: systematic review, Materials Research Express, 5 (2018).

[18] L.T. Gibson, Mesosilica materials and organic pollutant adsorption: part B removal from aqueous solution, Chem Soc Rev, 43 (2014) 5173-5182.

[19] Faisal I. Khan , A.K. Ghoshal, Removal of Volatile Organic Compounds from polluted air, Journal of Loss Prevention in the Process Industries, 527-545.

[20] P. Dwivedi, V. Gaur, A. Sharma, N. Verma, Comparative study of removal of volatile organic compounds by cryogenic condensation and adsorption by activated carbon fiber, Separation and Purification Technology, 39 (2004) 23-37.

[21] W. Raza, J. Lee, N. Raza, Y. Luo, K.-H. Kim, J. Yang, Removal of phenolic compounds from industrial waste water based on membrane-based technologies, Journal of Industrial and Engineering Chemistry, 71 (2019) 1-18.

[22] M.S. Kamal, S.A. Razzak, M.M. Hossain, Catalytic oxidation of volatile organic compounds (VOCs) – A review, Atmospheric Environment, 140 (2016) 117-134.

[23] Moo Been. Chang, C.C. Lee, Destruction of Formaldehyde with Dielectric Barrier Discharge Plasmas, Environ. Sci. Technol, 29 (1995) 181-186.

[24] J. Quiroz Torres, S. Royer, J.P. Bellat, J.M. Giraudon, J.F. Lamonier, Formaldehyde: catalytic oxidation as a promising soft way of elimination, ChemSusChem, 6 (2013) 578-592.

[25] Z. Liang, J. Wang, Y. Zhang, C. Han, S. Ma, J. Chen, G. Li, T. An, Removal of volatile organic compounds (VOCs) emitted from a textile dyeing wastewater treatment

plant and the attenuation of respiratory health risks using a pilot-scale biofilter, Journal of Cleaner Production, 253 (2020).

[26] RobertoAndreozzi, VincenzoCaprio, AmedeoInsol, RaffaeleMarott., Advanced oxidation processes (AOP) for water purification and recovery, Catalysis Today, 53 (1999) 51-59.

[27] E.Pelizzetti, C.Minero, Mechanism of the photo-oxidative degradation of organic pollutants over TiO2 particles, Electrochimica Acta, 38 (1993) 47-55.

[28] T. Fukumura, E. Sambandan, H. Yamashita, Synthesis and VOC degradation ability of a CeO 2 /WO 3 thin-layer visible-light photocatalyst, Materials Research Bulletin, 94 (2017) 493-499.

[29] A. Enesca, Y. Yamaguchi, C. Terashima, A. Fujishima, K. Nakata, A. Duta, Enhanced UV–Vis photocatalytic performance of the CuInS 2 /TiO 2 /SnO 2 hetero-structure for air decontamination, Journal of Catalysis, 350 (2017) 174-181.

[30] R. Yang, Q. Chen, Y. Ma, R. Zhu, Y. Fan, J. Huang, H. Niu, Y. Dong, D. Li, Y. Zhang, L. Mei, B. Chen, Z. Zeng, Highly efficient photocatalytic hydrogen evolution and simultaneous formaldehyde degradation over Z-scheme ZnIn2S4-NiO/BiVO4 hierarchical heterojunction under visible light irradiation, Chemical Engineering Journal, 423 (2021).

[31] S. Song, C. Lu, X. Wu, S. Jiang, C. Sun, Z. Le, Strong base g-C3N4 with perfect structure for photocatalytically eliminating formaldehyde under visible-light irradiation, Applied Catalysis B: Environmental, 227 (2018) 145-152.

[32] Z. Shayegan, C.-S. Lee, F. Haghighat, TiO2 photocatalyst for removal of volatile organic compounds in gas phase – A review, Chemical Engineering Journal, 334 (2018) 2408-2439.

[33] Lijun Guo, Yuanmin Wang, H.P. Lu, Combined Single-Molecule Photon-Stamping Spectroscopy and Femtosecond Transient Absorption Spectroscopy Studies of Interfacial Electron Transfer Dynamics, J. Am. Chem. Soc., 132 (2010) 1999-2004.

[34] I. Dhada, P.K. Nagar, M. Sharma, Challenges of TiO2-Based Photooxidation of Volatile Organic Compounds: Designing, Coating, and Regenerating Catalyst,

Industrial & Engineering Chemistry Research, 54 (2015) 5381-5387.
[35] K. Ozawa, M. Emori, S. Yamamoto, R. Yukawa, S. Yamamoto, R. Hobara, K. Fujikawa, H. Sakama, I. Matsuda, Electron-Hole Recombination Time at TiO2 Single-Crystal Surfaces: Influence of Surface Band Bending, J Phys Chem Lett, 5 (2014) 1953-1957.
[36] D. Vildozo, C. Ferronato, M. Sleiman, J.-M. Chovelon, Photocatalytic treatment of indoor air: Optimization of 2-propanol removal using a response surface methodology (RSM), Applied Catalysis B: Environmental, 94 (2010) 303-310.
[37] Y. Yamada, Y. Kanemitsu, Determination of electron and hole lifetimes of rutile and anatase TiO2 single crystals, Applied Physics Letters, 101 (2012).
[38] L. Xiong, J. Tang, Strategies and Challenges on Selectivity of Photocatalytic Oxidation of Organic Substances, Advanced Energy Materials, 11 (2021).
[39] Y. Wang, A. Liu, D. Ma, S. Li, C. Lu, T. Li, C. Chen, TiO2 Photocatalyzed C–H Bond Transformation for C–C Coupling Reactions, Catalysts, 8 (2018).
[40] D. Jiang, T.A. Otitoju, Y. Ouyang, N.F. Shoparwe, S. Wang, A. Zhang, S. Li, A Review on Metal Ions Modified TiO2 for Photocatalytic Degradation of Organic Pollutants, Catalysts, 11 (2021).
[41] J. Zhang, Y. Nosaka, Mechanism of the OH Radical Generation in Photocatalysis with TiO2 of Different Crystalline Types, The Journal of Physical Chemistry C, 118 (2014) 10824-10832.
[42] J. Zhang, Y. Nosaka, Quantitative Detection of OH Radicals for Investigating the Reaction Mechanism of Various Visible-Light TiO2 Photocatalysts in Aqueous Suspension, The Journal of Physical Chemistry C, 117 (2013) 1383-1391.
[43] Akihito Imanishi, Tomoaki Okamura, Naomichi Ohashi, Ryuhei Nakamura, Y. Nakato, Mechanism of Water Photooxidation Reaction at Atomically Flat TiO2 (Rutile) (110) and (100) Surfaces: Dependence on Solution pH, J. Am. Chem. Soc., 129 (2007) 11569-11578.
[44] M. Pelaez, N.T. Nolan, S.C. Pillai, M.K. Seery, P. Falaras, A.G. Kontos, P.S.M. Dunlop, J.W.J. Hamilton, J.A. Byrne, K. O'Shea, M.H. Entezari, D.D. Dionysiou, A

review on the visible light active titanium dioxide photocatalysts for environmental applications, Applied Catalysis B: Environmental, 125 (2012) 331-349.

[45] Q. Zeng, X. Wang, X. Xie, G. Lu, Y. Wang, S. Cheng Lee, J. Sun, TiO2/TaS2 with superior charge separation and adsorptive capacity to the photodegradation of gaseous acetaldehyde, Chemical Engineering Journal, 379 (2020).

[46] M. Sansotera, S. Geran Malek Kheyli, A. Baggioli, C.L. Bianchi, M.P. Pedeferri, M.V. Diamanti, W. Navarrini, Absorption and photocatalytic degradation of VOCs by perfluorinated ionomeric coating with TiO2 nanopowders for air purification, Chemical Engineering Journal, 361 (2019) 885-896.

[47] J.J.M. Vequizo, H. Matsunaga, T. Ishiku, S. Kamimura, T. Ohno, A. Yamakata, Trapping-Induced Enhancement of Photocatalytic Activity on Brookite TiO2 Powders: Comparison with Anatase and Rutile TiO2 Powders, ACS Catalysis, 7 (2017) 2644-2651.

[48] H.T.T. Tran, H. Kosslick, M.F. Ibad, C. Fischer, U. Bentrup, T.H. Vuong, L.Q. Nguyen, A. Schulz, Photocatalytic Performance of Highly Active Brookite in the Degradation of Hazardous Organic Compounds Compared to Anatase and Rutile, Applied Catalysis B: Environmental, 200 (2017) 647-658.

[49] Wei-Kun Li, Xue-Qing Gong, Guanzhong Lu, A. Selloni, Different Reactivities of TiO2 Polymorphs: Comparative DFT Calculations of Water and Formic Acid Adsorption at Anatase and Brookite TiO2 Surfaces, J. Phys. Chem. C, 112 (2008) 6594-6596.

[50] Z. Li, S. Cong, Y. Xu, Brookite vs Anatase TiO2 in the Photocatalytic Activity for Organic Degradation in Water, ACS Catalysis, 4 (2014) 3273-3280.

[51] M. Addamo, M. Bellardita, A. Di Paola, L. Palmisano, Preparation and photoactivity of nanostructured anatase, rutile and brookite TiO2 thin films, Chem Commun (Camb), (2006) 4943-4945.

[52] J. Zhang, S. Yan, L. Fu, F. Wang, M. Yuan, G. Luo, Q. Xu, X. Wang, C. Li, Photocatalytic Degradation of Rhodamine B on Anatase, Rutile, and Brookite TiO2, Chinese Journal of Catalysis, 32 (2011) 983-991.

[53] N. Guo, Y. Liang, S. Lan, L. Liu, J. Zhang, G. Ji, S. Gan, Microscale Hierarchical Three-Dimensional Flowerlike TiO2/PANI Composite: Synthesis, Characterization, and Its Remarkable Photocatalytic Activity on Organic Dyes under UV-Light and Sunlight Irradiation, The Journal of Physical Chemistry C, 118 (2014) 18343-18355.
[54] Xiaobo Chen, Lei Liu, Peter Y. Yu, S.S. Mao, Increasing Solar Absorption for Photocatalysis with Black Hydrogenated Titanium Dioxide Nanocrystals, SCIENCE, 331 (2011) 746-750.
[55] F. Yu, X. Bai, C. Yang, L. Xu, J. Ma, Reduced Graphene Oxide–P25 Nanocomposites as Efficient Photocatalysts for Degradation of Bisphenol A in Water, Catalysts, 9 (2019).
[56] X. Bi, G. Du, A. Kalam, D. Sun, Y. Yu, Q. Su, B. Xu, A.G. Al-Sehemi, Tuning oxygen vacancy content in TiO2 nanoparticles to enhance the photocatalytic performance, Chemical Engineering Science, 234 (2021).
[57] S. Bagheri, N.M. Julkapli, Modified iron oxide nanomaterials: Functionalization and application, Journal of Magnetism and Magnetic Materials, 416 (2016) 117-133.
[58] A. Zaleska, Doped-TiO2: A Review, Recent Patents on Engineering, 2 (2008) 157-164.
[59] S.A. Ansari, M.M. Khan, M.O. Ansari, M.H. Cho, Nitrogen-doped titanium dioxide (N-doped TiO2) for visible light photocatalysis, New Journal of Chemistry, 40 (2016) 3000-3009.
[60] H. Pan, Y.-W. Zhang, V.B. Shenoy, H. Gao, Effects of H-, N-, and (H, N)-Doping on the Photocatalytic Activity of TiO2, The Journal of Physical Chemistry C, 115 (2011) 12224-12231.
[61] M. Chen, L.-L. Shao, Y.-P. Liu, T.-Z. Ren, Z.-Y. Yuan, Nitrogen-doped ordered cubic mesoporous carbons as metal-free counter electrodes for dye-sensitized solar cells, Journal of Power Sources, 283 (2015) 305-313.
[62] Y. Zhang, F. Du, X. Yan, Y. Jin, K. Zhu, X. Wang, H. Li, G. Chen, C. Wang, Y. Wei, Improvements in the electrochemical kinetic properties and rate capability of anatase titanium dioxide nanoparticles by nitrogen doping, ACS Appl Mater Interfaces, 6 (2014)

4458-4465.

[63] X. Xiang, X.-Y. Shi, X.-L. Gao, F. Ji, Y.-J. Wang, C.-M. Liu, X.-T. Zu, Effect of N-Doping on Absorption and Luminescence of Anatase TiO

2

Films, Chinese Physics Letters, 29 (2012).

[64] A. Samokhvalov, Hydrogen by photocatalysis with nitrogen codoped titanium dioxide, Renewable and Sustainable Energy Reviews, 72 (2017) 981-1000.

[65] A.P. Bhirud, S.D. Sathaye, R.P. Waichal, J.D. Ambekar, C.J. Park, B.B. Kale, In-situ preparation of N-TiO2/graphene nanocomposite and its enhanced photocatalytic hydrogen production by H2S splitting under solar light, Nanoscale, 7 (2015) 5023-5034.

[66] J. Dai, J. Yang, X. Wang, L. Zhang, Y. Li, Enhanced visible-light photocatalytic activity for selective oxidation of amines into imines over TiO2(B)/anatase mixed-phase nanowires, Applied Surface Science, 349 (2015) 343-352.

[67] A.E. Giannakas, M. Antonopoulou, C. Daikopoulos, Y. Deligiannakis, I. Konstantinou, Characterization and catalytic performance of B-doped, B–N co-doped and B–N–F tri-doped TiO2 towards simultaneous Cr(VI) reduction and benzoic acid oxidation, Applied Catalysis B: Environmental, 184 (2016) 44-54.

[68] M. Iwase, K. Yamada, T. Kurisaki, O.O. Prieto-Mahaney, B. Ohtani, H. Wakita, Visible-light photocatalysis with phosphorus-doped titanium(IV) oxide particles prepared using a phosphide compound, Applied Catalysis B: Environmental, 132-133 (2013) 39-44.

[69] S. Wang, S. Zhou, Photodegradation of methyl orange by photocatalyst of CNTs/P-TiO(2) under UV and visible-light irradiation, J Hazard Mater, 185 (2011) 77-85.

[70] C. Xu, R. Killmeyer, M.L. Gray, S.U.M. Khan, Photocatalytic effect of carbon-modified n-TiO2 nanoparticles under visible light illumination, Applied Catalysis B: Environmental, 64 (2006) 312-317.

[71] C. Yuan, C.H. Hung, H.W. Li, W.H. Chang, Photodegradation of ibuprofen by TiO2 co-doping with urea and functionalized CNT irradiated with visible light - Effect

of doping content and pH, Chemosphere, 155 (2016) 471-478.

[72] J. Liu, R. Han, Y. Zhao, H. Wang, W. Lu, T. Yu, Y. Zhang, Enhanced Photoactivity of V−N Codoped TiO2 Derived from a Two-Step Hydrothermal Procedure for the Degradation of PCP−Na under Visible Light Irradiation, The Journal of Physical Chemistry C, 115 (2011) 4507-4515.

[73] D. Lu, H. Wang, X. Zhao, K.K. Kondamareddy, J. Ding, C. Li, P. Fang, Highly Efficient Visible-Light-Induced Photoactivity of Z-Scheme g-C3N4/Ag/MoS2 Ternary Photocatalysts for Organic Pollutant Degradation and Production of Hydrogen, ACS Sustainable Chemistry & Engineering, 5 (2017) 1436-1445.

[74] D.S. Bhachu, S. Sathasivam, C.J. Carmalt, I.P. Parkin, PbO-modified TiO2 thin films: a route to visible light photocatalysts, Langmuir, 30 (2014) 624-630.

[75] Q.R. Deng, X.H. Xia, M.L. Guo, Y. Gao, G. Shao, Mn-doped TiO2 nanopowders with remarkable visible light photocatalytic activity, Materials Letters, 65 (2011) 2051-2054.

[76] Hiroshi Irie, Kazuhide Kamiya, Toshihiko Shibanuma, Shuhei Miura, Donald A. Tryk, Toshihiko Yokoyama, K. Hashimoto, Visible Light-Sensitive Cu(II)-Grafted TiO2 Photocatalysts: Activities and X-ray Absorption Fine Structure Analyses, J. Phys. Chem. C, 113 (2009) 10761–10766.

[77] Huogen Yu, Hiroshi Irie, Yoshiki Shimodaira, Yasuhiro Hosogi, Yasushi Kuroda, Masahiro Miyauchi, K. Hashimoto, An Efficient Visible-Light-Sensitive Fe(III)-Grafted TiO2 Photocatalyst, J. Phys. Chem. C, 114 (2010) 16481–16487.

[78] Y. Ishibai, J. Sato, T. Nishikawa, S. Miyagishi, Synthesis of visible-light active TiO2 photocatalyst with Pt-modification: Role of TiO2 substrate for high photocatalytic activity, Applied Catalysis B: Environmental, 79 (2008) 117-121.

[79] M. Iwasaki, M. Hara, H. Kawada, H. Tada, S. Ito, Cobalt Ion-Doped TiO(2) Photocatalyst Response to Visible Light, J Colloid Interface Sci, 224 (2000) 202-204.

[80] S. Kitano, N. Murakami, T. Ohno, Y. Mitani, Y. Nosaka, H. Asakura, K. Teramura, T. Tanaka, H. Tada, K. Hashimoto, H. Kominami, Bifunctionality of Rh3+ Modifier on TiO2 and Working Mechanism of Rh3+/TiO2 Photocatalyst under Irradiation of Visible

Light, The Journal of Physical Chemistry C, 117 (2013) 11008-11016.

[81] S. Kitano, A. Tanaka, K. Hashimoto, H. Kominami, Metal ion-modified TiO2 photocatalysts having controllable oxidative performance under irradiation of visible light, Applied Catalysis A: General, 521 (2016) 202-207.

[82] Masato Takeuchi, Hiromi Yamashita, Masaya Matsuoka, Masakazu Anpo, Takashi Hirao, Nobuhisa Itoh, N. Iwamoto, Photocatalytic decomposition of NO under visible light irradiation on the Cr-ion-implanted TiO2 thin film photocatalyst, Catalysis Letters, 67 (2000) 135–137

[83] Ryuhei Nakamura, Akihiro Okamoto, Hitoshi Osawa, Hiroshi Irie, K. Hashimoto, Design of All-Inorganic Molecular-Based Photocatalysts Sensitive to Visible Light: Ti(IV)−O−Ce(III) Bimetallic Assemblies on Mesoporous Silica, J. Am. Chem. Soc., 129 (2007) 9596–9597.

[84] Huogen Yu, Hiroshi Irie, Yoshiki Shimodaira, Yasuhiro Hosogi〃, Yasushi Kuroda〃, Masahiro Miyauchi, K. Hashimoto, An Efficient Visible-Light-Sensitive Fe(III)-Grafted TiO2 Photocatalyst, J. Phys. Chem. C, 114 (2010) 16481-16487.

[85] H. Irie, S. Miura, K. Kamiya, K. Hashimoto, Efficient visible light-sensitive photocatalysts: Grafting Cu(II) ions onto TiO2 and WO3 photocatalysts, Chemical Physics Letters, 457 (2008) 202-205.

[86] D. Finkelstein-Shapiro, S.K. Davidowski, P.B. Lee, C. Guo, G.P. Holland, T. Rajh, K.A. Gray, J.L. Yarger, M. Calatayud, Direct Evidence of Chelated Geometry of Catechol on TiO2 by a Combined Solid-State NMR and DFT Study, The Journal of Physical Chemistry C, 120 (2016) 23625-23630.

[87] S. Chakrabarti, B. Chaudhuri, S. Bhattacharjee, P. Das, B.K. Dutta, Degradation mechanism and kinetic model for photocatalytic oxidation of PVC-ZnO composite film in presence of a sensitizing dye and UV radiation, J Hazard Mater, 154 (2008) 230-236.

[88] D. Chatterjee, S. Dasgupta, N. N Rao, Visible light assisted photodegradation of halocarbons on the dye modified TiO2 surface using visible light, Solar Energy Materials and Solar Cells, 90 (2006) 1013-1020.

[89] Youngmin Cho, Wonyong Choi, Chung-Hak Lee, Taeghwan Hyeon, H.-I. Lee,

Visible Light-Induced Degradation of Carbon Tetrachloride on Dye-Sensitized TiO2, Environ. Sci. Technol., 35 (2001) 966–970.

[90] P. Chowdhury, J. Moreira, H. Gomaa, A.K. Ray, Visible-Solar-Light-Driven Photocatalytic Degradation of Phenol with Dye-Sensitized TiO2: Parametric and Kinetic Study, Industrial & Engineering Chemistry Research, 51 (2012) 4523-4532.

[91] Eunyoung Bae, W. Choi, Highly Enhanced Photoreductive Degradation of Perchlorinated Compounds on Dye-Sensitized Metal/TiO2 under Visible Light, Environ. Sci. Technol., 37 (2003) 147-152.

[92] E. Safaralizadeh, S.J. Darzi, A.R. Mahjoub, R. Abazari, Visible light-induced degradation of phenolic compounds by Sudan black dye sensitized TiO2 nanoparticles as an advanced photocatalytic material, Research on Chemical Intermediates, 43 (2016) 1197-1209.

[93] A. Gołąbiewska, A. Malankowska, M. Jarek, W. Lisowski, G. Nowaczyk, S. Jurga, A. Zaleska-Medynska, The effect of gold shape and size on the properties and visible light-induced photoactivity of Au-TiO2, Applied Catalysis B: Environmental, 196 (2016) 27-40.

[94] G. Sanzone, M. Zimbone, G. Cacciato, F. Ruffino, R. Carles, V. Privitera, M.G. Grimaldi, Ag/TiO2 nanocomposite for visible light-driven photocatalysis, Superlattices and Microstructures, 123 (2018) 394-402.

[95] Christoph Langhammer, Zhe Yuan, Igor Zorić, B. Kasemo, Plasmonic Properties of Supported Pt and Pd Nanostructures, Nano Lett., 6 (2006) 833-838.

[96] X. Zhang, Y.L. Chen, R.S. Liu, D.P. Tsai, Plasmonic photocatalysis, Rep Prog Phys, 76 (2013) 046401.

[97] C. Cai, S. Han, W. Caiyang, R. Zhong, Y. Tang, M.J. Lawrence, Q. Wang, L. Huang, Y. Liang, M. Gu, Tracing the Origin of Visible Light Enhanced Oxygen Evolution Reaction, Advanced Materials Interfaces, 6 (2019).

[98] M. Sachs, E. Pastor, A. Kafizas, J.R. Durrant, Evaluation of Surface State Mediated Charge Recombination in Anatase and Rutile TiO2, J Phys Chem Lett, 7 (2016) 3742-3746.

[99] J. Gao, J. Xue, S. Jia, Q. Shen, X. Zhang, H. Jia, X. Liu, Q. Li, Y. Wu, Self-Doping Surface Oxygen Vacancy-Induced Lattice Strains for Enhancing Visible Light-Driven Photocatalytic H2 Evolution over Black TiO2, ACS Appl Mater Interfaces, 13 (2021) 18758-18771.

[100] Y. Nam, L. Li, J.Y. Lee, O.V. Prezhdo, Strong Influence of Oxygen Vacancy Location on Charge Carrier Losses in Reduced TiO2 Nanoparticles, J Phys Chem Lett, 10 (2019) 2676-2683.

[101] Cristiana Di Valentin, Gianfranco Pacchioni, Annabella Selloni, Stefano Livraghi, E. Giamello, Characterization of Paramagnetic Species in N-Doped TiO2 Powders by EPR Spectroscopy

and DFT Calculations, J. Phys. Chem. B, 109 (2005) 11414–11419.

[102] Y. Yang, K. Ye, D. Cao, P. Gao, M. Qiu, L. Liu, P. Yang, Efficient Charge Separation from F(-) Selective Etching and Doping of Anatase-TiO2{001} for Enhanced Photocatalytic Hydrogen Production, ACS Appl Mater Interfaces, 10 (2018) 19633-19638.

[103] R. Katoh, A. Furube, K.-i. Yamanaka, T. Morikawa, Charge Separation and Trapping in N-Doped TiO2 Photocatalysts: A Time-Resolved Microwave Conductivity Study, The Journal of Physical Chemistry Letters, 1 (2010) 3261-3265.

[104] Z. Qin, L. Chen, R. Ma, R. Tomovska, X. Luo, X. Xie, T. Su, H. Ji, TiO2/BiYO3 composites for enhanced photocatalytic hydrogen production, Journal of Alloys and Compounds, 836 (2020).

[105] B. Lin, H. Li, H. An, W. Hao, J. Wei, Y. Dai, C. Ma, G. Yang, Preparation of 2D/2D g-C3N4 nanosheet@ZnIn2S4 nanoleaf heterojunctions with well-designed high-speed charge transfer nanochannels towards high-efficiency photocatalytic hydrogen evolution, Applied Catalysis B: Environmental, 220 (2018) 542-552.

[106] H. Heng, Q. Gan, P. Meng, X. Liu, The visible-light-driven type III heterojunction H3PW12O40/TiO2-In2S3: A photocatalysis composite with enhanced photocatalytic activity, Journal of Alloys and Compounds, 696 (2017) 51-59.

[107] A. Hiskia, A. Mylonas, E. Papaconstantinou, Comparison of the photoredox properties of polyoxometallates and semiconducting particles, Chemical Society Reviews, 30 (2001) 62-69.

[108] M. Xie, X. Dai, S. Meng, X. Fu, S. Chen, Selective oxidation of aromatic alcohols to corresponding aromatic aldehydes using In2S3 microsphere catalyst under visible light irradiation, Chemical Engineering Journal, 245 (2014) 107-116.

[109] J. Fu, S. Cao, J. Yu, Dual Z-scheme charge transfer in TiO2–Ag–Cu2O composite for enhanced photocatalytic hydrogen generation, Journal of Materiomics, 1 (2015) 124-133.

[110] J. Hu, L. Wang, P. Zhang, C. Liang, G. Shao, Construction of solid-state Z-scheme carbon-modified TiO2/WO3 nanofibers with enhanced photocatalytic hydrogen production, Journal of Power Sources, 328 (2016) 28-36.

[111] K. Xie, Q. Wu, Y. Wang, W. Guo, M. Wang, L. Sun, C. Lin, Electrochemical construction of Z-scheme type CdS–Ag–TiO2 nanotube arrays with enhanced photocatalytic activity, Electrochemistry Communications, 13 (2011) 1469-1472.

[112] F. Xu, W. Xiao, B. Cheng, J. Yu, Direct Z-scheme anatase/rutile bi-phase nanocomposite TiO 2 nanofiber photocatalyst with enhanced photocatalytic H 2 -production activity, International Journal of Hydrogen Energy, 39 (2014) 15394-15402.

[113] D. Zhou, Z. Chen, Q. Yang, X. Dong, J. Zhang, L. Qin, In-situ construction of all-solid-state Z-scheme g-C3N4/TiO2 nanotube arrays photocatalyst with enhanced visible-light-induced properties, Solar Energy Materials and Solar Cells, 157 (2016) 399-405.

[114] Hexing Li, Zhenfeng Bian, Jian Zhu, Yuning Huo, Hui Li, Y. Lu, Mesoporous Au/TiO2 Nanocomposites with Enhanced Photocatalytic Activity, J. Am. Chem. Soc., 129 (2007) 4538–4539.

[115] X.H. Li, M. Antonietti, Metal nanoparticles at mesoporous N-doped carbons and carbon nitrides: functional Mott-Schottky heterojunctions for catalysis, Chem Soc Rev, 42 (2013) 6593-6604.

[116] P. Wang, B. Huang, X. Qin, X. Zhang, Y. Dai, J. Wei, M.H. Whangbo, Ag@AgCl:

a highly efficient and stable photocatalyst active under visible light, Angew Chem Int Ed Engl, 47 (2008) 7931-7933.

[117] S.B. Nair, K.A. John, J.A. Joseph, S. Babu, V.K. Shinoj, S.K. Remillard, S. Shaji, R.R. Philip, Fabrication and Characterization of Type-II Heterostructure n:In2O3/p:in-TiO2 for Enhanced Photocatalytic Activity, physica status solidi (b), 258 (2020).

Section 2. Fe(III)-Pt(II) Oxide-Co-Sensitized Brookite TiO_2 Nanorods for Photocatalytic Degradation of Acetaldehyde under Visible Light

Abstract

Platinum is widely investigated as co-catalysts for photocatalytic degradation of volatile organic compounds but studies seldom focus on their visible light sensitizing properties. Herein, Pt sensitizers of different oxidation states (0, II, IV) were modified on brookite TiO_2 nanorods and investigated for acetaldehyde degradation under visible light. Pt(II) oxide/TiO_2 showed the best photocatalytic activity but its stability was compromised by its self-oxidation to Pt(IV) during photo-oxidation reaction. Surface modification of an Fe(III) oxide thin film sensitizer layer around the Pt(II) oxide sensitizer was found to enhance both the stability and activity of Pt(II) oxide/TiO_2. *In situ* double beam photoacoustic spectroscopy (DB-PAS) supported by DFT modelling showed the rapid injection of photoexcited electrons from Fe(III) oxide to Pt(II) oxide promote the stability of Pt(II) oxide, leading to enhanced performance. The findings provide guidance for the rational design of visible light-active metal oxide sensitizers for oxidative removal of indoor air pollutants.

Keywords

TiO_2, indoor VOCs degradation, visible light sensitizers, Pt sensitizers, Fe sensitizers

2.1 Introduction

In our contemporary society, people spend on average 80% of their time indoors. Indoor air quality has therefore become an important issue for human health.[1] Volatile organic compounds (VOCs) are notable indoor air pollutants as well as other compounds such as NO_x, SO_2, ozone and particulate matters.[2-5] Indoor VOCs such as aldehydes, amines and aromatic compounds can be emitted from indoor sources and activities including cooking, secondhand smoke, cleaning, consumer products, home furnishings and building materials. Moreover, in

recent years, indoor air pollutants have been increasingly associated with sick building syndrome (SBS).[6-9]

Photocatalytic systems that can decompose VOCs to CO_2 are promising methods for removing indoor VOCs. Photocatalytic degradation of VOCs with various materials such as TiO_2, C_3N_4, WO_3, SnO_2 and $BiVO_4$ has been demonstrated.[10-13] Although photocatalytic systems can remove VOCs by photooxidative destruction, the removal efficiency is very low under normal indoor light conditions due to the lack of adequate energetic photons. The development of photo-conversion materials that can utilize visible light photons at the maximum capacity should enable effective removal of indoor air pollutants under indoor light conditions.

Metallic Pt (i.e., Pt(0)) is widely used as a cocatalyst for various photocatalytic reactions including hydrogen evolution reaction and NO_x and CO_2 reduction reaction owing to its ability to promote interfacial charge separation as well as its favorable catalytic properties.[14-16] Recently, Pt in its 2+ and 4+ oxidation state, (Pt(II) and Pt(IV)), respectively, have also been reported to be visible light active catalysts (or sensitizers) for NO_x oxidation[17, 18], organic compounds degradation[19, 20] and hydrogen evolution reaction.[21] However, it is unclear if Pt in its metallic form or oxide form is the most active form of visible light sensitizer for photocatalytic degradation of VOCs.

TiO_2 is a non-toxic and relatively cheap photoconversion material. TiO_2 exists in three crystalline structures: anatase, rutile and brookite phases. Most photocatalytic studies have focused on the anatase and rutile phases of TiO_2 due to their relatively high thermal stability and ease of preparation.[22, 23] Although brookite TiO_2 is not as commonly used as that of anatase or rutile TiO_2 owing to its metastability, brookite TiO_2 has shown high photocatalytic activities for the degradation of various recalcitrant pollutants.[24, 25] W.-K. Li et al. found the exposed {210} facet of brookite TiO_2 is more reactive than the {101} facet of

anatase TiO_2, which is thus beneficial for improving photocatalytic reactions.[26] Brookite TiO_2 also showed higher surface affinity for O_2 adsorption than anatase TiO_2 in oxygen reduction reaction to produce H_2O_2.[27] Moreover, brookite TiO_2 was demonstrated to oxidize propanone to CO_2 and H_2O much faster than anatase TiO_2. Brookite TiO_2 also exhibited higher areal photocatalytic activity for RhB degradation than rutile TiO_2 and anatase TiO_2.[28, 29] These observations suggest brookite TiO_2 is a promising photoconversion material for solving environmental issues.

In this study, brookite TiO_2 nanorods with well-defined {210} and {111} facets were synthesized by a hydrothermal process utilizing TALH and urea as precursors. Acetaldehyde was used as a representative indoor VOC. Pt(0) metal sensitizer and Pt(II) and Pt(IV) oxide sensitizers were incorporated on the surfaces of the brookite TiO_2 nanorods by a photodeposition method or a chemisorption method.

Our results show Pt(II) oxide-sensitized brookite TiO_2 (Pt(II)/TiO_2) exhibits higher photocatalytic activity than that of Pt(0)/TiO_2 or Pt(IV) oxide/TiO_2 for acetaldehyde degradation under visible light. However, the photocatalytic activity of Pt(II)/TiO_2 is hindered by the low stability of Pt(II) oxide, which readily oxidizes to Pt(IV) oxide with increased reaction time. We then developed strategies to overcome the stability issues of a Pt(II) oxide sensitizer. We found a simultaneous photodeposition of Pt(IV) ions and Fe(II) cations onto brookite TiO_2 nanorods resulted in selective formation of island-like PtO and $Pt(OH)_2$ nanoclusters on the {210} facet of brookite TiO_2 nanorods with a film-like Fe(III) oxide layer covering the entire surface of the Pt(II)/TiO_2 nanorods. The Fe(III) oxide thin film layer not only serves as a protective layer preventing Pt(II) oxide from ambient oxidation but also acts as a visible light sensitizer. The Fe(III)/Pt(II)-oxide-co-sensitized brookite TiO_2 nanorods (Fe(III)-Pt(II)/TiO_2) show dramatic enhancements in both activity and stability for acetaldehyde

degradation under visible light illumination. The electron transfer mechanisms leading to the enhanced photocatalytic performance were unraveled by *in situ* double beam photoacoustic spectroscopy (DB-PAS), XPS and UV-Vis spectroscopy and supported by density functional theorem (DFT) computational modeling.

2.2 Experiment

2.2.1 Preparation of pure brookite TiO_2

Pure brookite TiO_2 nanorods were prepared by hydrothermal reaction according to a previously reported method.[30, 31] First, 21.02 g of urea (Wako, Guaranteed Reagent, min. 99.0%) and 5 ml of titanium (IV) bis (ammonium lactate) dihydroxide (TALH) (Sigma Aldrich, ~50wt% in H_2O) were mixed and stirred in 45 ml of Mill-q water for 2 h. The solution was then transferred into a Teflon-lined hydrothermal reactor. Hydrothermal reaction was performed at 200 ℃ for 48 h. The resultant powder and supernatant were separated by centrifugation and washed with Mill-q water until the ionic conductivity of the supernatant was lower than 10 μS cm^{-1}. Finally, the TiO_2 powder was dried in a vacuum oven at 60ºC.

2.2.2 Preparation of Fe(III)-sensitized brookite TiO_2

0.3 g of brookite TiO_2 powder and the required amount of iron(III) nitrate nonahydrate (Wako, 99.9%) were mixed and stirred in 80 ml of Milli-q water with addition of 20 ml of ethanol (Wako, Extra Pure, 95%). After nitrogen bubbling for 1 h, photodeposition was carried out under a mercury lamp (Ushio, SX-UI501UO) for 6 h. The light intensity was 1.0 mW cm^{-2}. The resultant powder and supernatant were separated by filtration and washed with Mill-q water until the ionic conductivity of the supernatant was lower than 10 μS cm^{-1}. The resultant powder was dried in a vacuum oven at 25ºC.

2.2.3 Preparation of Pt(0)-sensitized brookite TiO_2

0.3 g of brookite TiO_2, the required amount of chloroplatinic acid hexahydrate (Wako, 99.9%) and 20 ml of ethanol (Wako, Extra Pure, 95%) were mixed and stirred in 80 ml of Milli-q water. After nitrogen bubbling for 1 h, photoirradiation was carried out under a mercury lamp (Ushio, SX-UI501UO) for 6 h. The light intensity was 100 mW cm^{-2}. The resultant powder and supernatant were separated by filtration and washed with Milli-q water until the ionic conductivity of the supernatant was lower than 10 μS cm^{-1}. The resultant powder was dried in a vacuum oven at 25°C.

2.2.4 Preparation of Pt(IV) or Pt(II)-sensitized brookite TiO_2

0.3 g of brookite TiO_2 and the required amount of chloroplatinic acid hexahydrate (Wako, 99.9%) or potassium tetrachloroplatinate(II) (Sigma Aldrich, >99.9% trace metal basis) were mixed and stirred in 100 ml of Milli-q water. Then nitrogen bubbling was performed for 1 h for removing oxygen in the environment. Subsequently, the mixed solution was continuously stirred for 5 h under dark conditions. The resultant powder and supernatant were separated by filtration and washed with Mill-q water until the ionic conductivity of the supernatant was lower than 10 μS cm^{-1}. The resultant powder was dried in a vacuum oven at 25°C.

2.2.5 Preparation of Fe(III)-Pt(II)-co-sensitized brookite TiO_2

The preparation scheme for Fe(III)-Pt(II)-co-sensitized brookite TiO_2 is presented in Scheme 1. First, 0.3 g of brookite TiO_2 powder and the required amount of chloroplatinic acid (Wako, 99.9%) (equivalent to 0.4wt%Pt in the final product) were mixed and stirred in 100 ml of Milli-q water with constant nitrogen bubbling for 1 h. The resulting powder-suspension was then photo-irradiated under a mercury lamp (Ushio, SX-UI501UO) for 45 min. Upon photo-irradiation, the required amount of ferrous sulfate heptahydrate (Sigma Aldrich, reagent grade, 99.5%) that was pre-dissolved in Milli-q water (equivalent to a nominal loading of 0.4wt%Fe(II)) was injected into the flask. The light intensity was 100 mW cm^{-2}. Subsequently, the resultant powder and supernatant were separated by filtration and washed with Mill-q

water until the ionic conductivity of the supernatant was lower than 10 μS cm^{-1}. The resultant powder was then dried in vacuum oven at 25°C.

2.2.6 Characterization

The crystal structure of the produced materials was analyzed by X-ray diffraction (Rigaku, MiniFlex II). Transmission electron microsocopy (TEM) was conducted using a Hitachi H-9000NAR at an accelerating voltage of 200 kV. Specific surface areas of the samples were determined by Quantachrome Nova 4200e surface area measurement. Inductively coupled plasma optical emission spectroscopy (ICP-OES; Shimadzu, ICPS-8000) was used to determine the concentrations of Fe or Pt cations loaded on TiO_2. UV-Vis diffuse reflectance spectra were obtained by a UV-2500PC (Shimadzu) equipped with an integrating sphere unit. X-ray photoelectron spectra (XPS) of as-prepared samples were obtained by a Thermo ESCALAB 250Xi system at room temperature using Al Kα with monochromatic radiation. Raman measurements were conducted using a NRS-5100 Laser Raman Spectrometer with Ar-ion laser excitation at a wavelength of 523.5 nm.

2.2.7 Photocatalytic activity tests

Photocatalytic activities of as-prepared pure TiO_2 samples and metal-loaded TiO_2 samples were evaluated by photocatalytic decomposition of acetaldehyde under visible light photoirradiation. First, 250 mg of TiO_2 powder was spread on a glass dish with a diameter of 3.4 cm. The glass dish was put into a Tedlar bag and degassed. Then 125 cm^{-3} of standard gas that contained 79% N_2, 21% O_2, <0.01 ppm of CO_2 and 500 ppm acetaldehyde was injected into the Tedlar bag. The photocatalyst was left in the dark for 1 h to achieve an absorption equilibrium. Then a light-emitting diode (LED) was turned on for the required amount of time. The wavelength of the LED light was 455 nm, and the light intensity was 1.0 mW cm^{-2}. Gas chromatography (Shimadzu, GC-8A, FID detector) was used to estimate the concentrations of acetaldehyde and CO_2 per hour.

2.2.9 Double-beam photoacoustic spectroscopic (DB-PAS) measurement

A gas-exchangeable photoacoustic (PA) cell equipped with two valves for gas flow was used and a sample was placed in the cell. The atmosphere was controlled by a flow of artificial air containing 2-propanol vapor (air+2-PrOH) or artificial air. The measurements were conducted after shutting off the valves, i.e., in a closed system at room temperature. An LED emitting light at ca. 940 nm (OSRAM, SFH4751) was used as a probe light for detection of electron accumulation, and the output intensity was modulated at 40 Hz. In addition to the modulated light, a blue-LED (OptoSupply, OSB5XNE3C1S, emitting light at ca. 470 nm) was also used as simultaneous continuous irradiation for photoexcitation. The PA signal acquired by a MEMS microphone (INMP401, TDK InvenSense) buried in the cell was amplified and monitored by a digital lock-in amplifier (LI5640, NF). Detailed setups of DB-PAS measurements have been reported previously. [32]

2.2.10 DFT calculations

First principle DFT calculations were performed by Vienna Ab initio Simulation Package (VASP) [33] with the projector augmented wave (PAW) method. [34] The exchange-functional was treated using the generalized gradient approximation (GGA) of the Perdew-Burke-Emzerhof (PBE) functional. [35] The energy cutoff for the plane wave basis expansion was set to 450 eV and the force on each atom of less than 0.03 eV/Å was set for the convergence criterion of geometry relaxation. Grimme's DFT-D3 methodology was used to describe the dispersion interactions. [36] Partial occupancies of the Kohn−Sham orbitals were allowed using the Gaussian smearing method and a width of 0.05 eV. The Brillourin zone was sampled with Monkhorst mesh 3× 3 × 1 through all the computational process. The self-consistent calculations applied a convergence energy threshold of 10^{-5} eV. A 15 Å vacuum space along the z direction was added to avoid the interaction between two neighboring images. The

DFT + U correction for strong-correlation 3d electrons of transition metal was taken into account, and the U-J value of 4.0 for Ti was used. [37]

2.2.11 Apparent Quantum Efficiency (AQE) calculations:[38, 39]

$$\mathbf{AQE} = \frac{\mathbf{X}\mathbf{n}N_A}{tN_p} \times 100\% \quad \mathbf{(1)}$$

$$\frac{1}{2}CH_3CHO \rightarrow CO_2 + 2H_2O + 5e^- \quad \mathbf{(2)}$$

$$\mathbf{n} = V \times \Phi_i \div V_m \quad \mathbf{(3)}$$

$$N_p = \frac{\lambda WS}{hc} \quad \mathbf{(4)}$$

The apparent quantum efficiency, AQE, is gotten by calculating the ratio of the number of electrons transferred in the reaction to the actual number of incident photons. The number of electrons transferred in the reaction is equal to XnN_A. The actual number of incident photons is equal to tN_p. Where, n is the number of CO_2 molecules, N_A is the Avogadro's constant (6.02×10^{-23}). V is the total volume of the gas, which is 125mL. Φ_i is volume fraction of CO_2 (ppm). V_m is molar volume of gas (22.4 L/mol). X is the number of electrons require to produce one molecule of CO_2, for acetaldehyde degradation, X = 5,[40] N_p is the number of incident photons, t is the reaction time (s). λ is wavelength of light, W is intensity of the monochromatic light (W/m^2), S is irradiation area, in this work, S = 9.07×10^{-4} m^2, h is Planck constant (6.63×10^{-34}), c is speed of light in vacuum (3×10^8 m/s), Equation (2) shows the equation for photocatalytic degradation of acetaldehyde to generate CO_2 and water.

2.3 Results and Discussion

2.3.1 Surface and Structural Properties

Scheme 1 shows the material flowchart leading to the synthesis of metallic Pt-sensitized brookite TiO_2 nanorods (Pt(0)/TiO_2), Pt(II)-sensitized brookite TiO_2 nanorods

(Pt(II)/TiO_2) and Pt(IV)-sensitized brookite TiO_2 nanorods (Pt(VI)/TiO_2). In brief, Pt(0)/TiO_2 is prepared by photodeposition of Pt^{4+} ions onto TiO_2 nanorod surfaces using an aqueous solution containing chloroplatinic acid ($H_2Pt(IV)Cl_6$) and ethanol as the hole scavenger. Pt(II) and Pt(IV)-sensitized TiO_2 are synthesized by chemisorption of Pt(II) and Pt(IV) ions under dark conditions from an aqueous solution of potassium tetrachloroplatinate ($K_2Pt(II)Cl_4$) or $H_2Pt(IV)Cl_6$.

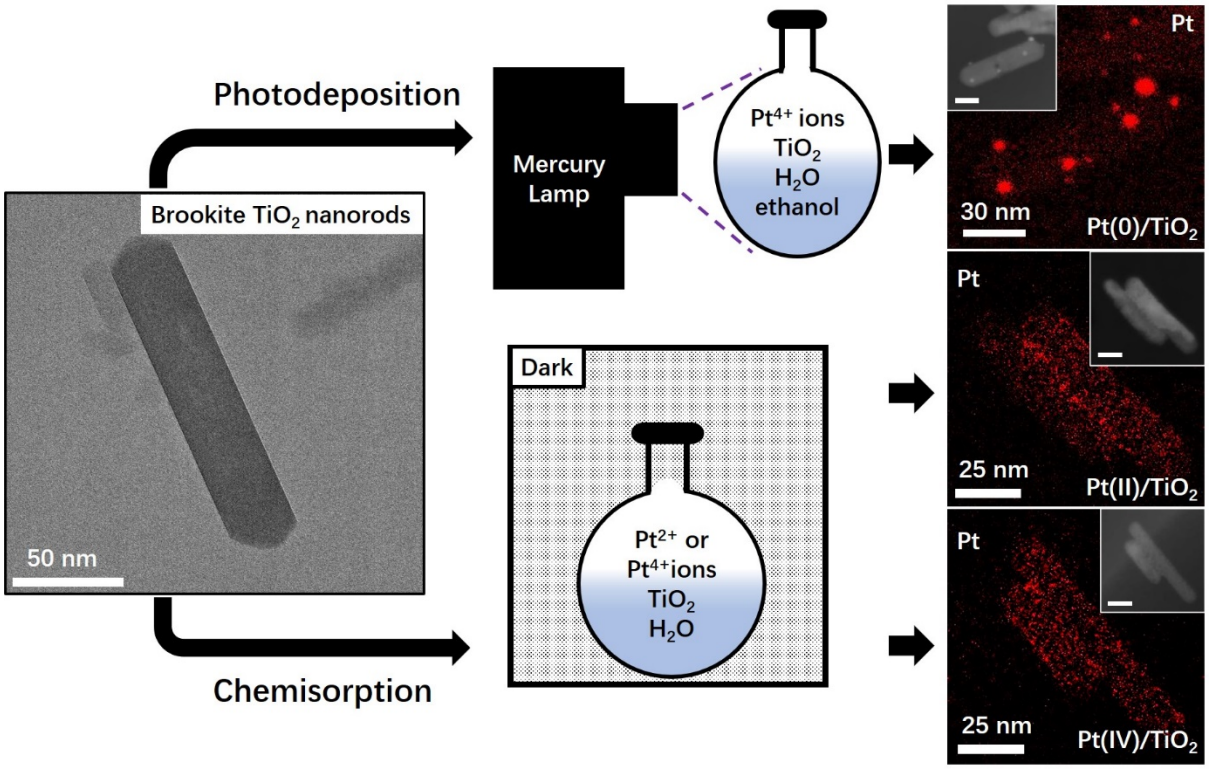

Scheme 1. A material flowchart showing the synthesis of metallic Pt-sensitized brookite TiO_2 nanorods (Pt(0)/TiO_2) by a photo-deposition method and, Pt(II) oxide-sensitized brookite TiO_2 nanorods (Pt(II)/TiO_2) and Pt(IV) oxide-sensitized brookite TiO_2 nanorods (Pt(VI)/TiO_2) by a chemisorption method. Scale bar in inset for Pt(0)/TiO_2 represents 30 nm and 25 nm for Pt(II)/TiO_2 and Pt(IV)/TiO_2. The Pt TEM-EDX spectrum and HRTEM image (inset) of a Pt(0)/TiO_2 sample showed the metallic Pt exists as small Pt nanoparticles with diameters in the range of 2-10 nm on the surfaces of the brookite TiO_2 nanorods. On the other hand, for Pt(II)/TiO_2 and Pt(IV)/TiO_2 samples, the entire surfaces of the brookite TiO_2 nanorods were uniformly coated with a thin film layer of Pt(II) oxides or Pt(IV) oxides.

Fig. 2-1 shows the high-resolution transmission electron microscopy (HRTEM) images and a selected area electron diffraction (SAED) pattern of a pure brookite TiO_2 nanorod sample. The HRTEM images (Fig. 2-1c) show the brookite TiO_2 rods have a prismatic morphology with tapered ends and smooth surfaces. The length and width of the brookite TiO_2 nanorods are ~150.0 nm and 26.7 nm, respectively. In addition, the lattice plane imaging (Fig. 2-1c) shows the brookite TiO_2 nanorods possess a well-defined {210} body facet and a {111} tapered end facet. [41, 42] Moreover, the single bright spots of an SAED pattern of a brookite TiO_2 nanorod, as shown in Fig. 2-1d, indicate the brookite TiO_2 nanorods are single crystalline brookite TiO_2. Fig. 2-2 shows the XRD spectra of the as-prepared brookite TiO_2 sample. The XRD spectra show only diffraction peaks of brookite phase TiO_2 (JCPDS NO. 29-1360). No diffraction peak associated with other phase (anatase or rutile phase) of TiO_2 was observed, indicating the as-prepared TiO_2 are pure brookite-phase TiO_2[43]. The high purity of the as-prepared brookite TiO_2 was also collaborated by a Raman spectrum, as shown in Fig. 2-3.[44]

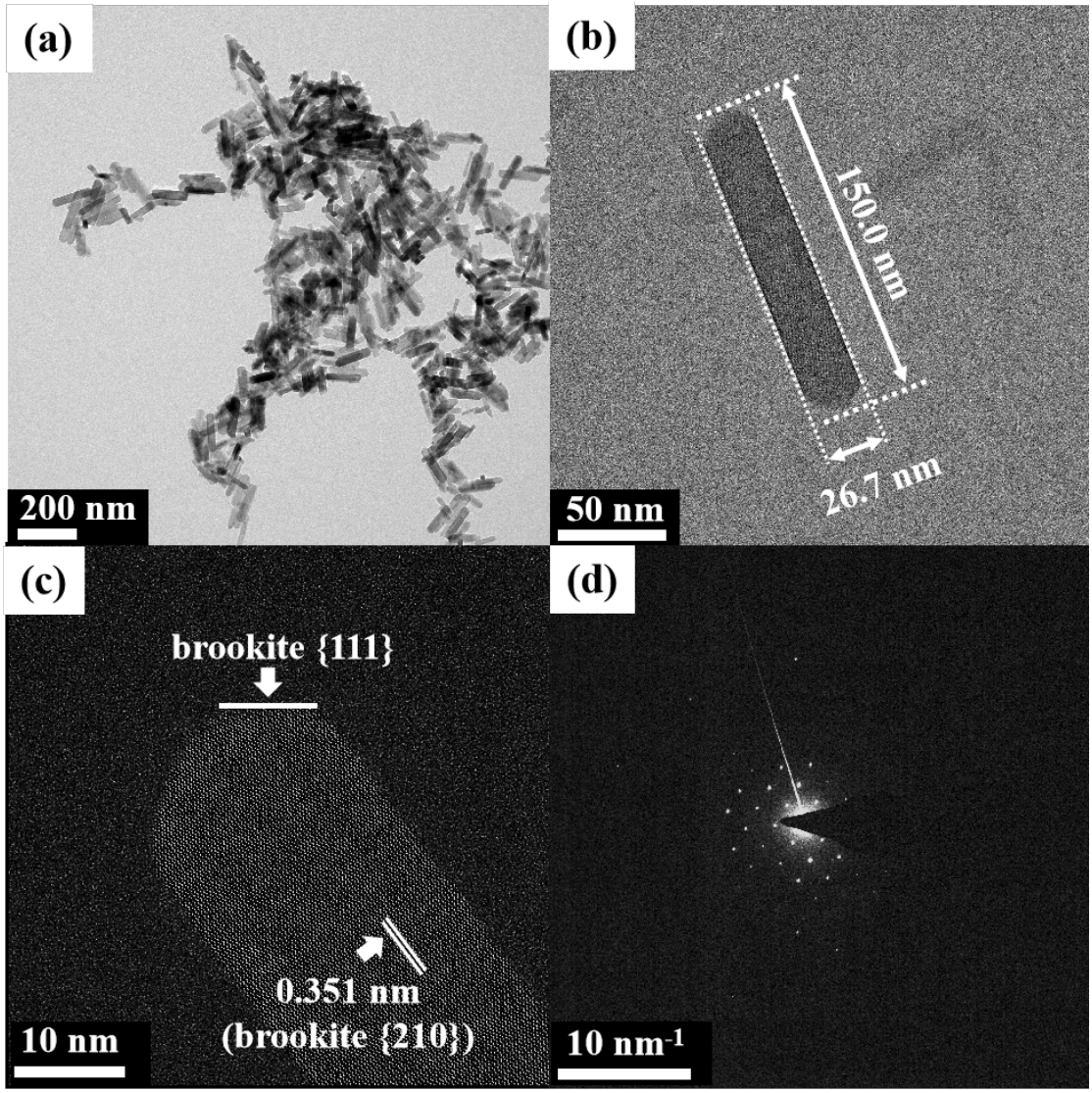

Fig. 2-1(a-c) HRTEM images and (d) SAED pattern of as-prepared brookite TiO_2 samples.

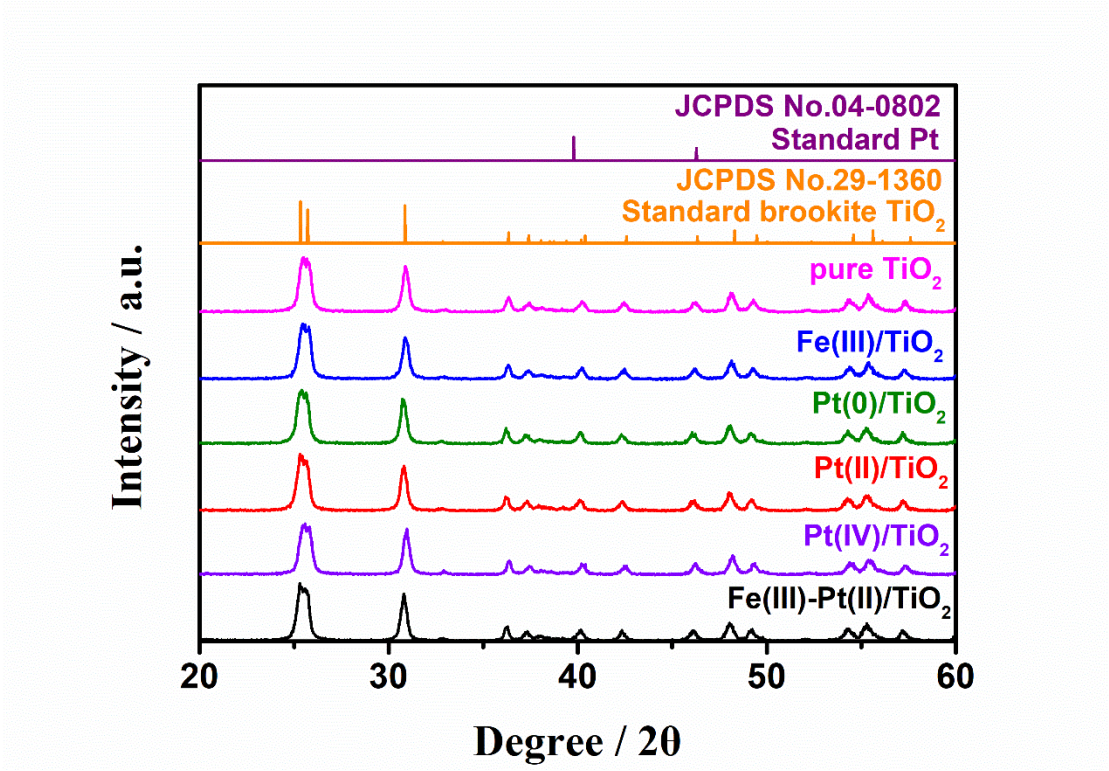

Fig. 2-2 XRD patterns of as-prepared brookite TiO_2, Pt(0)/TiO_2, Fe(III)/TiO_2, Pt(II)/TiO_2 and Fe(III)-Pt(II)/TiO_2 photocatalysts.

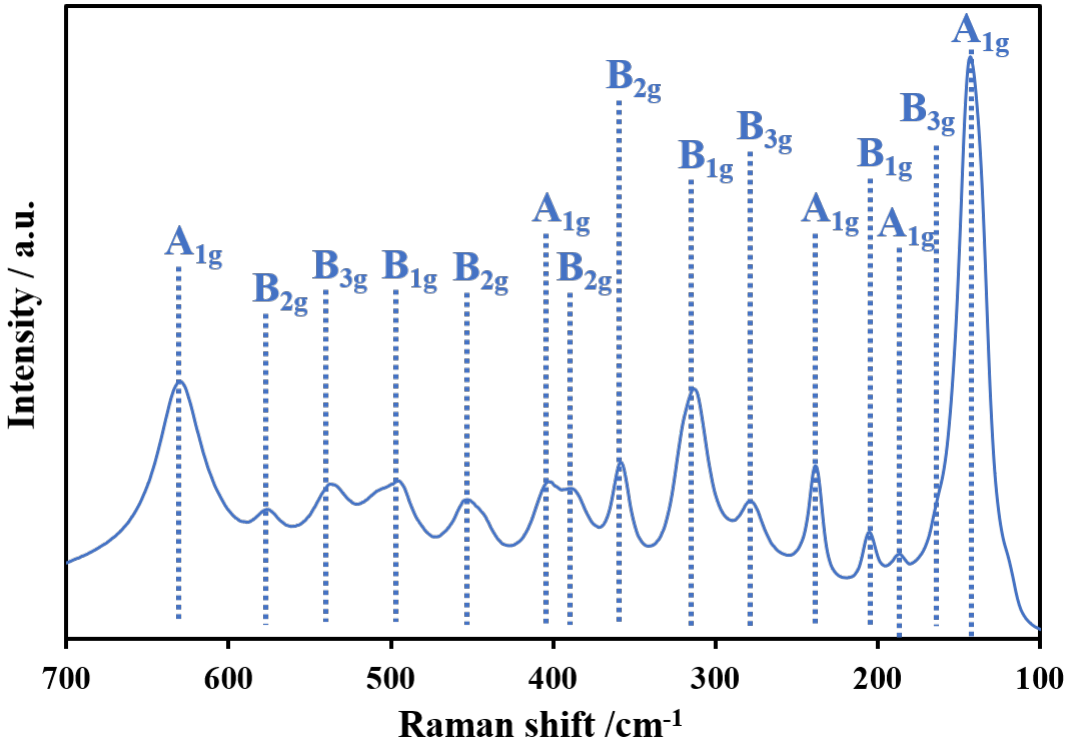

Fig. 2-3 Raman spectrum of as-prepared brookite TiO_2 nanorods.

Fig. 2-4 a-c show the Pt 4f XPS spectra for Pt(0)/TiO_2, Pt(II)/TiO_2 and Pt(IV)/TiO_2 samples. The XPS results show the photodeposition of Pt^{4+} ions onto the TiO_2 nanorod surfaces in an ethanol-containing aqueous solution resulted in the deposition of metallic Pt (or Pt(0)) on the brookite TiO_2 nanorod surface with a small proportion of PtO (or Pt(II)). The surface concentrations of Pt(0) and PtO were determined from the XPS spectrum to be 83.5% and 16.5%, respectively. In the Pt(II)/TiO_2 sample, Pt XPS spectrum indicate the presence of four types of Pt species on the TiO_2 nanorod surfaces: PtO, $[Pt(II)Cl_4]^{2-}$ (abbreviated as Pt(II)-Cl), PtO_2 and $[Pt(IV)Cl_6]^{2-}$ (abbreviated as Pt(IV)-Cl).[45] From the XPS spectrum, the surface concentrations of PtO, Pt(II)-Cl, PtO_2 and Pt(IV)-Cl were determined to be 39.7%, 23.3%, 10.0% and 27.1%, respectively. In the Pt(IV)/TiO_2 sample, the chemisorption of $[Pt(IV)Cl_6]^{2-}$ on the TiO_2 nanorod surfaces formed high concentration of PtO_2 (~79.4%) and some Pt(IV)-Cl (~20.6%). The chemisorption of $[Pt(II)Cl_4]^{2-}$ or $[Pt(IV)Cl_6]^{2-}$ onto TiO_2 nanoparticle surfaces is known to lead to the formation of covalently bounded surface complex.[46-48] Chloride substitution by surface [Ti]-O^- is feasible, and in addition, very stable Ti–O–Pt bonds can be formed under ambient conditions.[48] Hence, PtO and PtO_2 are the associated chemisorbed products in the Pt(II)/TiO_2 sample while PtO_2 is a chemisorbed product in the Pt(IV)/TiO_2 sample.

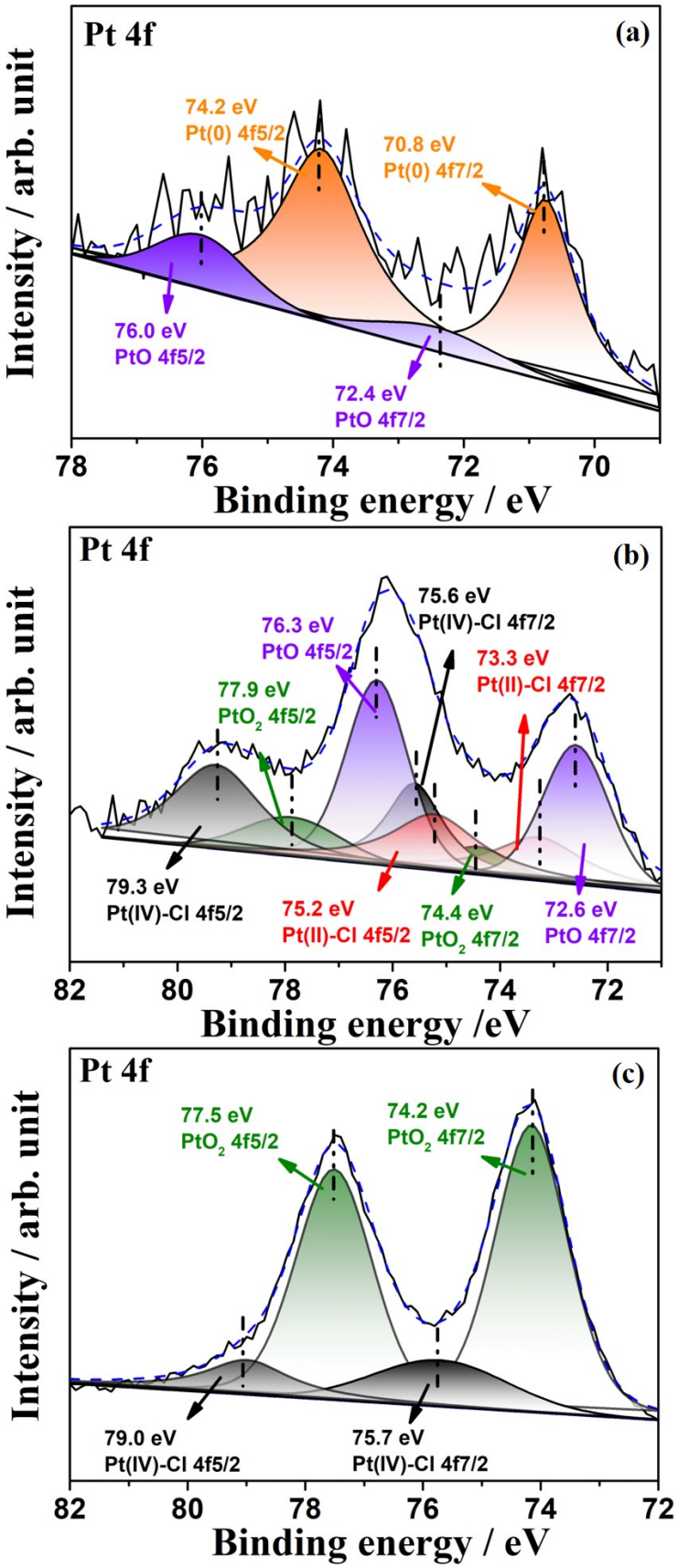

Fig. 2-4 Pt 4f XPS spectrum of (a) Pt(0)/TiO_2, (b) Pt(II)/TiO_2, and (c) Pt(IV)/TiO_2

Fig. 2-5, 2-6 and 2-7 shows the HRTEM images and EDX elemental mapping of Pt(0)/TiO_2, Pt(II)/TiO_2 and Pt(IV)/TiO_2 samples, respectively. The HRTEM image of Pt(0)/TiO_2 revealed the metallic Pt exists as small Pt nanoparticles with diameters in the range of 2-10 nm on the surfaces of the brookite TiO_2 nanorods. On the other hand, for the Pt(II)/TiO_2 and Pt(IV)/TiO_2 samples, the entire surfaces of the brookite TiO_2 nanorods were uniformly coated with a thin film layer of Pt(II) oxides or Pt(IV) oxides.

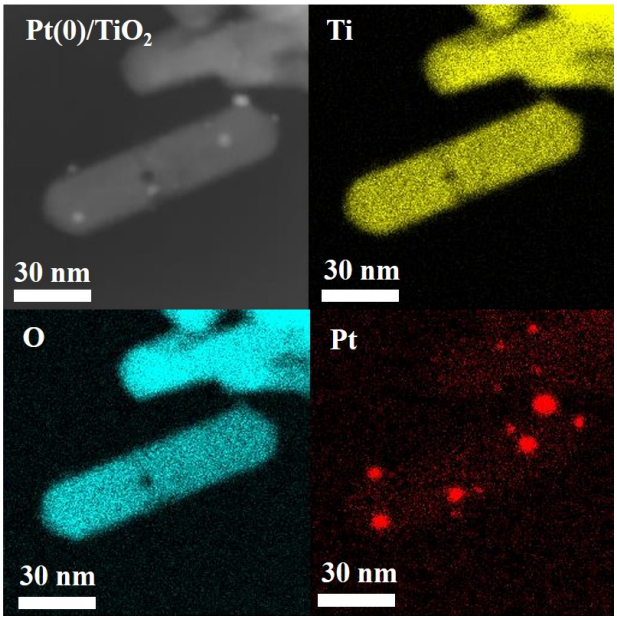

Fig. 2-5 HRTEM image and EDX elemental mapping of a Pt(0)/TiO_2 sample.

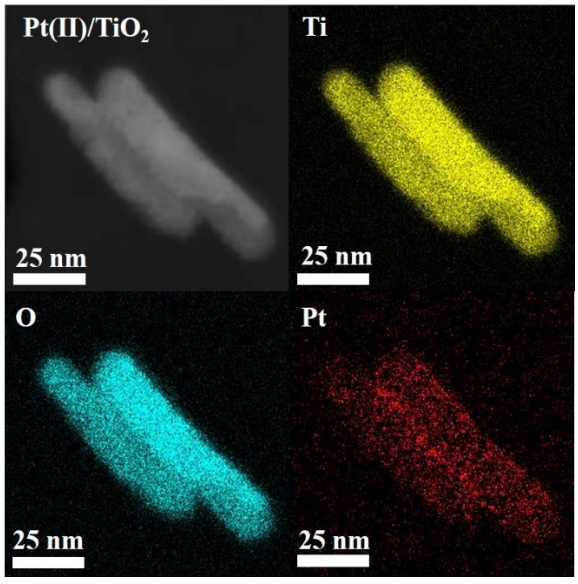

Fig. 2-6 HRTEM image and EDX elemental mapping of a Pt(II)/TiO_2 sample.

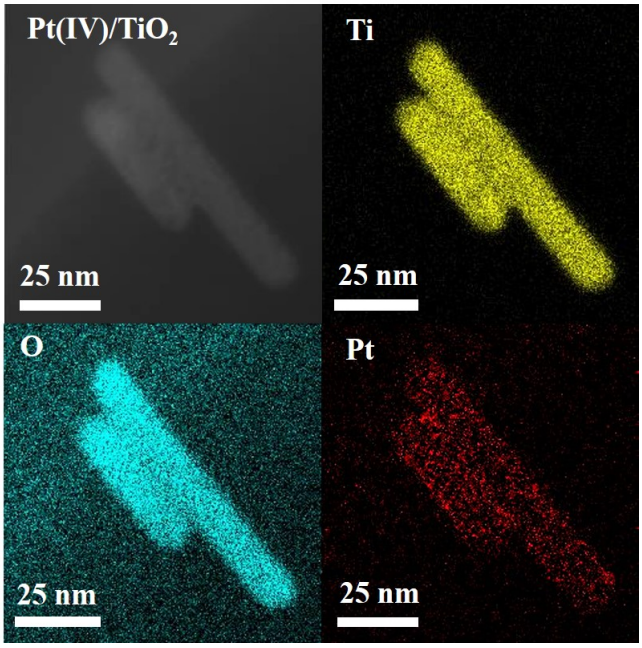

Fig. 2-7 HRTEM image and EDX elemental mapping of a Pt(IV)/TiO_2 sample.

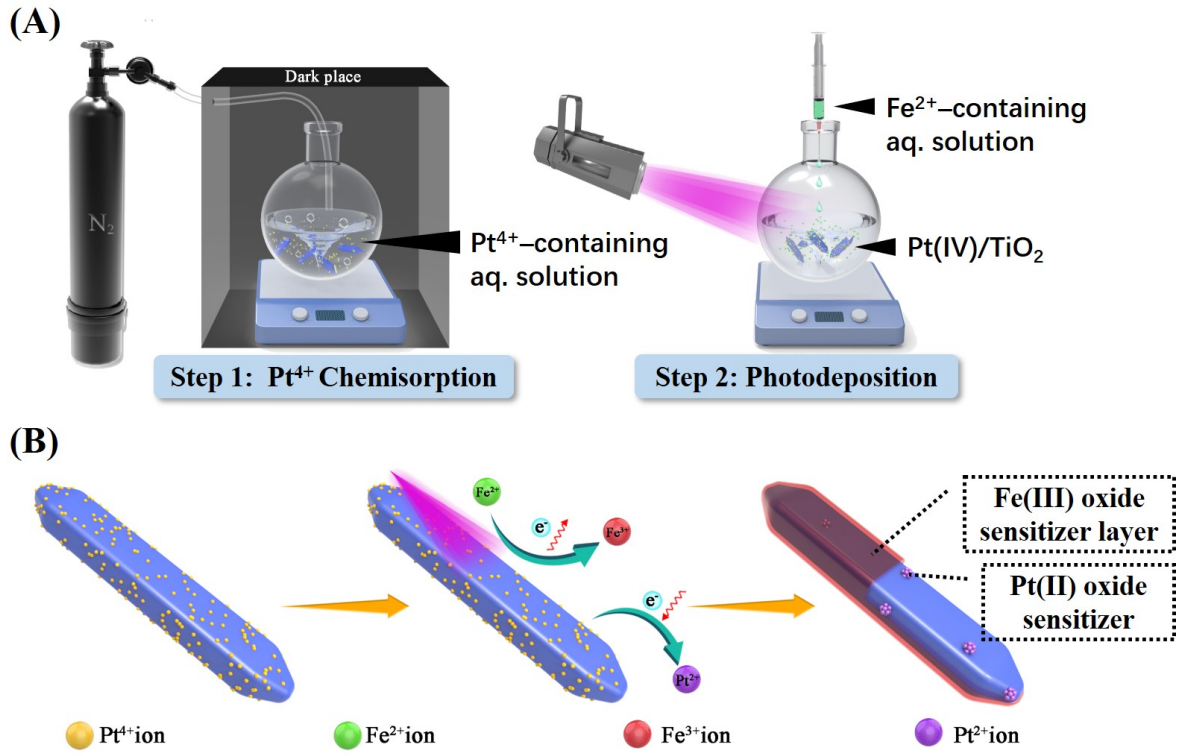

Scheme 2. (A) The preparation steps of Fe(III)-Pt(II)-oxide-co-sensitized brookite TiO_2 nanorods (Fe(II)-Pt(II)/TiO_2). Pt^{4+} cations were first chemisorbed onto the brookite TiO_2 nanorods under dark conditions and anoxic conditions. Subsequently, an aqueous

solution of Fe(II) sulfate was injected into the Pt^{4+}-containing solution upon light-irradiation and the co-photodeposition of Pt^{4+} and Fe^{2+} cations onto the brookite TiO_2 nanorods occurred to form Fe(III)-Pt(II)/TiO_2 nanorods. **(B)** Proposed formation mechanism of Fe(III)-Pt(II)/TiO_2 nanorods. The chemisorbed Pt^{4+} cations on the TiO_2 nanorod surfaces were reduced by the photogenerated electrons of TiO_2 to form Pt(II) oxide nanoparticles on the brookite TiO_2 nanorod surfaces. Owing to the low surface affinity of the brookite TiO_2 nanorods for Fe(II) cations, the brookite TiO_2 nanorod surfaces contained low concentration of surface-adsorbed Fe(II) cations, which were subsequently oxidized by the photogenerated holes of TiO_2 to form a very thin layer of the Fe(III) oxide sensitizer over the entire surfaces of the Pt(II) oxide-sensitized TiO_2 nanorods.

Scheme 2A shows the preparation steps of the Fe(II)-Pt(II)/TiO_2 samples. The brookite TiO_2 nanorods were initially dispersed and stirred in an aqueous solution containing only $[Pt(IV)Cl_6]^{2-}$ with nitrogen bubbling and sonication. Subsequently, UV photo-irradiation was provided while an aqueous Fe(II) sulfate solution was simultaneously injected into the Pt(IV)/TiO_2 powder-suspension to initiate the co-deposition of Pt and Fe sensitizers onto the TiO_2 nanorods.

Fig. 2-8 A-D show the XPS spectra of the Fe(III)-Pt(II)/TiO_2 sample. The Pt 4f XPS spectrum in Fig. 2-8D shows the presences of PtO (65.3%), Pt(II)-Cl (~18.1%) and PtO_2 (~16.6%). XPS peaks associated with Pt(IV)-Cl were not detected on the nanorod surfaces implying the $[Pt(IV)Cl_6]^{2-}$ on the TiO_2 surfaces had been photo-reduced to PtO and Pt(II)-Cl. The PtO_2 was likely formed from the subsequent oxidation of the PtO in ambient environment. The Fe 2p XPS spectrum in Fig. 2-8C indicates the presence of Fe oxide sensitizers with an oxidation state of +3 on the TiO_2 nanorod surface. The Fe(III) 2p3/2 at band energies of 710.0 eV and 712.2eV can be associated with nano-sized Fe_2O_3[49]and γ-FeOOH[50], respectively, suggesting that Fe(II) cations was oxidized to Fe(III) oxide nanoparticles by the photogenerated holes during the photodeposition process. Fe_2O_3 was the predominant species formed on the surface of

the brookite TiO_2 nanorods with a small amount of γ-FeOOH. In addition, the formation of Fe_2O_3 and γ-FeOOH on the brookite TiO_2 nanorod surfaces can be further observed in an Fe 2p XPS spectrum when the photodeposition of the Fe(II) cations was conducted at higher precursor loading of 10wt% Fe(II), as shown in Fig. 2-9. At higher loading of Fe(III) oxides, the Fe_2O_3 and γ-FeOOH exhibit surface properties resembling that of Fe_2O_3 and γ-FeOOH bulk materials, as indicated by the Fe(III) 2p3/2 bands at higher binding energies of 710.7 eV and 712.1 eV, respectively.[51]

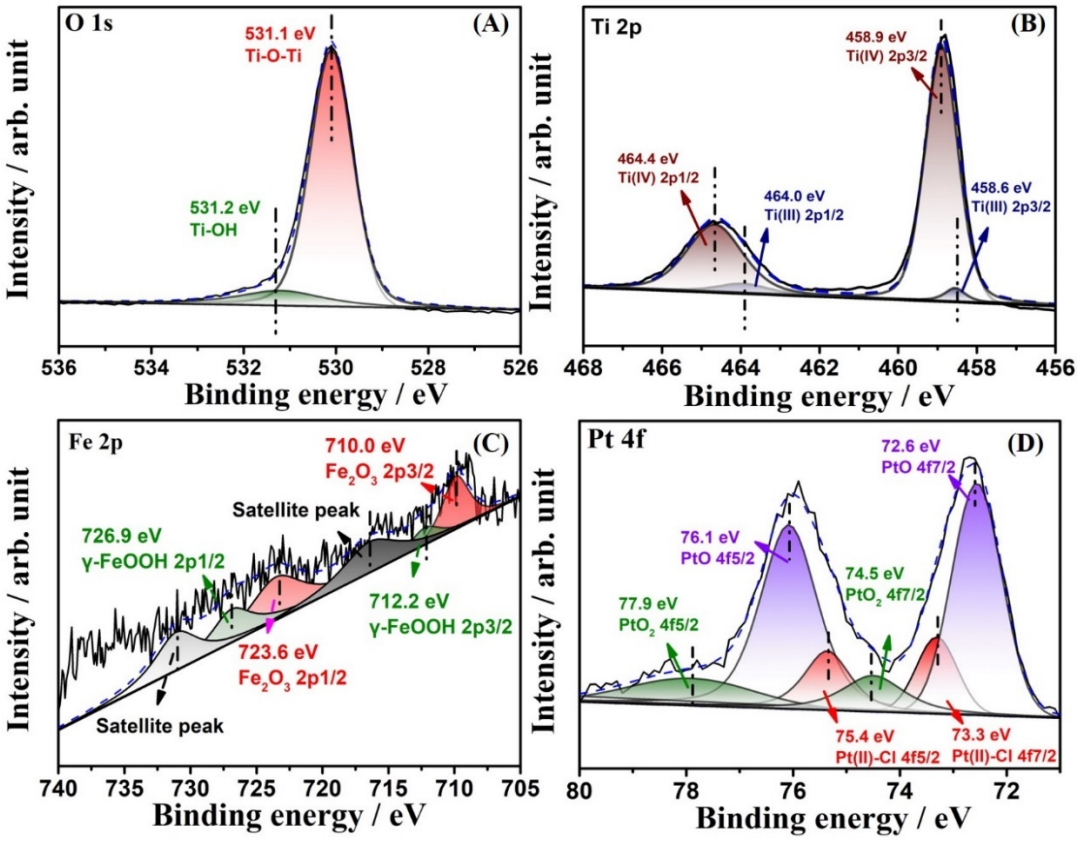

Fig. 2-8 XPS spectra of Fe(III)-Pt(II)/TiO_2 (a) O 1s, (b) Ti 2p, (c) Fe 2p and (d) Pt 4f region.

Overall, the XPS results show the photodeposition of $[Pt(IV)Cl_6]^{2-}$ on the brookite TiO_2 nanorod surfaces in the presence of Fe(II) cations led to the co-formation of Fe(III) oxide sensitizers and Pt(II)/(IV) sensitizers. In addition, it can be observed the concentration of Pt(II) sensitizers in the Fe(III)-Pt(II)/TiO_2 sample is significantly higher than that of the Pt(II)/TiO_2 sample. The Fe(III)-Pt(II)/TiO_2 sample contains 65.3% PtO and 18.1% Pt(II)-Cl, corresponding to a total Pt(II) concentration of 83.4%.

On the other hand, the Pt(II)/TiO_2 sample, which contains 39.7 % PtO and 23.3% Pt(II)-Cl, has a lower total Pt(II) concentration of 63%. Hence, the merit of co-depositing Fe(III) oxide sensitizers with Pt sensitizers is that the Fe(III) oxides can limit the oxidation of the Pt(II) species (PtO and Pt(II)-Cl) to Pt(IV) species (PtO_2 and Pt(IV)-Cl), thereby stabilizing the Pt sensitizer oxidation state in a 2+ state. By contrast, if ethanol was used as the hole scavenger instead of Fe(II) cations, the Pt^{4+} ($[Pt(IV)Cl_6]^{2-}$) would be photoreduced to Pt(0) metal, as demonstrated by the Pt(0)/TiO_2 sample.

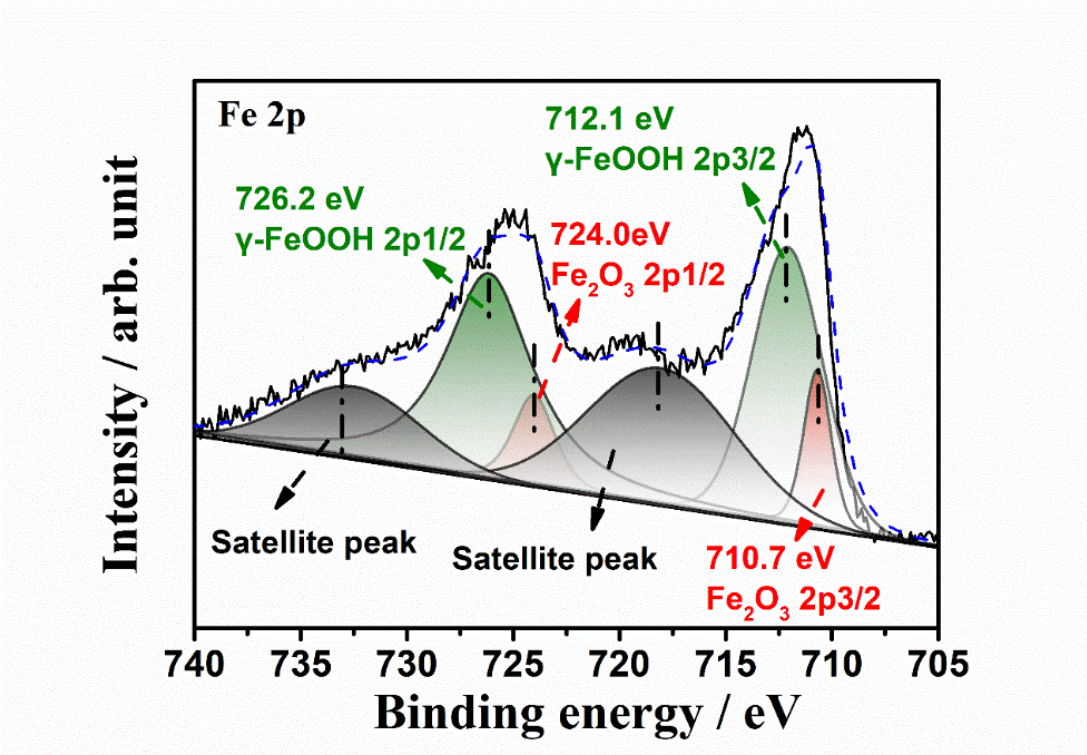

Fig. 2-9 Fe 2p XPS spectrum of an Fe(III)/TiO_2 sample with an Fe(III) concentration of 10wt%.

Fig. 2-10A-F shows HRTEM images and EDX (energy dispersive X-ray spectroscopy) elemental mapping of the as-prepared Fe(III)-Pt(II)/TiO_2 nanorods. The elemental mapping of the Fe(III)-Pt(II)/TiO_2 nanorods clearly showed the Pt(II) sensitizer was selectively photo-deposited on the {210} facet of the brookite TiO_2 nanorods and accumulated in nanometer-sized island-like structures on the {210} facet. Unlike Pt(II) nanoparticles, the Fe(III) oxide sensitizer was not selectively photo-

deposited on any particular facet of the brookite TiO_2 nanorods. Instead, the Fe(III) oxide sensitizer formed a uniform thin film layer coating on the entire Pt(II)/TiO_2 nanorods.

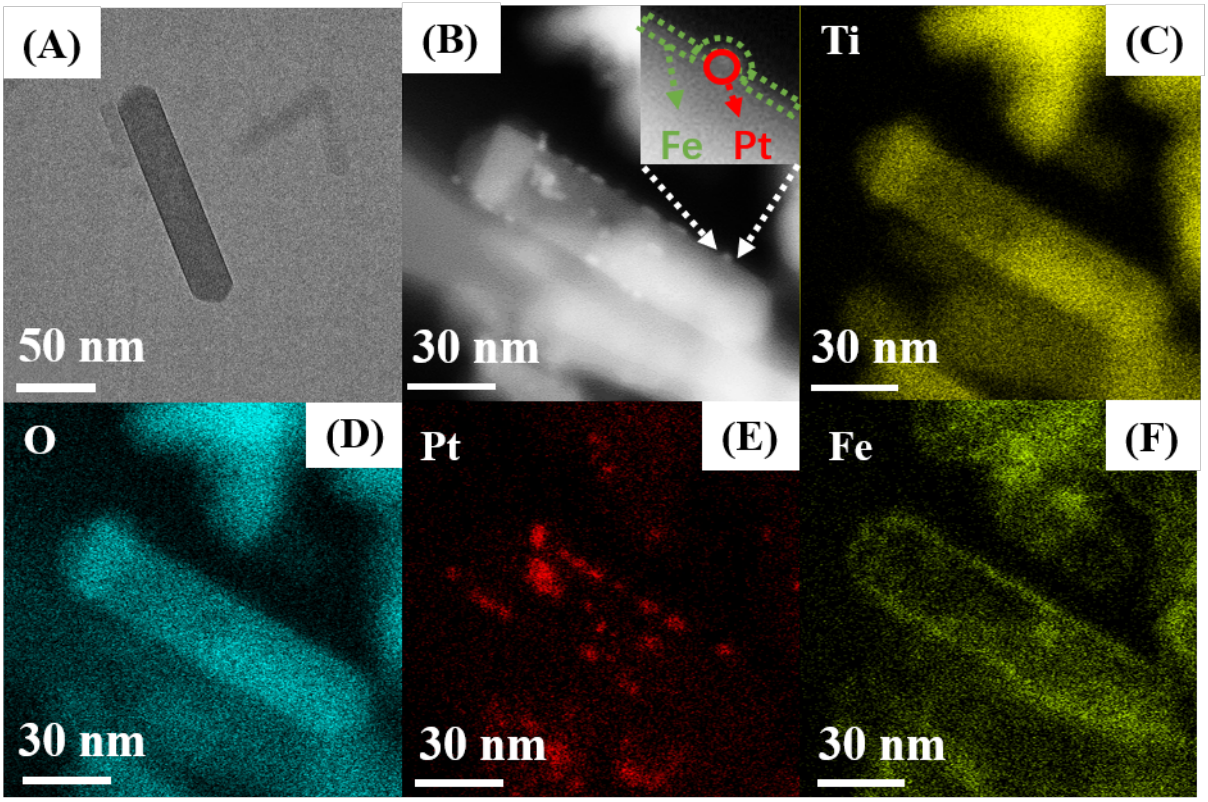

Fig. 2-10 HRTEM images of (A) pure brookite TiO_2 nanorods and (B) Fe(III)-Pt(II)-oxide-co-sensitized brookite TiO_2 nanorods (B) and the associated EDX elemental mapping of the as-prepared Fe(III)-Pt(II)-oxide-co-sensitized brookite TiO_2 nanorods (C) Ti, (D) O, (E) Pt and (F) Fe.

Fig. 2-2 also shows the XRD spectra of the Pt(0)/TiO_2, Pt(II)/TiO_2, Fe(III)/TiO_2 (prepared by chemisorption method) and Fe(III)-Pt(II)/TiO_2 sample. The XRD spectra indicate the modification of the as-prepared brookite TiO_2 with Pt/Fe sensitizers did not result in any XRD peak shift or the formation of new diffraction peaks belonging to metallic Pt or $Fe(OH)_3$. These observations suggest the Fe(III) and Pt sensitizers are not embedded into the bulk structures of brookite TiO_2 but are likely only deposited on the surfaces of the brookite TiO_2 nanorods.

2.3.2 Surface Affinities of Brookite TiO_2 for Fe^{2+}, Fe^{3+} and Pt^{4+} Cations

To elucidate how the Fe(III) oxide sensitizer layer was formed on the surfaces of the Pt(II)/TiO_2 nanorods upon photodeposition of Fe(II) and Pt(IV) ions , the surface adsorption capability of brookite TiO_2 nanorods for Fe(II), Fe(III) and Pt(IV) ions was investigated. Table 2-1 summarized the concentrations of Fe cations that were found deposited on the brookite TiO_2 samples after stirring the TiO_2 samples in known concentrations of Fe(II) or Fe(III)-containing solutions under dark conditions. The brookite TiO_2 nanorods could adsorb as much as 3.7wt% of Fe(III) cations when the brookite TiO_2 nanorods were stirred in in an Fe(III)-containing solution containing 4wt% Fe(III) cations. However, the brookite TiO_2 nanorods could only adsorb at maximum 0.23wt% of Fe(II) cations when the TiO_2 nanorods were stirred in a 4wt% Fe(II) solution. The results of ICP-MS show brookite TiO_2 exhibits high surface affinity for Fe(III) adsorption but low surface affinity for Fe(II) adsorption. The adsorption of Fe(II) and by TiO_2 was previously studied by Nano and Strathmann,[52] Zhang[53] and Hiemstra.[54] At the TiO_2 surface, the Fe^{2+} ion is presumably bound as a quattro-dentate surface complex ($\equiv(TiO)_2(TiOH)_2$-Fe(II)). This quattro-dentate surface complex exhibits high surface charge attribution with the TiO_2 surface.[53] Consequently, the hydrolysis and adsorption of Fe^{2+} on TiO_2 shows high pH dependency.[52] The adsorption of Fe(II) on TiO_2 is favored at pH>~7.5 (>80%) while significantly low at lower pH (<10%). In the current chemisorption conditions, the Fe(II) solution exhibits a pH of ~6 while the Fe(II)/Pt(IV) photo-deposition solution has a pH of ~3.8, these pH are relatively low for effective Fe(II) adsorption on TiO_2. In contrast, for Fe(III), the major Fe(III) species in solution at ~pH 3.5 are $[Fe(OH)(H_2O)_5]^{2+}$ and $[Fe(H_2O)_6]^{3+}$.[55] These hydrolyzed monomers can effectively adsorb onto TiO_2 surfaces.

Table 2-1. Net amounts of Fe(III) cations deposited on the surfaces of brookite TiO_2 nanorods.

Sample name	Nominal loading amount	Actual loading amount
0.1wt% Fe(III)-dark-adsorption	0.1wt% Fe	0.1wt% Fe
0.2wt% Fe(III)-dark-adsorption	0.2wt% Fe	0.2wt% Fe
0.4wt% Fe(III) -dark-adsorption	0.4wt% Fe	0.4wt% Fe
0.6wt% Fe(III) -dark-adsorption	0.6wt% Fe	0.6wt% Fe
4wt% Fe(III)-dark-adsorption	4wt% Fe	3.57wt% Fe
0.1wt% Fe(III)-light-photodeposition	0.1wt% Fe	0.09wt% Fe
0.2wt% Fe(III)-light-photodeposition	0.2wt% Fe	0.17wt% Fe
0.4wt% Fe(III) -light-photodeposition	0.4wt% Fe	0.23wt% Fe
0.6wt% Fe(III)-light-photodeposition	0.6wt% Fe	0.24wt% Fe
4wt% Fe(II)-dark-adsorption	4wt%	0.23wt%Fe

The surface adsorption capability of brookite TiO_2 nanorods for Pt(IV) ions in the dark was also elucidated. The brookite TiO_2 nanorods exhibit high surface affinity for Pt(IV) ions. ICP results indicate that all of the Pt(IV) ions were adsorbed onto the brookite TiO_2 nanorod surfaces when the brookite TiO_2 nanorods were stirred in aqueous solutions containing 0.1-0.6 wt% Pt(IV) in dark conditions, as shown in Table 2-2. As mentioned above, the chemisorption of $[Pt(IV)Cl_6]^{2-}$ onto TiO_2 surface forms a covalently bound surface complex by chloride substitution at the surface [Ti]-O^-. Under ambient conditions, these Pt(IV)-Cl surface complexes are partly converted to highly stable Ti-O-Pt bonds.[56]

The results of ICP-MS show for the TiO_2 nanorod sample co-deposited with Fe(II) and Pt(IV) ions, both at nominal loadings of 0.4wt%, only 0.07wt% of Fe(II) cations in the aqueous solution was eventually deposited on the TiO_2 nanorod surfaces to form the Fe(III) oxide thin film sensitizer coating (see Table 2-2). On the other hand, for Pt, all of the 0.4wt% of Pt(IV) ions in the solution were adsorbed onto the TiO_2 nanorod surfaces.

Table 2-2. Net amounts of Pt cations deposited on the surfaces of brookite TiO_2 nanorods.

Sample name	Nominal loading amount	Actual loading amount
0.1wt% Pt(IV) solution	0.1wt% Pt	0.1wt% Pt
0.2wt% Pt(IV) solution	0.2wt% Pt	0.2wt% Pt
0.4wt% Pt(IV) solution	0.4wt% Pt	0.4wt% Pt
0.6wt% Pt(IV) solution	0.6wt% Pt	0.6wt% Pt
0.4wt% Fe(II) ion and 0.4wt% Pt(IV) solution	0.4wt% Fe	0.07wt% Fe
	0.4wt% Pt	0.4wt% Pt

2.3.3 Proposed Formation Mechanism of Fe(III)- Pt(II)/TiO_2 Nanorods

Scheme 2b shows the proposed formation mechanism of Fe(III)-Pt(II)/TiO_2 nanorods. The $[Pt(IV)Cl_6]^{2-}$ were reduced by the photogenerated electrons of TiO_2 to form Pt(II) nanoparticles (i.e., PtO, Pt(II)-Cl) on the brookite TiO_2 nanorod surfaces. Attributed to the low surface affinity of the brookite TiO_2 nanorods for Fe(II) cations, as revealed by ICP-MS and discussed above, the brookite TiO_2 nanorod surfaces contained only small amounts of surface-adsorbed Fe(II) cations. Consequently, when the surface-adsorbed Fe(II) cations on the TiO_2 nanorods were oxidized by the photogenerated holes, the

Fe(II) cations formed a very thin layer of the Fe(III) oxide sensitizer (i.e., Fe_2O_3/FeOOH) on the entire surfaces of the Pt(II)-sensitized TiO_2 nanorods. Notably, the presence of the Fe(III) oxide thin film sensitization layer inhibits further reduction of the Pt(II) to Pt(IV) species, resulting in the formation of significantly high surface concentrations of Pt(II) sensitizers on the TiO_2 nanorod surfaces (~83.4%). Since TiO_2 is a demonstrated water oxidation photocatalyst, the electron used for the oxidation of Fe(II) and the reduction of Pt(IV) during the photo-deposition reaction is balanced by a concurrent oxidation of water.[57]

2.3.4 Optical Properties

Optical properties of the as-prepared brookite TiO_2 photocatalysts were elucidated using UV-Vis spectra. Fig. 2-11A shows the UV-Vis diffuse absorption spectra of pure brookite TiO_2, Fe(III)/TiO_2, Pt(II)/TiO_2 and Fe(III)-Pt(II)/TiO_2. Pure brookite TiO_2 shows an absorption edge at 380 nm, corresponding to an optical band gap of ~3.3 eV. Owing to the photo-sensitizing effects of the Fe(III) and Pt(II)/(IV) sensitizers, the brookite TiO_2 nanorod samples exhibit visible light absorption tails in the wavelength region of 400-600 nm upon surface modifications with the Fe and/or Pt sensitizers.[58-60] The visible light absorption tail is observed to be stronger for the Pt(II)/TiO_2 sample than for the Fe(III)/TiO_2 sample. This observation indicates the Pt(II)/(IV)sensitizers have greater visible light responses than that of the Fe(III) oxide sensitizers suggesting that Pt(II)/(IV) sensitizers are likely to be better visible light-driven sensitizers than Fe(III) oxide sensitizers. For the Fe(III)-Pt(II)/TiO_2 nanorod sample, the co-loading of Pt(II) and Fe(III) oxide sensitizers onto brookite TiO_2 nanorods results in the most apparent red shift in the visible light absorption. Since the Fe(III)-Pt(II)/TiO_2 nanorod sample contains higher concentrations of Pt(II) sensitizers and lower concentration of Pt(IV) sensitizers compared to that of the Pt(II)/TiO_2 sample, the enhanced visible light absorption property of Fe(III)-Pt(II)/TiO_2 nanorod sample can be attributed to the Pt(II) sensitizers. Furthermore, we also loaded Pt(II) on rutile and anatase TiO_2. As shown in the Fig. 2-11(E), the concentration of CO2 produced from acetaldehyde degradation

over brookite phase TiO_2 is higher than that over rutile and anatase TiO_2, indicating that brookite phase TiO_2 can better promote acetaldehyde degradation than other two phases under visible light.

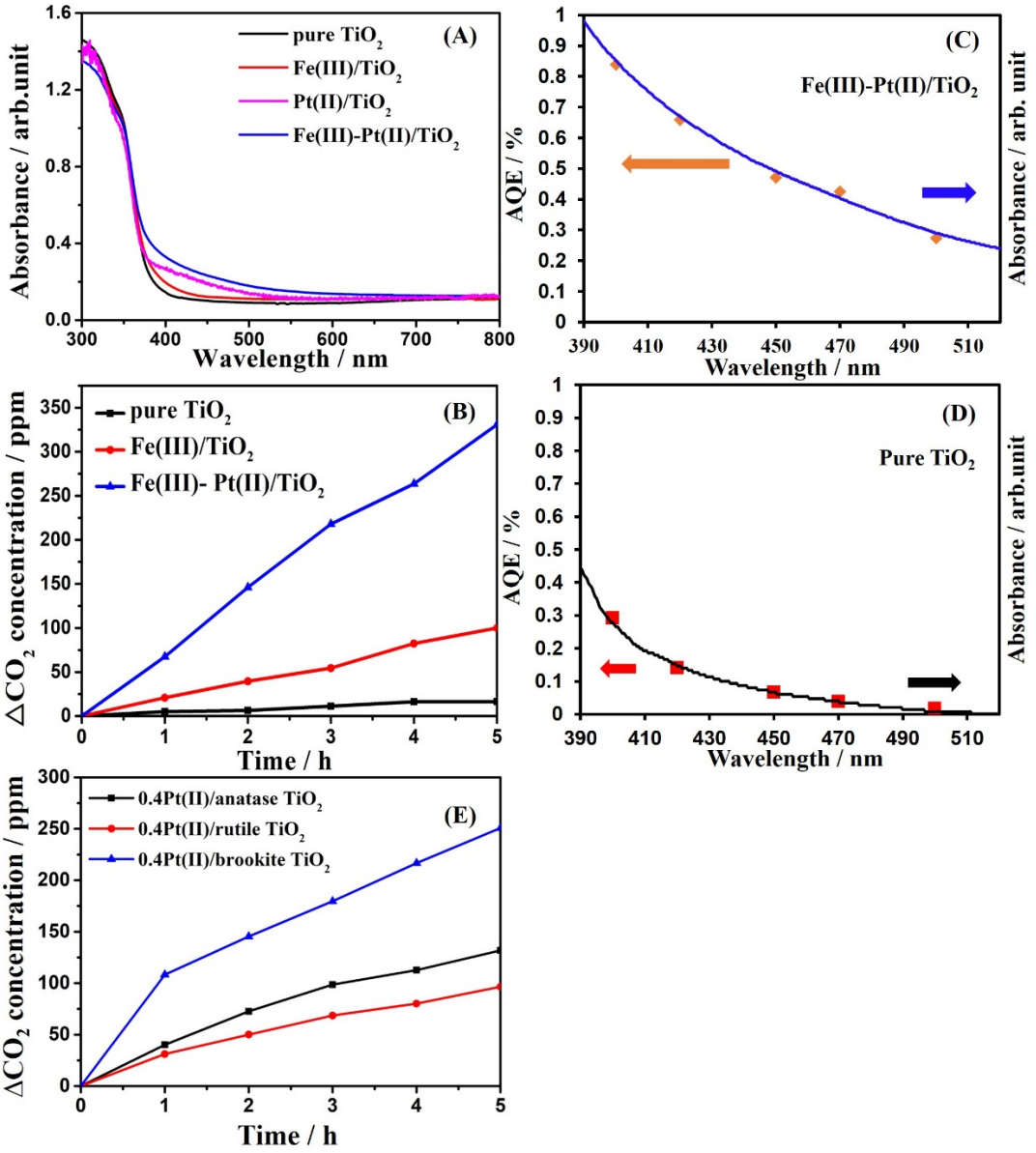

Fig. 2-11 (A) UV-Vis diffuse absorption spectra of pure brookite TiO_2, Fe(III)/TiO_2, Pt(II)/TiO_2 and Fe(III)-Pt(II)/TiO_2 samples, (B) CO_2 concentrations generated from photocatalytic degradation of acetaldehyde under visible light using Fe(III)-Pt(II)/TiO_2, Fe(III)/TiO_2 and pure brookite TiO_2 photocatalysts and, wavelength-dependent action spectrum of (C) Fe(III)-Pt(II)/TiO_2 and (D)pure TiO_2. (E) CO_2 concentrations generated

from photocatalytic degradation of acetaldehyde under visible light using 0.4wt%Pt(II) loaded rutile, anatase and brookite TiO_2.

2.3.5 Photocatalytic Activities of Fe(III) and Pt-sensitized TiO_2 and Fe(III)-Pt(II)-oxide-co-sensitized TiO_2 nanorods

The activities of as-prepared brookite TiO_2 nanorods and Fe(III) or Pt-sensitized brookite TiO_2 nanorod samples for photocatalytic degradation of acetaldehyde under visible light illumination were investigated. Prior to the light irradiation, the samples were investigated under dark conditions. Fig. 2-12 shows the CO_2 concentration-time profiles of the samples upon exposure to acetaldehyde under dark conditions. In all samples, low concentrations of CO_2 (~20-50 ppm) were detected within 30 min exposure to acetaldehyde and the CO_2 levels remained unchanged therefore. Since adsorbed CO_2 are naturally present on a TiO_2 oxide surface, the detection of CO_2 under dark conditions suggests there is a surface-exchange of CO_2 for acetaldehyde on the TiO_2 surfaces.[60-62] That is, adsorbed CO_2 desorbed from the TiO_2 surfaces upon exposure to acetaldehyde and acetaldehyde was re-adsorbed onto the TiO_2 surfaces. It is energetically infeasible for pure TiO_2 or the Pt/Fe-sensitized TiO_2 to degrade acetaldehyde spontaneously under dark conditions and evolve CO_2, particularly at CO_2 levels of ~20-50 ppm within 30 min.[60]

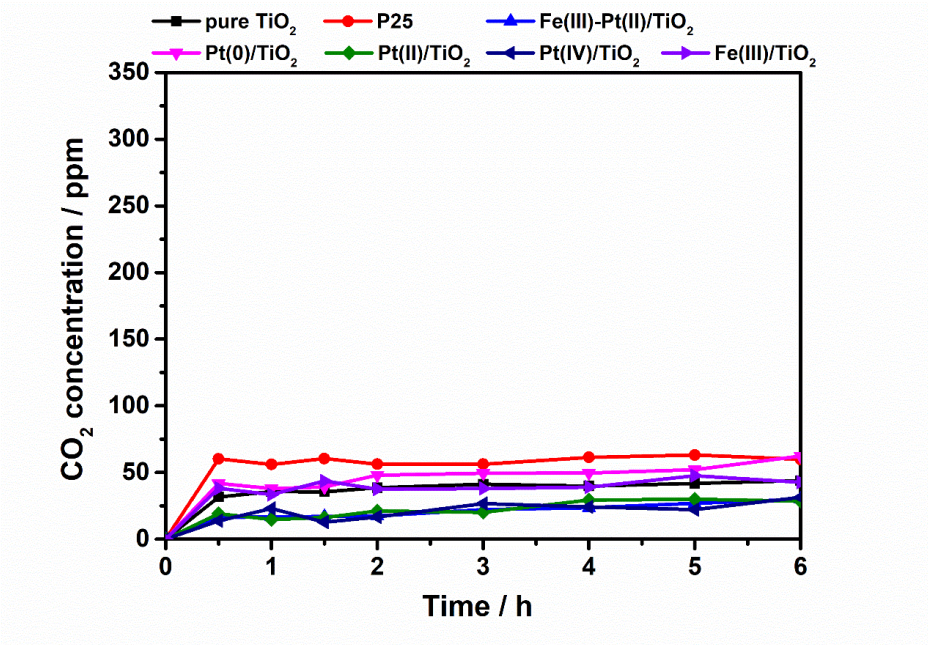

Fig. 2-12 Concentrations of CO_2 produced in the dark in the presence of various photocatalysts, pure brookite TiO_2, Pt(0)/TiO_2, Pt(II)/TiO_2, Pt(IV)/TiO_2, Fe(III)-Pt(II)/TiO_2 Fe(III)/TiO_2 and Degussa P25 TiO_2 (P25) (as a reference material).

For all samples, the CO_2 concentration generated from photocatalytic acetaldehyde degradation is determined after subtracting the amount of CO_2 that were desorbed under dark conditions (abbreviated as ΔCO_2). Fig. 2-13 shows the concentrations of CO_2 generated from acetaldehyde degradation when Pt(II)/TiO_2 and Fe(III)/TiO_2 with varied nominal loading of Pt sensitizers or Fe(III) oxide sensitizer were utilized as the photocatalysts. For both Pt(II)/TiO_2 and Fe(III)/TiO_2, the photocatalytic activities increased with increase in the weight loading of Pt sensitizers or Fe(III) oxide sensitizers until an optimum concentration was derived, whereby the photocatalytic activity was highest. A further increase in concentrations of Pt or Fe(III) sensitizers resulted in a decrease in activities, probably due to an excessive coverage of Pt or Fe(III) sensitizers on the active sites of TiO_2, which hinders efficient transport of photoexcited electrons. The optimum weight loading of Pt sensitizers and Fe(III) oxide sensitizers on brookite TiO_2 for photocatalytic degradation of acetaldehyde were both found to be at a nominal loading of 0.4wt% Fe or Pt. While the actual loading of Pt in the optimal Pt(II)/TiO_2 sample is also 0.4wt% due to the high surface affinity of brookite TiO_2 for

Pt ions, the actual loading of Fe element in the optimal Fe(III)/TiO_2 sample is 0.23% (see Table 2-3). Hence, for the co-deposition of Pt(IV) ions and Fe(II) cations on brookite TiO_2 nanorods to form an Fe(III)-Pt(II)/TiO_2 photocatalyst, nominal loading of 0.4wt% was applied for both Fe(II) and Pt(IV).

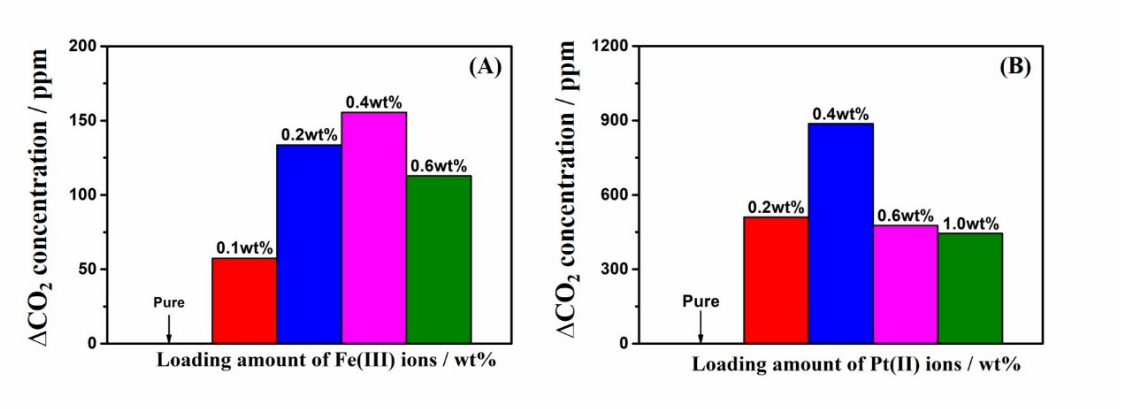

Fig. 2-13 Concentrations of CO_2 produced from photocatalytic acetaldehyde degradation using TiO_2 photocatalysts deposited with different nominal loading amounts of Fe(III) or Pt(II), (A) Fe(III)/TiO_2 and (B) Pt(II)/TiO_2, under visible light (455 nm).

Table 2-3. BET measurements of as-prepared brookite TiO_2 photocatalysts.

Samples	pure TiO_2	Fe(III)/TiO_2	Pt(II)/TiO_2	Fe(III)-Pt(II)/TiO_2
BET (m^2/g)	54.010	54.496	56.368	55.976

Fig. 2-11B shows the CO_2 concentrations from photocatalytic degradation of acetaldehyde over Fe(III)-Pt(II)/TiO_2, Fe(III)/TiO_2 and pure brookite TiO_2 photocatalysts. The Fe(III)-Pt(II)/TiO_2 photocatalyst shows the highest activity among the three samples. In a 5-h photocatalytic test, Fe(III)-Pt(II)/TiO_2 generated more than 300 ppm of CO_2, which is approximately two-times higher than that generated by Fe(III)/TiO_2(<100 ppm CO_2). The pure brookite TiO_2 photocatalyst shows some visible

light activity, it generated minor amount of CO_2 in 5h (~16.5 ppm CO_2). The Ti XPS spectrum of pure brookite TiO_2 nanorods, Fig. 2-14, indicate the presence of low concentration of Ti^{3+} defect states on the surface of the brookite TiO_2 nanorods. The visible light activity of the brookite TiO_2 can be attributed to the visible light absorption at the Ti^{3+} defect centers. Low concentrations of oxygen vacancies are commonly observed in TiO_2 nanorods due to the ease of formation of oxygen vacancies in TiO_2 nanostructures.[63, 64] Fig. 2-11C and D show the action spectra of Fe(III)-Pt(II)/TiO_2 and pure TiO_2 samples. The wavelength-dependent action spectra of Fe(III)-Pt(II)/TiO_2 indicate the apparent quantum efficiencies (AQE) of the Fe(III)-Pt(II)/TiO_2 photocatalyst and pure TiO_2 match well with their UV-Vis absorbance. The dependence of photocatalytic activities with different wavelengths of light indicate the light absorption by the Fe(III)-Pt(II)/TiO_2 and pure TiO_2 photocatalysts is the main factor contributing to the photocatalytic reactions. The Fe(III)-Pt(II)/TiO_2 photocatalyst exhibited an AQE of 0.84% under 420 nm monochromatic light irradiation. It should be noted the BET surface area analyses show the as-prepared brookite TiO_2 nanorods with and without modifications with Fe and/or Pt sensitizers exhibit equivalent surface areas of ~54-56 m^2/g. The BET surface areas of as-prepared TiO_2 samples are summarized in Table 2-3.

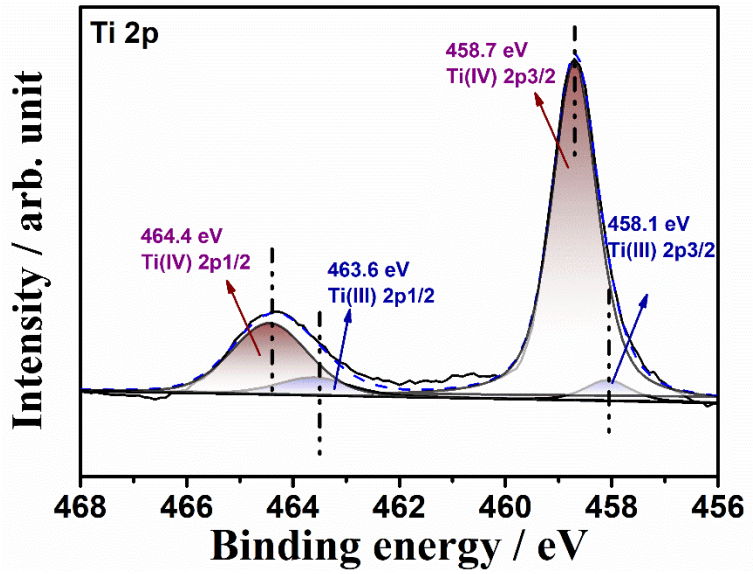

Fig. 2-14 Ti 2p XPS spectrum of an pure brookite TiO_2 sample.

2.3.6 Photocatalytic Activities of Pt(0) and Pt(II) and Pt(IV) Sensitizer-modified Brookite TiO_2 Nanorods

In order to investigate the activities and stabilities of Pt sensitizers with different oxidation states for photocatalytic degradation of acetaldehyde under visible light, photocatalytic tests were conducted for Pt(0)/TiO_2, Pt(II)/TiO_2, Pt(IV)/TiO_2 and Fe(III)-Pt(II)/TiO_2 over three repeated cycles. Fig. 2-15 shows the CO_2 concentrations produced from the photocatalytic degradation of acetaldehyde over Pt(0)/TiO_2, Pt(II)/TiO_2, Pt(IV)/TiO_2 and Fe(III)-Pt(II)/TiO_2. Among the Pt-sensitized TiO_2 samples (without Fe(III) co-loading), Pt(II)/TiO_2 shows the highest photocatalytic activity. When Pt(II)/TiO_2 was used, 250 ppm of CO_2 was generated from the degradation of acetaldehyde in the first photocatalytic cycle of 5 h. In contrast, <100 ppm and <90 ppm of CO_2 were generated in the first cycle tests with Pt(IV)/TiO_2 and Pt(0)/TiO_2, respectively. Although Pt(II)/TiO_2 shows the highest activity for photocatalytic degradation of acetaldehyde in the first 5-h cycle, the Pt(II)/TiO_2 sample shows poor stability on subsequent 5-h cycles. The CO_2 concentrations generated in the second and third 5-h cycles decreased to 76% and 50%, respectively, of the concentration in the first cycle. On the other hand, the Pt(IV)/TiO_2 and Pt(0)/TiO_2 samples show strong stability with no deterioration in activities over the three 5-h cycles.

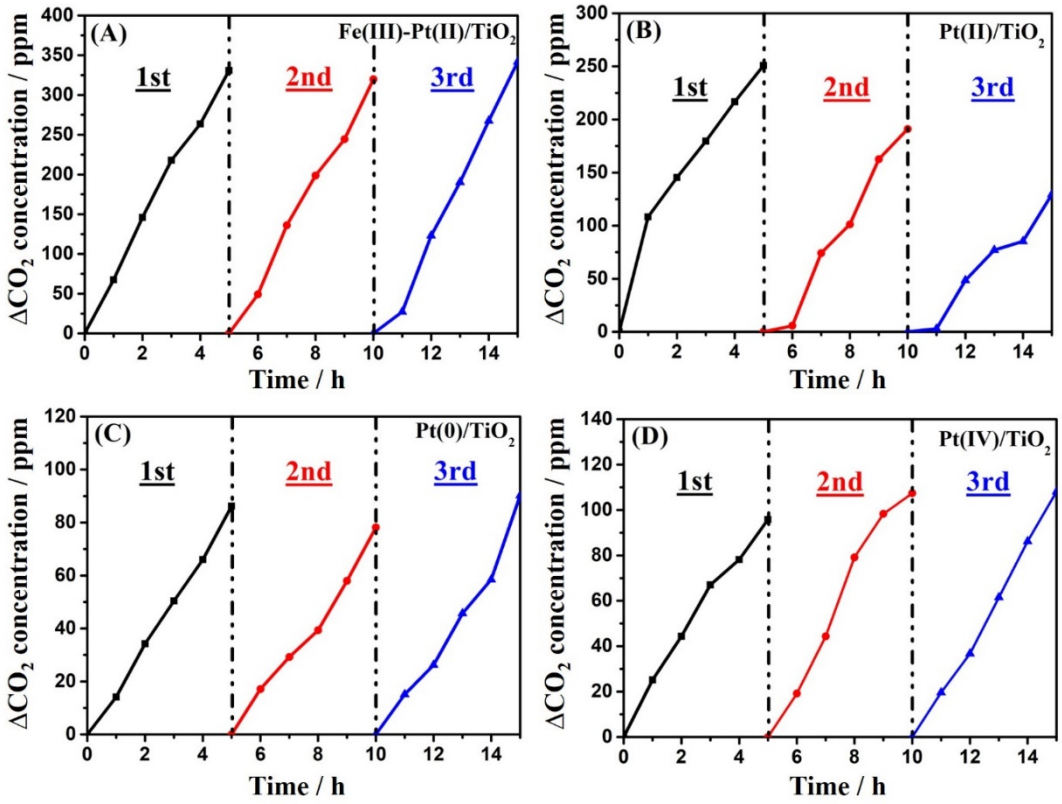

Fig. 2-15 CO_2 concentrations generated from the photocatalytic degradation of acetaldehyde under visible light using (A) Fe(III)-Pt(II)/TiO_2, (B) Pt(II)/TiO_2, (C) Pt(0)/TiO_2, and (D) Pt(IV)/TiO_2 samples. All samples contained 0.4wt% Pt. Fe(III)-Pt(II)/TiO_2 contained 0.07 wt%Fe.

To elucidate the structural change in Pt(II)/TiO_2 after photocatalytic tests leading to the decreased activities, the Pt(II)/TiO_2 sample was investigated by XPS before and after a photocatalytic test. Fig. 2-16 shows the Pt 4f XPS spectra of a fresh Pt(II)/TiO_2 sample and a spent Pt(II)/TiO_2 sample that was photo-irradiated in acetaldehyde under visible light for 24 h. As aforementioned, the as-prepared Pt(II)/TiO_2 sample consists of PtO (39.7%), Pt(II)-Cl (23.3%), PtO_2 (10.0%) and Pt(IV)-Cl (27.1%). After the 24-h photocatalytic reaction with acetaldehyde, the XPS results of the spent Pt(II)/TiO_2 sample, as can be seen in Fig. 2-16B, show significant reductions in peak intensities for PtO and Pt(II)-Cl. On the other hand, the peak intensities for PtO_2 and Pt(IV)-Cl showed significant increased. The Pt compositions in the spent Pt(II)/TiO_2 sample are as follows: PtO (20.7%), Pt(II)-Cl (12.3%), PtO_2 (29.6%) and Pt(IV)-Cl (37.4%) Hence,

the reduced photocatalytic activity of the Pt(II)/TiO_2 sample can be attributed to the oxidation of PtO and Pt(II)-Cl to PtO_2 and Pt(IV)-Cl, respectively. The results imply the Pt(II) sensitizers are more effective visible light sensitizers than the Pt(IV) sensitizers, albeit with lower stability.

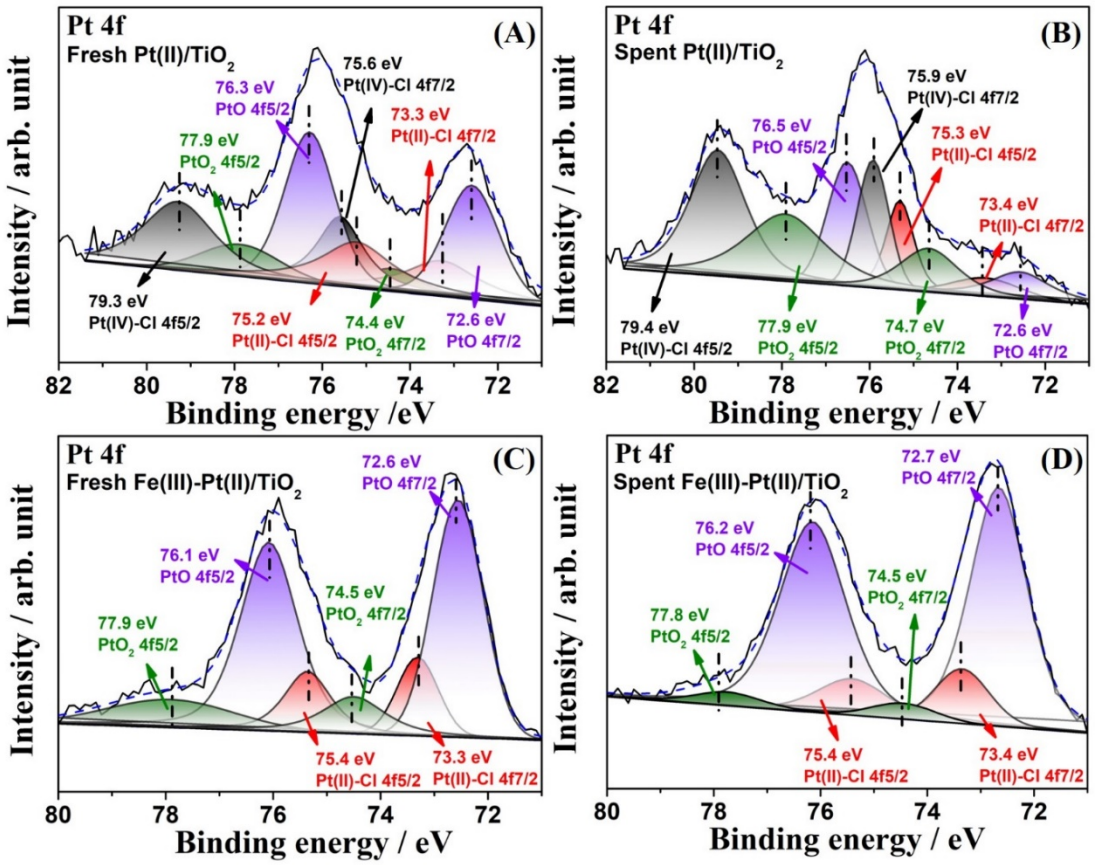

Fig. 2-16 Pt 4f XPS spectra of a fresh Pt(II)/TiO_2 sample (A), a spent Pt(II)/TiO_2 sample that was photo-irradiated in acetaldehyde for 24 h (B), a fresh Fe(III)-Pt(II)/TiO_2 sample (C) and a spent Fe(III)-Pt(II)/TiO_2 sample (D) that was photo-irradiated in acetaldehyde for 24 h.

The optical properties of a Pt(II)/TiO_2 sample before and after the 24-h photocatalytic reaction with acetaldehyde as well as those of a fresh Pt(IV)/TiO_2 sample were also measured by UV-Vis spectroscopy. UV-Vis diffuse absorption spectra of these samples are shown in Fig. 2-17 and 2-18. The as-prepared Pt(II)/TiO_2 shows a stronger visible light absorption tail in the 400-600 nm wavelength region compared to the as-prepared

Pt(IV)/TiO_2 sample. After the 24-h photocatalytic test, the UV-Vis spectra of the post-treated Pt(II)/TiO_2 sample shows a reduction in visible light absorption intensity in the 400-600 nm wavelength region. Hence, the decrease in photocatalytic activities of the Pt(II)/TiO_2 sample in the repeated photocatalytic tests can be attributed to a reduced ability of the Pt(II)/TiO_2 sample to absorb visible light due to an increased conversion of Pt(II) to Pt(IV) during the photocatalytic degradation process.

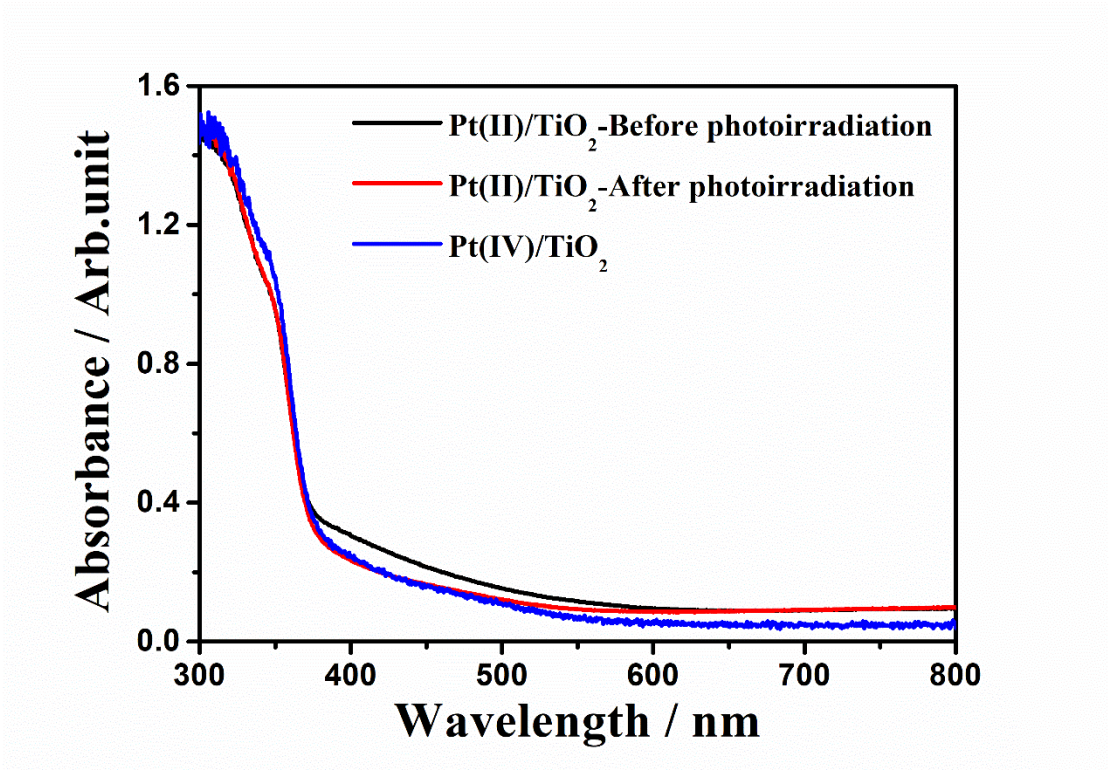

Fig. 2-17 UV-Vis diffuse absorption spectra of a Pt(II)/TiO_2 sample before photoirradiation and after irradiation in acetaldehyde under visible light for 24 h and a fresh Pt(IV)/TiO_2 sample.

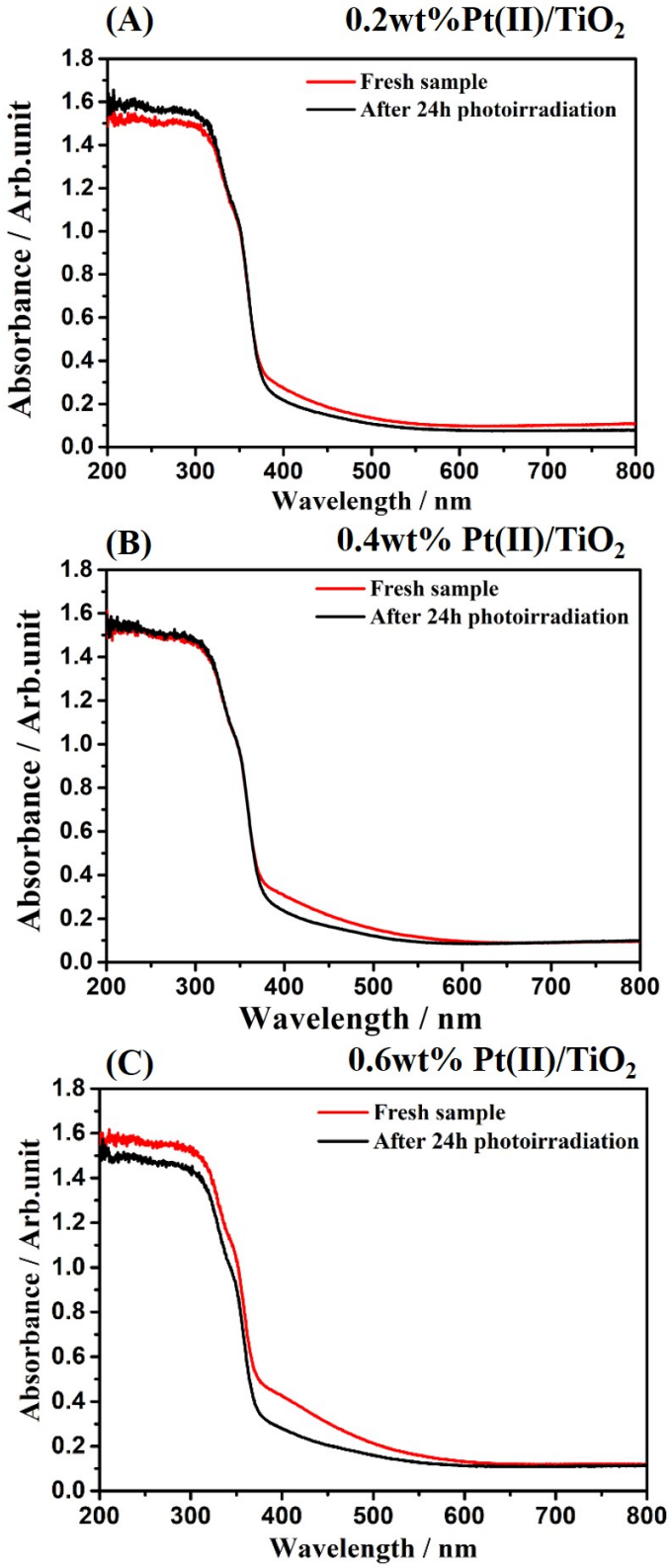

Fig. 2-18 UV-vis diffuse absorption spectra of (A) 0.2wt%, (B) 0.4wt% and (C) 0.6wt% Pt(II)/TiO_2 samples before and after photoirradiation in acetaldehyde under visible light for 24 h.

2.3.7 Importance of Fe(III) Oxide Sensitizer Outer Layer for Enhancing the Photocatalytic Activity and Stability of Pt(II)/TiO_2

Fig. 2-15 also shows the CO_2 concentration from photocatalytic degradation of acetaldehyde over the Fe(III)-Pt(II)/TiO_2 photocatalyst. It is notable that the co-modifications of the Fe(III) and Pt(II) sensitizers on the brookite TiO_2 nanorods improved not only the photocatalytic activity of Pt(II)/TiO_2 but also the cycling stability of the sample. The Fe(III)-Pt(II)/TiO_2 photocatalyst generated 325 ppm of CO_2 for all three 5-h cycles with no deterioration, which is a significant enhancement compared to the 250 ppm of CO_2 generated by Pt(II)/TiO_2 in the first cycle (Fig. 2-15). Fig. 2-19 shows the cycling stability test for Fe(III)/TiO_2. Similar to Fe(III)-Pt(II)/TiO_2 photocatalyst, the Fe(III)/TiO_2 shows stability for photocatalytic acetaldehyde degradation over three 5-h cycles, it generated ~100-110 ppm of CO_2 in each cycle. XPS was also utilized to examine the Fe(III)-Pt(II)/TiO_2 photocatalyst after 24-h photocatalytic degradation of acetaldehyde. Fig. 2-16C and D show the Pt spectra of the Fe(III)-Pt(II)/TiO_2 sample before and after the photocatalytic test. The XPS indicate an increased in PtO concentration in the spent- Fe(III)-Pt(II)/TiO_2 sample (from 65.3% in the fresh sample to 77.8% in the spent sample). On the other hand, the concentrations of Pt(II)-Cl and PtO_2 showed reductions in the spent sample. The Pt(II)-Cl and PtO_2 in the fresh Fe(III)-Pt(II)/TiO_2 sample were 18.1% and 16.6%, respectively, while 15.3% and 5.1% in the spent Fe(III)-Pt(II)/TiO_2 sample, respectively. The increased in PtO concentration accompanied with concurrent reductions of Pt(II)-Cl and PtO_2 concentrations in the spent Fe(III)-Pt(II)/TiO_2 sample indicate some of the PtO_2 were photoreduced to PtO while some of the Pt(II)-Cl were also converted to PtO during the photocatalytic degradation of acetaldehyde. It is energetically feasible for the Cl^- ligands to form free Cl^- radicals during the photocatalytic oxidation reactions.[56, 65, 66]

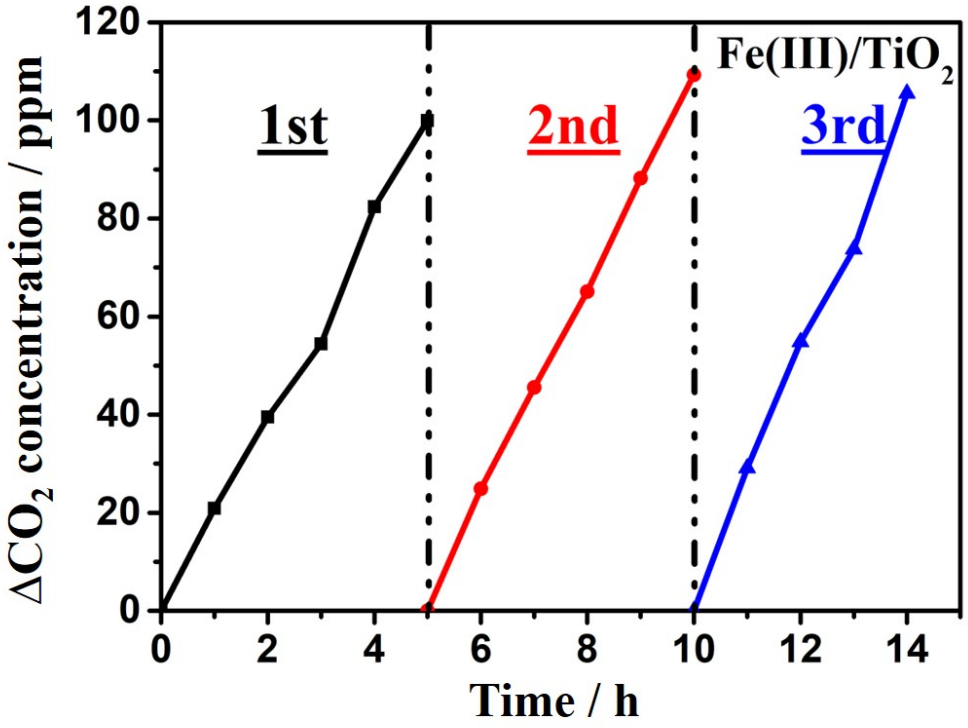

Fig. 2-19 CO_2 concentrations generated from the photocatalytic degradation of acetaldehyde under visible light using Fe (III) /TiO_2.

2.3.8 Direct Visualization of Electron Transfer in Fe/Pt-sensitized TiO_2 Nanorods under Visible Light Irradiation using *in situ* DB-PAS

In order to elucidate the electron transfer mechanisms of Fe/Pt-sensitized TiO_2 leading to the obtained activities, the behaviors of injected electrons in pure brookite TiO_2 and Fe/Pt-sensitized TiO_2 were investigated by *in situ* DB-PAS. Fig. 2-20A shows the time-course curves of PA intensity under visible light irradiation in the presence of air and 2-PrOH vapor for pure brookite TiO_2, Fe(III)/TiO_2, Pt(II)/TiO_2 and Fe(III)-Pt(II)/TiO_2. The PA intensity increased upon visible light irradiation because Ti(IV) was reduced to Ti(III) by the injected electrons from the loaded metal cations into TiO_2. However, the number of electrons accumulated in the TiO_2 by visible light irradiation was much smaller, compared to the maximum capacity of electron accumulation in the TiO_2. The steady-state values of PA intensity show dependence on the kind of metal oxide sensitizer(s) loaded onto TiO_2 in the order of Fe(III)-Pt(II)/TiO_2 > Pt(II)/TiO_2 >

Fe(III)/TiO_2 > TiO_2. Because these measurements were carried out in the presence of an electron acceptor such as O_2, the PA intensity is related to the difference between the amount of injected electrons and electrons consumed on TiO_2. Previous studies show some metal oxide compounds function as not only visible light sensitizers but also electron acceptor.[67] Therefore, it is difficult to estimate the amount of electron injection only from PA intensity measured in the presence of O_2. However, the almost same increases in PA intensity for Fe(III)-Pt(II)/TiO_2 and Pt(II)/TiO_2 under visible light irradiation indicate that electron consumption was hardly changed by the co-loading of Fe(III) oxides on Pt(II)/TiO_2. Overall, the PA intensities indicate Pt(II) oxide works as a more efficient visible light sensitizer than Fe(III) oxide sensitizer, in good agreement with the UV-Vis light absorption spectra (Fig. 2-11A). By contrast, the Fe(III)/TiO_2 showed a lower PA intensity than the Pt(II)/TiO_2 or the Fe(III)-Pt(II)/TiO_2 because the amount of injected electrons from the Fe(III)/TiO_2 was much smaller due to the lower photoabsorption of the Fe(III)/TiO_2.

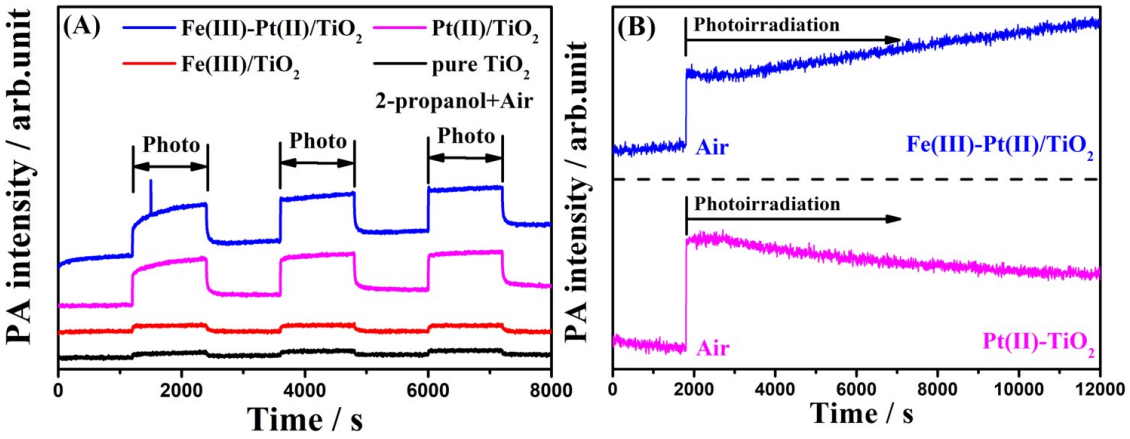

Fig. 2-20 (A) The time-course curves of the PA intensity under intermittent visible light irradiation in the presence of air and 2-PrOH vapor for pure brookite TiO_2, Fe(III)/TiO_2, Pt(II)/TiO_2 and Fe(III)-Pt(II)/TiO_2 samples and (B) the time-course curves of the PA intensity under continuous visible light irradiation in the presence of air for Pt(II)/TiO_2 and Fe(III)-Pt(II)/TiO_2 samples.

Fig. 2-20B shows time-course curves of PA intensity for Fe(III)-Pt(II)/TiO_2 and Pt(II)/TiO_2 under visible light irradiation in artificial air only. The PA intensity for both samples increased under visible light irradiation even in the absence of electron donor, i.e., 2-PrOH vapor. However, the PA intensity of Pt(II)/TiO_2 decreased after prolonged light irradiation, indicating the efficiency of electron injection was decreased in the absence of 2-PrOH electron donor. The decrease in PA intensity is likely to be due to the self-oxidation of Pt(II) to Pt(IV), as indicated by XPS results (Fig. 2-16) and UV-Vis spectra (Fig. 2-17 and 2-18). In contrast, the PA intensity for Fe(III)-Pt(II)/TiO_2 increased under prolonged light irradiation even in the absence of 2-PrOH electron donor. This observation is presumably because the co-loaded Fe(III) oxide sensitizer retards the self-oxidation of Pt(II) oxide sensitizer and the rate of electron injection from Pt(II) stabilized by Fe(III) is continuously faster than that of electron consumption.

2.3.9 Proposed Mechanisms of Photocatalytic Acetaldehyde Degradation over Pt(II)/TiO_2 and Fe(III)-Pt(II)/TiO_2 under Visible Light

The proposed mechanisms for acetaldehyde degradation over Pt(II)/TiO_2 and Fe(III)-Pt(II)/TiO_2 photocatalyts under visible light is presented in Fig. 2-21A. For Pt(II)/TiO_2, upon visible light photoexcitation of the Pt(II) oxide sensitizer, photoexcited electrons are transferred from the Pt(II) oxide sensitizer to the conduction band of TiO_2 and O_2 is reduced to superoxide radicals ($O_2^{\cdot-}$) at the TiO_2 surface active sites. Simultaneously, the photoexcited holes oxidize acetaldehyde to CO_2 at the Pt(II) oxide sensitizer photocatalytic sites. However, the oxygen in the air can also extract electrons from the Pt(II) oxide sensitizer and directly oxidize Pt(II) to Pt(IV). The decrease in the concentration of the Pt(II) oxide sensitizer in the Pt(II)/TiO_2 sample with time reduces both the light absorption ability and photocatalytic activity of the Pt(II)/TiO_2 photocatalyst.

In the case of the Fe(III)-Pt(II)/TiO_2 photocatalyst, upon photoexcitation of both Fe(III) and Pt(II) oxide sensitizers with visible light, photocatalytic degradation of acetaldehyde occurs on both the Fe(III) and Pt(II) oxide sensitizers. The Fe(III) oxide

sensitizer protective layer around the Pt(II)/TiO_2 nanorods can protect the Pt(II) oxide sensitizer from oxidation by continuously injecting its photoexcited electrons into the Pt(II) oxide sensitizer, as evidenced by the *in situ* DB-PAS, leading to enhanced photocatalytic activity and sustained stability.

In addition, the electron injected into the conduction band of TiO_2 is expected to reduce O_2 to superoxide anions ($\bullet O_2^-$), which is further reduced into hydrogen peroxide (H_2O_2) and hydroxyl (OH) radicals by subsequent second and third electron transfer, respectively, [23, 68, 69] as shown in Fig. 2-21A. As the H_2O_2 and OH radicals have high oxidizing powers,[70] they will be consumed in the oxidation reaction of acetaldehyde.

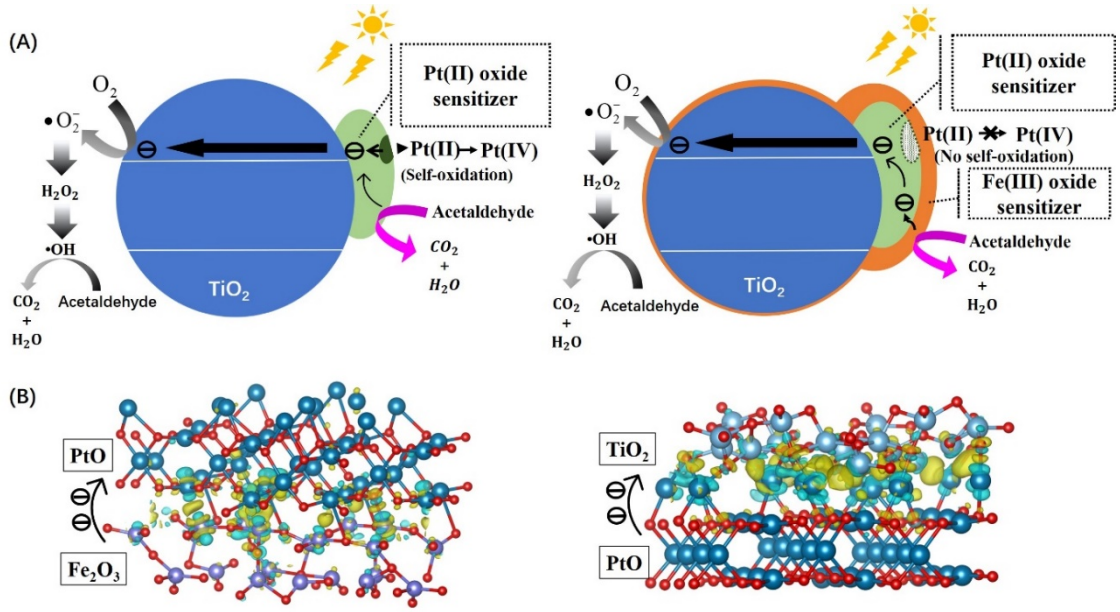

Fig. 2-21 (A) Proposed mechanisms for acetaldehyde degradation over Pt(II)/TiO_2 and Fe(III)-Pt(II)/TiO_2 photocatalyts under visible light and (B) electron density distribution maps of PtO and brookite TiO_2 (left) and Fe_2O_3 and PtO heterojunction interfaces (right), color of spheres: red = O, dark blue = Pt, light blue = Ti and purple = Fe, yellow and green areas represent higher and lower electron density.

Besides the direct experimental evidence from *in situ* DB-PAS, the first principle DFT calculations also support the proposed charge transfer mechanisms. Since PtO and Fe_2O_3 are the dominant components of Pt(II) and Fe(III) oxide sensitizers, we modeled

the heterojunction interface of PtO and Fe_2O_3 and that of PtO and brookite TiO_2. The obtained electron density distribution maps are presented in Fig. 2-21B. The electron density distribution map of the Fe_2O_3 and PtO heterojunction interface indicates electrons are accumulating at the PtO sites, suggesting that electrons are spontaneously transferring from Fe_2O_3 to PtO. On the other hand, at the heterojunction interface of PtO and TiO_2, electrons are accumulating at the TiO_2 sites, suggesting that electrons are migrating spontaneously from PtO to TiO_2. Taken together, the favorable tri-component interfaces of Fe_2O_3/PtO/TiO_2 allow rapid transfer of photoexcited electrons from Fe_2O_3 to PtO and then to TiO_2, where the electrons are eventually scavenged by ambient O_2 at the TiO_2 surface. The rapid removal of photoexcited electrons from Fe_2O_3 and PtO also extends the lifetime of photoexcited holes at the Fe_2O_3 and PtO surfaces, which in turn enhances the hole oxidation reaction of acetaldehyde to CO_2 at the Fe(III) and Pt(II) oxide photocatalytic sites.

2.4 Conclusions

In summary, single-crystalline brookite TiO_2 nanorods with well-defined {210} and {111} facets were successfully fabricated by a hydrothermal process using TALH as a shaping agent. Among the Pt sensitizers of different oxidation states, Pt(II) oxide-sensitized TiO_2 shows the highest photocatalytic activity for degradation of acetaldehyde under visible light. However, the stability of Pt(II) oxide is compromised by its self-oxidation to Pt(IV) during the photocatalytic reaction with acetaldehyde. Surface coating of a Fe(III) oxide sensitizer thin film layer around the Pt(II)/TiO_2 nanorods can prevent the self-oxidation of Pt(II) oxide sensitizer through electron injection, enabling enhanced stability and enhanced activity. The energetically favorable tri-component interfaces of Fe_2O_3/PtO/TiO_2 allow photoexcited electrons to migrate rapidly from the outermost Fe(III) oxide sensitizer to the mid-zone Pt(II) oxide sensitizer and then to TiO_2. The enhanced separation of electrons and holes promotes the hole oxidation reaction of acetaldehyde at the Fe(III) and Pt(II) oxide photocatalytic sites. The Fe(III)-Pt(II)/TiO_2 photocatalyst exhibited an AQE of 0.84% under 420 nm

monochromatic light irradiation for acetaldehyde degradation, which is significantly higher than that of pure brookite TiO_2 (0.14%)**.**

References

[1] Z.N. Tong, Discussion on the health problems of indoor living, IOP Conference Series: Earth and Environmental Science, 186 (2018).

[2] C. Guo, Z. Gao, J. Shen, Emission rates of indoor ozone emission devices: A literature review, Building and Environment, 158 (2019) 302-318.

[3] P. Harb, N. Locoge, F. Thevenet, Treatment of household product emissions in indoor air: Real scale assessment of the removal processes, Chemical Engineering Journal, 380 (2020).

[4] Y.-J. Hu, L.-J. Bao, C.-L. Huang, S.-M. Li, P. Liu, E.Y. Zeng, Exposure to air particulate matter with a case study in Guangzhou: Is indoor environment a safe haven in China?, Atmospheric Environment, 191 (2018) 351-359.

[5] H. Salonen, T. Salthammer, L. Morawska, Human exposure to NO_2 in school and office indoor environments, Environ Int, 130 (2019) 104887.

[6] R.M. Alberici., W.F. Jardim, Photocatalytic destruction of VOCs in the gas-phase using titanium dioxide, Applied Catalysis B: Environmental, 14 (1997) 55-68.

[7] M. Meisutovic-Akhtarieva, T. Prasauskas, D. Ciuzas, E. Krugly, K. Keraityte, D. Martuzevicius, V. Kauneliene, Impacts of exhaled aerosol from the usage of the tobacco heating system to indoor air quality: A chamber study, Chemosphere, 223 (2019) 474-482.

[8] M. Salaspuro, Key role of local acetaldehyde in upper GI tract carcinogenesis, Best Pract Res Clin Gastroenterol, 31 (2017) 491-499.

[9] X. Zhang, J. Cao, J. Wei, Y. Zhang, Improved C-history method for rapidly and accurately measuring the characteristic parameters of formaldehyde/VOCs emitted from building materials, Building and Environment, 143 (2018) 570-578.

[10] T. Fukumura, E. Sambandan, H. Yamashita, Synthesis and VOC degradation ability of a CeO_2 /WO_3 thin-layer visible-light photocatalyst, Materials Research

Bulletin, 94 (2017) 493-499.

[11] S. Song, C. Lu, X. Wu, S. Jiang, C. Sun, Z. Le, Strong base g-C3N4 with perfect structure for photocatalytically eliminating formaldehyde under visible-light irradiation, Applied Catalysis B: Environmental, 227 (2018) 145-152.

[12] A. Enesca, Y. Yamaguchi, C. Terashima, A. Fujishima, K. Nakata, A. Duta, Enhanced UV–Vis photocatalytic performance of the $CuInS_2$ /TiO_2 /SnO_2 hetero-structure for air decontamination, Journal of Catalysis, 350 (2017) 174-181.

[13] R. Yang, Q. Chen, Y. Ma, R. Zhu, Y. Fan, J. Huang, H. Niu, Y. Dong, D. Li, Y. Zhang, L. Mei, B. Chen, Z. Zeng, Highly efficient photocatalytic hydrogen evolution and simultaneous formaldehyde degradation over Z-scheme ZnIn2S4-NiO/BiVO4 hierarchical heterojunction under visible light irradiation, Chemical Engineering Journal, 423 (2021).

[14] Y. Peng, S. Kang, Z. Hu, Pt Nanoparticle-Decorated CdS Photocalysts for CO_2 Reduction and H2 Evolution, ACS Applied Nano Materials, 3 (2020) 8632-8639.

[15] S. Song, Z. Sheng, Y. Liu, H. Wang, Z. Wu, Influences of pH value in deposition-precipitation synthesis process on Pt-doped TiO2 catalysts for photocatalytic oxidation of NO, Journal of Environmental Sciences, 24 (2012) 1519-1524.

[16] M. Yoshida., A. Yamakata., K. Takanabe., J. Kubota., M. Osawa., K. Domen, ATR-SEIRAS Investigation of the Fermi Level of Pt Cocatalyst on a GaN Photocatalyst for Hydrogen Evolution under Irradiation, Journal of the American Chemical Society, 131 (2009) 13218-13219.

[17] Y. Hu, X. Song, S. Jiang, C. Wei, Enhanced photocatalytic activity of Pt-doped TiO_2 for NOx oxidation both under UV and visible light irradiation: A synergistic effect of lattice Pt^{4+} and surface PtO, Chemical Engineering Journal, 274 (2015) 102-112.

[18] C.-H. Huang, I.K. Wang, Y.-M. Lin, Y.-H. Tseng, C.-M. Lu, Visible light photocatalytic degradation of nitric oxides on PtOx-modified TiO_2 via sol-gel and impregnation method, Journal of Molecular Catalysis A: Chemical, 316 (2010) 163-170.

[19] F. Dong, H. Wang, G. Sen, Z. Wu, S.C. Lee, Enhanced visible light photocatalytic

activity of novel Pt/C-doped TiO_2/$PtCl_4$ three-component nanojunction system for degradation of toluene in air, J Hazard Mater, 187 (2011) 509-516.

[20] M. Nishikawa, H. Sakamoto, Y. Nosaka, Reinvestigation of the photocatalytic reaction mechanism for Pt-complex-modified TiO_2 under visible light irradiation by means of ESR spectroscopy and chemiluminescence photometry, J Phys Chem A, 116 (2012) 9674-9679.

[21] C. Wang, H. Fan, X. Ren, Y. Wen, W. Wang, Highly dispersed PtO nanodots as efficient co-catalyst for photocatalytic hydrogen evolution, Applied Surface Science, 462 (2018) 423-431.

[22] M. Sansotera, S. Geran Malek Kheyli, A. Baggioli, C.L. Bianchi, M.P. Pedeferri, M.V. Diamanti, W. Navarrini, Absorption and photocatalytic degradation of VOCs by perfluorinated ionomeric coating with TiO_2 nanopowders for air purification, Chemical Engineering Journal, 361 (2019) 885-896.

[23] Q. Zeng, X. Wang, X. Xie, G. Lu, Y. Wang, S. Cheng Lee, J. Sun, TiO_2/TaS_2 with superior charge separation and adsorptive capacity to the photodegradation of gaseous acetaldehyde, Chemical Engineering Journal, 379 (2020).

[24] J.J.M. Vequizo, H. Matsunaga, T. Ishiku, S. Kamimura, T. Ohno, A. Yamakata, Trapping-Induced Enhancement of Photocatalytic Activity on Brookite TiO2 Powders: Comparison with Anatase and Rutile TiO_2 Powders, ACS Catalysis, 7 (2017) 2644-2651.

[25] H.T.T. Tran, H. Kosslick, M.F. Ibad, C. Fischer, U. Bentrup, T.H. Vuong, L.Q. Nguyen, A. Schulz, Photocatalytic Performance of Highly Active Brookite in the Degradation of Hazardous Organic Compounds Compared to Anatase and Rutile, Applied Catalysis B: Environmental, 200 (2017) 647-658.

[26] W.-K. Li., X.-Q. Gong., G. Lu., A. Selloni., Different Reactivities of TiO_2 Polymorphs: Comparative DFT Calculations of Water and Formic Acid Adsorption at Anatase and Brookite TiO_2 Surfaces, The Journal of Physical Chemistry C, 112 (2008) 6594-6596.

[27] Z. Li, S. Cong, Y. Xu, Brookite vs Anatase TiO2 in the Photocatalytic Activity for

Organic Degradation in Water, ACS Catalysis, 4 (2014) 3273-3280.

[28] M. Addamo, M. Bellardita, A. Di Paola, L. Palmisano, Preparation and photoactivity of nanostructured anatase, rutile and brookite TiO_2 thin films, Chem Commun (Camb), (2006) 4943-4945.

[29] J. Zhang, S. Yan, L. Fu, F. Wang, M. Yuan, G. Luo, Q. Xu, X. Wang, C. Li, Photocatalytic Degradation of Rhodamine B on Anatase, Rutile, and Brookite TiO_2, Chinese Journal of Catalysis, 32 (2011) 983-991.

[30] M. Kobayashi., H. Kato., M. Kakihana., Synthesis of Titanium Dioxide Nanocrystals with Controlled Crystal- and Micro-Structures from Titanium Complexes, Nanomaterials and Nanotechnology, 3.

[31] Y. Ma, K. Kobayashi, Y. Cao, T. Ohno. Development of visible-light-responsive morphology-controlled brookite TiO_2 nanorods by site-selective loading of AuAg bimetallic nanoparticles. Applied Catalysis B: Environmental, 245, 15 (2019) 681-690.

[32] T. Ohno, K. Sarukawa, M. Matsumura, Crystal faces of rutile and anatase TiO_2 particles and their roles in photocatalytic reactions, New Journal of Chemistry, 26 (2002) 1167-1170.

[33] G.Kressea., J.Furthmüller., Efficiency of ab-initio total energy calculations for metals and semiconductors using a plane-wave basis set, Computational Materials Science, 6 (1996) 15-50.

[34] P.E. Blochl, Projector augmented-wave method, Phys Rev B Condens Matter, 50 (1994) 17953-17979.

[35] J.P. Perdew, J.A. Chevary, S.H. Vosko, K.A. Jackson, M.R. Pederson, D.J. Singh, C. Fiolhais, Atoms, molecules, solids, and surfaces: Applications of the generalized gradient approximation for exchange and correlation, Phys Rev B Condens Matter, 46 (1992) 6671-6687.

[36] S. Grimme, J. Antony, S. Ehrlich, H. Krieg, A consistent and accurate ab initio parametrization of density functional dispersion correction (DFT-D) for the 94 elements H-Pu, J Chem Phys, 132 (2010) 154104.

[37] H. Xu, D. Cheng, D. Cao, X.C. Zeng, A universal principle for a rational design of

single-atom electrocatalysts, Nature Catalysis, 1 (2018) 339-348.
[38] S. Xiao, W. Dai, X. Liu, D. Pan, H. Zou, G. Li, G. Zhang, C. Su, D. Zhang, W. Chen, H. Li, Microwave-Induced Metal Dissolution Synthesis of Core–Shell Copper Nanowires/ZnS for Visible Light Photocatalytic H2 Evolution, Advanced Energy Materials, 9 (2019).

[39] F. Yu, C. Wang, Y. Li, H. Ma, R. Wang, Y. Liu, N. Suzuki, C. Terashima, B. Ohtani, T. Ochiai, A. Fujishima, X. Zhang, Enhanced Solar Photothermal Catalysis over Solution Plasma Activated TiO_2, Adv Sci (Weinh), 7 (2020) 2000204.
[40] S.W. Verbruggen, K. Masschaele, E. Moortgat, T.E. Korany, B. Hauchecorne, J.A. Martens, S. Lenaerts, Factors driving the activity of commercial titanium dioxide powders towards gas phase photocatalytic oxidation of acetaldehyde, Catalysis Science & Technology, 2 (2012).

[41] X.-Q. Gong, A. Selloni, First-principles study of the structures and energetics of stoichiometric brookiteTiO2surfaces, Physical Review B, 76 (2007).
[42] T. Ohno, T. Higo, H. Saito, S. Yuajn, Z. Jin, Y. Yang, T. Tsubota, Dependence of photocatalytic activity on aspect ratio of a brookite TiO_2 nanorod and drastic improvement in visible light responsibility of a brookite TiO_2 nanorod by site-selective modification of Fe^{3+} on exposed faces, Journal of Molecular Catalysis A: Chemical, 396 (2015) 261-267.
[43] J. Jin, J. Luo, L. Zan, T. Peng, One-Pot Synthesis of Cu-Nanocluster-Decorated Brookite TiO_2 Quasi-Nanocubes for Enhanced Activity and Selectivity of CO_2 Photoreduction to CH_4, Chemphyschem, 18 (2017) 3230-3239.
[44] I.A. Mkhalid, J.L.G. Fierro, R.M. Mohamed, A.A. Alshahri, Visible light driven photooxidation of imazapyr herbicide over highly efficient mesoporous $Ag/Ag_2O–TiO_2$ p-n heterojunction photocatalysts, Ceramics International, 46 (2020) 25822-25832.
[45] A. Romanchenko, M. Likhatski, Y. Mikhlin, X-ray Photoelectron Spectroscopy (XPS) Study of the Products Formed on Sulfide Minerals Upon the Interaction with Aqueous Platinum (IV) Chloride Complexes, Minerals, 8 (2018).

[46] Burgeth. G, K. H, Photocatalytic and photoelectrochemical properties of titania/ chloroplatinate(IV), Coordination Chemistry Reviews, 230 (2002) 41-47.

[47] W. Macyk, K. Szaciłowski, G. Stochel, M. Buchalska, J. Kuncewicz, P. Łabuz, Titanium(IV) complexes as direct TiO2 photosensitizers, Coordination Chemistry Reviews, 254 (2010) 2687-2701.

[48] Macyk. W, K. H, Photosensitization of Crystalline and Amorphous Titanium Dioxide by Platinum (IV) Chloride Surface Complexes, Chemistry-A European Journal, 7 (2001) 1862-1867.

[49] A.P. Grosvenor, B.A. Kobe, M.C. Biesinger, N.S. McIntyre, Investigation of multiplet splitting of Fe 2p XPS spectra and bonding in iron compounds, Surface and Interface Analysis, 36 (2004) 1564-1574.

[50] L. Shen, Y. Cao, Z. Du, W. Zhao, K. Lin, L. Jiang, Illuminate the active sites of γ-FeOOH for low-temperature desulfurization, Applied Surface Science, 425 (2017) 212-219.

[51] X.-q. Li, W.-x. Zhang, Iron Nanoparticles: the Core-Shell Structure and Unique Properties for Ni(II) Sequestration, Langmuir, 22 (2006) 4638-4642.

[52] G.V. Nano, T.J. Strathmann, Ferrous iron sorption by hydrous metal oxides, J Colloid Interface Sci, 297 (2006) 443-454.

[53] Z. Zhang, P. Fenter, L. Cheng, N. C. Sturchio, M. J. Bedzyk, M. Pr˘edota, A. Bandura, J. D. Kubicki, S. N. Lvov, P. T. Cummings, A. A. Chialvo, M. K. Ridley, P. Be´ne´zeth, L. Anovitz, D.A. Palmer, M. L. Machesky, a.D.J. Wesolowski, Ion Adsorption at the Rutile-Water Interface: Linking Molecular and Macroscopic Properties, Langmuir, 20 (2004) 4954-4969.

[54] T. Hiemstra, W.H. van Riemsdijk, Adsorption and surface oxidation of Fe(II) on metal (hydr)oxides, Geochimica et Cosmochimica Acta, 71 (2007) 5913-5933.

[55] E. Piera, M.I. Tejedor-Tejedor, M.E. Zorn, M.A. Anderson, Relationship concerning the nature and concentration of Fe(III) species on the surface of TiO2 particles and photocatalytic activity of the catalyst, Applied Catalysis B: Environmental,

46 (2003) 671-685.

[56] F.J. Gracia, J.T. Miller, A.J. Kropf, E.E. Wolf, Kinetics, FTIR, and Controlled Atmosphere EXAFS Study of the Effect of Chlorine on Pt-Supported Catalysts during Oxidation Reactions, Journal of Catalysis, 209 (2002) 341-354.

[57] H. Eidsvag, S. Bentouba, P. Vajeeston, S. Yohi, D. Velauthapillai, TiO_2 as a Photocatalyst for Water Splitting-An Experimental and Theoretical Review, Molecules, 26 (2021).

[58] Huogen Yu, Hiroshi Irie, Yoshiki Shimodaira, Yasuhiro Hosogi, Yasushi Kuroda, Masahiro Miyauchi, K. Hashimoto, An Efficient Visible-Light-Sensitive Fe(III)-Grafted TiO2 Photocatalyst, J. Phys. Chem. C, 114 (2010) 16481-16487.

[59] Jina Choi, Hyunwoong Park, M.R. Hoffmann, Effects of Single Metal-Ion Doping on the Visible-Light Photoreactivity of TiO_2, J. Phys. Chem. C, 114 (2010) 783-792.

[60] Alexis Markovits, Adil Fahmi, C. Minot, A theoretical study of CO_2 adsorption on TiO_2, Journal of Molecular Structure (Theochem), 371 (1996) 219-235.

[61] Y.-H. Lin, C.-H. Weng, J.-H. Tzeng, Y.-T. Lin, Adsorption and Photocatalytic Kinetics of Visible-Light Response N-Doped TiO_2 Nanocatalyst for Indoor Acetaldehyde Removal under Dark and Light Conditions, International Journal of Photoenergy, 2016 (2016) 1-9.

[62] Y. Ma, Q. Tang, W.-Y. Sun, Z.-Y. Yao, W. Zhu, T. Li, J. Wang, Assembling ultrafine TiO_2 nanoparticles on UiO-66 octahedrons to promote selective photocatalytic conversion of CO_2 to CH_4 at a low concentration, Applied Catalysis B: Environmental, 270 (2020).

[63] Fan Zuo, Le Wang, Tao Wu, Zhenyu Zhang, Dan Borchardt, P. Feng, Self-Doped Ti^{3+} Enhanced Photocatalyst for Hydrogen Production under Visible Light, J. Am. Chem. Soc., 132 (2010) 11856-11857.

[64] X. Wang, Y. Li, X. Liu, S. Gao, B. Huang, Y. Dai, Preparation of Ti^{3+} self-doped TiO2 nanoparticles and their visible light photocatalytic activity, Chinese Journal of Catalysis, 36 (2015) 389-399.

[65] G. I. STRAGUZZI, H. R. ADURIZ, C.E. GIGOLA, Redispersion of Platinum on

Alumina Support, JOURNAL OF CATALYSIS, 66 (1980) 171-183.

[66] E. Marceau, H. Lauron-Pernot, M. Che, Influence of the Metallic Precursor and of the Catalytic Reaction on the Activity and Evolution of Pt(Cl)/δ-Al_2O_3 Catalysts in the Total Oxidation of Methane, Journal of Catalysis, 197 (2001) 394-405.

[67] T. Ohno., D. Haga., K. Fujihara., K. Kaizaki., M. Matsumura., Unique Effects of Iron(III) Ions on Photocatalytic and Photoelectrochemical Properties of Titanium Dioxide, The Journal of Physical Chemistry B, 101 (1997) 6415-6419.

[68] T. Hirakawa, K. Yawata, Y. Nosaka, Photocatalytic reactivity for O_2^- and OH radical formation in anatase and rutile TiO_2 suspension as the effect of H_2O_2 addition, Applied Catalysis A: General, 325 (2007) 105-111.

[69] H. Kim, W. Choi, Effects of surface fluorination of TiO_2 on photocatalytic oxidation of gaseous acetaldehyde, Applied Catalysis B: Environmental, 69 (2007) 127-132.

[70] J.-H. Xu, F. Shiraishi, Photocatalytic decomposition of acetaldehyde in air over titanium dioxide, Journal of Chemical Technology and Biotechnology, 74 (1999) 1096-1100.

Section 3. H_2 and CH_4 production from Acetic acid reforming over metal loaded brookite TiO_2 in Ar atmosphere

Abstract

Brookite TiO_2 was reported to have stronger ability for organic compounds degradation than anatase and rutile, which may cause by stronger O_2 adsorption for brookite. Furthermore, brookite TiO_2 is easy for acetic acid and acetone adsorption than anatase. Pt, thought to be able to promote the charge separation, was used as the co-catalyst. The photocatalytic activity of acetic acid reforming was evaluated by detecting the production rate of CH_4 and H_2. Some other normal metals (Ag, Au, Ni, Cu) were loaded on the surface of TiO_2 as well. The Pt modification was the most suitable elements for acetic acid reforming. Furthermore, the optimal amount of loaded Pt is 0.4wt% (: $mTiO_2$). The influence of different valence state of Pt modification was researched as well. The Pt0 was estimated to be the best valence state for CH_4 and H_2 production from acetic acid reforming. The XPS indicated Pt^{2+} and Pt^{4+} will gradually be reduced to Pt0. And Pt0-loaded TiO_2 shows the good stability. The Pt0/brookite TiO_2 showed much better photocatalytic activity for acetic acid reforming. At the time, rutile TiO_2 has no efficiency for acetic acid reforming.

Key words

Metal modification, brookite TiO_2, photo-Kolbe reaction

3.1 Introduction

It was reported that only 2.5% of water in the world is fresh water. And only 0.007% fresh water is available and can be used directedly.[1] Industrial, agricultural production and people's daily life consume massive water resources and discharge wastewater.[2] According to reports, there are still 1.1 billion people in the world who do not have

access to clean drinking water.[3] Among these discharged wastewaters, organic pollutants are one of the important components. These pollutants are closely related to many diseases such as cancer.[4-6] Therefore, the removal of organic pollutants in waste water is an important topic. At present, common methods to remove organic substances in wastewater such as adsorption, membrane separation, electrochemical oxidation, etc, have been maturely used in daily life.[7-9] These methods still exist the problems of production of secondary pollution, high post-processing costs and so on.

Photocatalysis, which utilizes solar energy (a clean and recyclable energy) as the energy source, is a promising way to remove the organic compounds. Bernhard Kraeutler et al researched a photoelectric system with using the rutile TiO_2 as the electrode and succeeded converts a variety of organic acids to methane, ethane, vinyl and so on.[10-13] This reaction, which can reform organic acids to alkanes and CO_2, is name as photo-Kolbe reaction and is a very valuable reaction for recycling organic matter in wastewater.[14]

Many materials have been developed for photo-Kolbe reaction. Ailin et al. A. Ana developed a crystal-surface controlled anatase TiO_2 loaded with Cu in-situ. A stronger photocatalytic activity for photo-Kolbe reaction than commercial P25 sample was found by this material.[15] Fe was modified on P25 by the method of calcination by M. Sylwia and used for acetic acid reforming. Except CH_4 and H_2, many other alkanes were also produced during the reaction. [16] The researchers, H. Saher et al and A. Ana, respectively synthesized and compared the different kinds of metal loaded P25 TiO_2 for acetic acid reforming, and detected the yield and composition of products. They found the large value of the work function of the employed co-catalyst was found to favor H_2 evolution. And a low value of the work function promoted alkane evolution.[17, 18] Choi et al researched the pH influence for acetic acid reforming upon a Pt loaded P25 sample.[19] Currently the main photo-Kolbe reactions are based on anatase, rutile and P25. The researches of photo-Kolbe reaction upon brookite phase still rare.

TiO_2 consists of 3 kinds of phases: rutile, anatase and brookite.[20] Limited by high difficulty of preparing high purity of brookite TiO_2, brookite phase is studied relatively

less than other two phases.[21] However, it was reported that brookite TiO_2 has suitable electron trapping level compared with anatase and rutile phase, which can effectively promote electron and hole pair separation.[22] Besides, brookite TiO_2 has similar capability for O_2 adsorption as anatase phase and stronger photocatalytic activity for organic compounds degradation to CO_2.[23, 24] Compared with anatase-type TiO_2, brookite-type TiO_2 can better adsorb acetic acid (weaker than rutile-type), suggesting higher photocatalytic activity of acetic acid reforming.[25]

In this research, the photocatalytic activity of rutile, anatase and brookite (loaded with Pt0) was estimated and compared by evaluating the production of CH_4 and H_2 from acetic acid reforming. The photocatalytic activity of brookite TiO_2 (loaded with Pt) is much higher anatase and rutile. Different kinds of metals were loaded on the surface of brookite TiO_2. The Pt was proved to be the most suitable elements for both CH_4 and H_2 production. We compared photocatalytic activity of the different valence state of Pt, the Pt0 was proved to be the best state. Finally, a 0.4%Pt0/ brookite TiO_2 is proved to be better for promoting acetic acid reforming and production of CH_4 and H_2.

3.2 Experiment

3.2.1 Preparation of metal loaded TiO_2

Metal loaded brookite TiO_2 was prepared by the method of photo-deposition. 0.3g of Commercial brookite TiO_2 powder (KOJUNDO CHEMICAL LABORATORY CO), metal ions (chloroplatinic acid (10mmM, Wako), silver nitrate (Wako, super pure), hydrogen tetrachloroaurate (III) tetrahydrate (Wako), copper chloride (Wako, super pure), Nickel nitrate (Wako, super pure)), 80mL of Mill-q water and 20mL ethanol (Wako, Extra Pure, 95%) was mixed in a flask. After N_2 bubbling for 1h, the mixture solution was irradiated under a mercury lamp for 6h. The light intensity was 100 mW cm^{-2}. After photoirradiation, the resultant powder was gotten by filtration and washed by ultrapure water until conductivity below than 10 μS cm^{-1}.

3.2.2 Characterization

The crystal structure of the produced materials was analyzed by X-ray diffraction (Rigaku, MiniFlex II). Transmission electron microsocopy (TEM) was conducted using a Hitachi H-9000NAR at an accelerating voltage of 200 kV. Specific surface areas of the samples were determined by Quantachrome Nova 4200e surface area measurement. Inductively coupled plasma optical emission spectroscopy (ICP-OES; Shimadzu, ICPS-8000) was used to determine the concentrations of Pt loaded on TiO_2. UV-Vis diffuse reflectance spectra were obtained by a UV-2500PC (Shimadzu) equipped with an integrating sphere unit. X-ray photoelectron spectra (XPS) of as-prepared samples were obtained by a Thermo ESCALAB 250Xi system at room temperature using Al Kα with monochromatic radiation. PL (Photoluminescence spectroscopy) spectra of different amount of Pt-loaded TiO_2 was analyzed by using a fluorescence spectrophotometer (Jasco. Inc, FP-8500) with excitation light of 420nm.

3.2.3 Photocatalytic activity tests

The photocatalytic activity test was estimated by evaluating CH_4 and H_2 production from acetic acid reforming. First, 40mg photocatalyst powder, 20 μL (0.1vol%, 1.75×10^{-2}mol/L) acetic acid was mixed together in a quartz container. Then ultrapure water was added to adjust the volume of the mixed solution to 20mL. After Ar gas bubbling for 30min, the mixed solution was irradiated under Xenon lamp for 3h. Micro-GC (Agilent Technologies 490 Micro GC with column: 10m MS5A) was used to detected the concentration of produced gas, for example H_2, CH_4, C_2H_6 and et al. The components of acetic acid water solution were evaluated by the liquid chromatography before and after experiment.

3.3 Results and Discussion

3.3.1 Surface and Structure properties

XRD spectra of pure brookite and metallic Pt loaded brookite TiO_2 (Pt0/TiO_2) are shown in the Fig. 3-1. According to diffraction peaks of standard brookite TiO_2 (JCPDS

NO. 29-1360), no peak of rutile and anatase phase was found, indicating high purity of brookite TiO_2.[26] Metallic Pt modification on brookite TiO_2 did not result in the peak shift or formation of new diffraction peak belonging to metallic Pt. This result suggests that metallic Pt modification is not embed into the bulk of TiO_2 but loaded on the surface of brookite TiO_2.

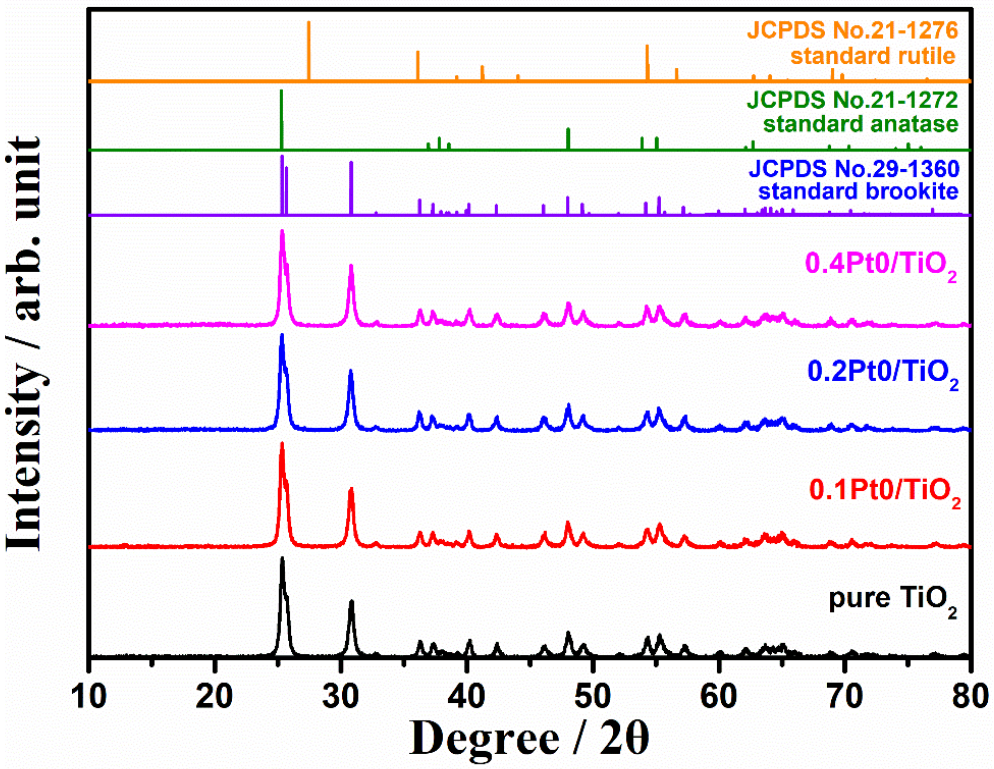

Fig. 3-1 XRD patterns of pure brookite TiO_2 and Pt(0)/TiO_2 photocatalysts.

Fig. 3-2 shows the high-resolution transmission electron microscopy (HRTEM) images of pure brookite TiO_2. The Fig. 3-2(A) shows a brookite TiO_2 nanoparticle contain a square crystal shape with pointed top head and smooth surface. The length and the width for one brookite nanorod is about 70nm and 30nm respectively. According to lattice plane imaging shown in the Fig.3-2 (B), the lattice width on the body surface of brookite nanorods of is 0.351nm, indicating the {210} facets.[27, 28] It also suggests that the top head belongs to {111} facets. Besides, the uniform lattice fringe surface indicates that the brookite TiO_2 contains a single-crystal structure.

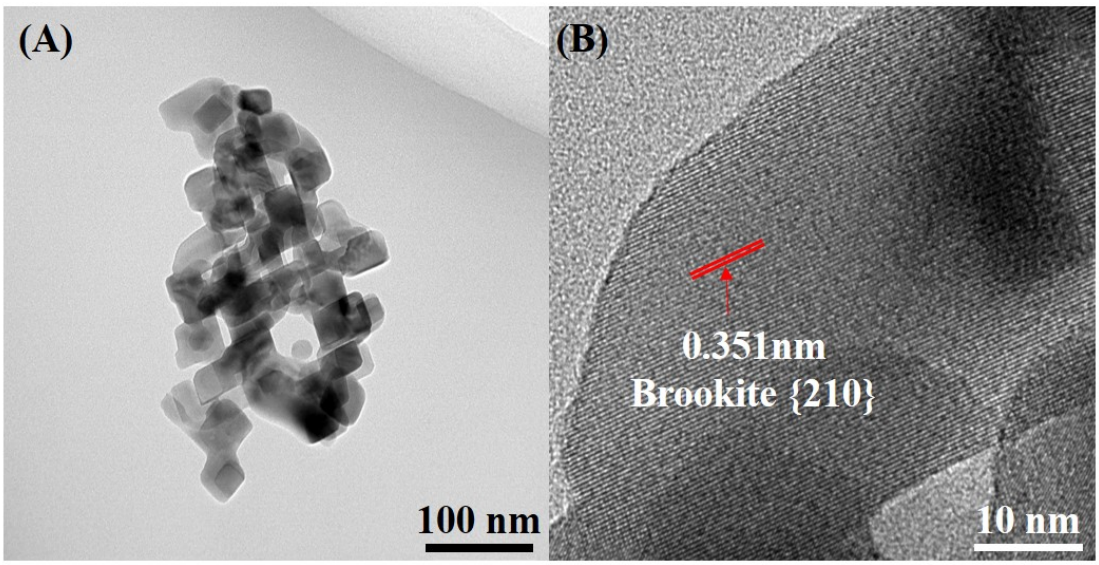

Fig. 3-2 HRTEM images of pure brookite TiO_2 sample.

For Pt-loaded brookite, the actual amount of loaded Pt is shown in the Table 3-1. The actual amount of loaded platinum was gotten by calculating the difference between the adding amount of Pt and the Pt ion in the filtrate. From the Table 3-1, all of the added Pt was loaded on the surface of TiO_2, indicating the good loading efficiency by photo-deposition. The EDX mapping images of Pt0/TiO_2 are shown in the Fig. 3-3. The TEM mapping pictures also show that Pt is successfully loaded onto the surface of TiO_2. The loaded Pt aggregates together and takes on a spherical shape. The average diameter of a Pt nanoparticle is about 5nm.

Table 3-1. Actual amounts of Pt0 deposited on the surfaces of brookite TiO_2 nanorods.

Sample name	Nominal loading amount	Actual loading amount
0.1%Pt0/TiO_2	0.1wt%	0.1wt%
0.2%Pt0/TiO_2	0.2wt%	0.2wt%
0.4%Pt0/TiO_2	0.4wt%	0.4wt%
0.6%Pt0/TiO_2	0.6wt%	0.6wt%

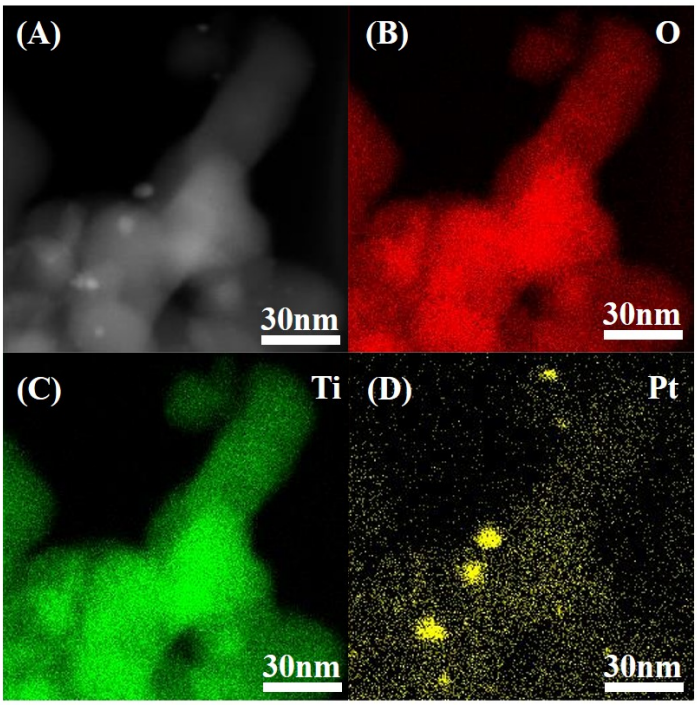

Fig. 3-3 HRTEM images of (A) Pt0-loaded brookite TiO_2 nanorods and the associated EDX elemental mapping of Pt0-loaded brookite TiO_2 nanorods (B) O, (C) Ti, (D) Pt.

3.3.2 Optical properties

Fig. 3-4 shows the UV-vis spectra of pure brookite TiO_2 and as-prepared Pt0/TiO_2. The absorbance spectra of pure brookite and all Pt0/TiO_2 samples exhibits an obvious decrease between ~370 and 380nm. The similar absorbance edges of all samples, 380nm, correspond to the band gap of about 3.3eV, indicating that metallic Pt modification don not change the valence band of photocatalyst compared with pure TiO_2. The light absorbance of different amount of Pt loaded TiO_2 increasing from 400nn to 800nm could be because of LEPR effect of Pt nanoparticles. The Fig. 3-5 shows the photostimulated luminescence (PL) spectra of pure TiO_2 and Pt0/TiO_2 for an excitation of 420nm. In semiconductors, photoexcited electron-hole pair recombination produces PL emission. PL spectroscopy is used to study the efficiency of charge carrier capture, migration, transfer and separation. From the Fig. 3-5, the weakening of the PL intensity represents the prolongation of the electron-hole recombination time, indicating that the carrier separation efficiency increases with the increase of the Pt concentration. In this experiment, the prolongation of electron-hole lifetime means that electrons and holes

have more time to participate in the oxidation reaction of acetic acid and the reduction reaction of protons, which is one of the ways to effectively improve the photocatalytic efficiency. [29]

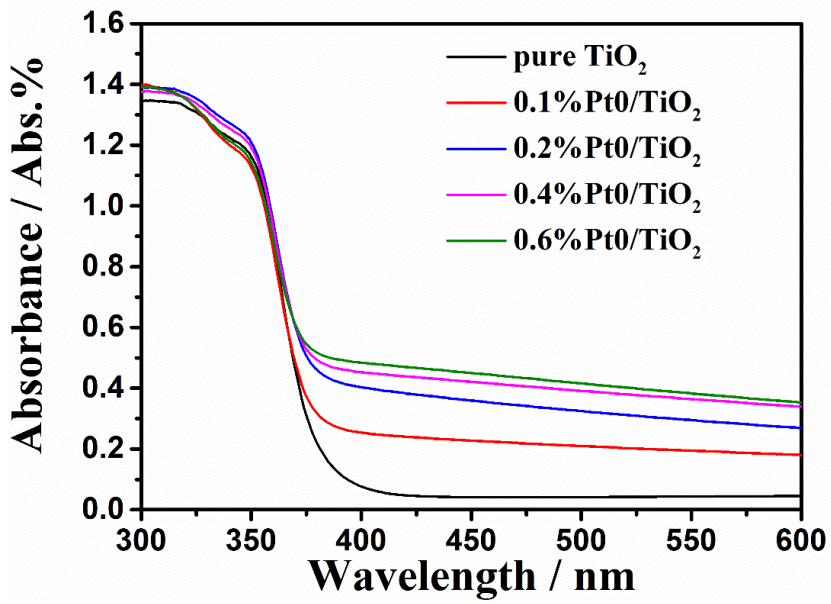

Fig. 3-4 UV-Vis diffuse absorption spectra of pure brookite TiO_2 and metallic Pt loaded TiO_2.

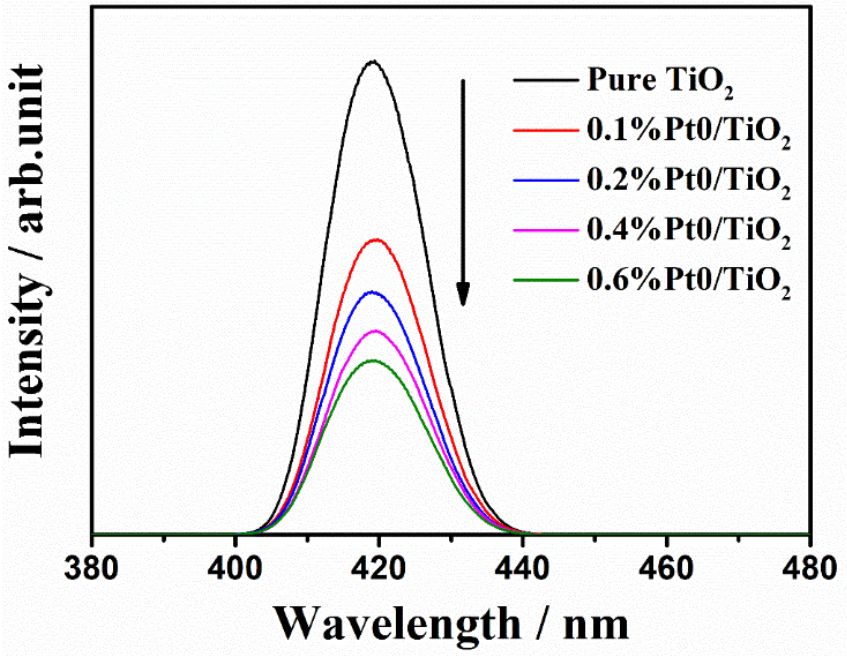

Fig. 3-5 Photostimulated luminescence (PL) spectra of pure TiO2 and metallic Pt loaded TiO_2.

3.3.3 The importance and optimal amount of Pt modification

In this experiment, 0.1vol% acetic acid (1.75×10^{-2}mol/L) was used as the raw material. Metallic Pt loaded brookite TiO_2 was used as the photocatalyst. The

photocatalytic activity of as-prepared photocatalyst samples was estimated by evaluation of production rate of produced gas. As can be seen the Fig. 3-6, putting the acetic acid solution under xenon lamp photoirradiation for 3h without photocatalyst participation, no gas products were detected, indicating that CH_4 production is not from thermal decomposition of acetic acid spontaneously. Furthermore, without photoirradiation, no gas or liquid products were detected as well. To sum up, the generation of acetic acid-reforming products is based on the photocatalytic reaction.

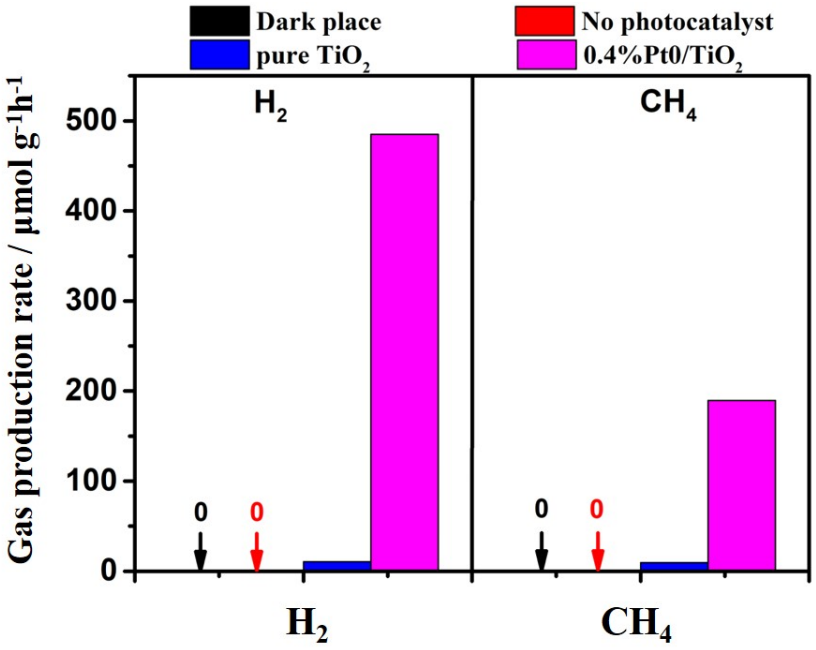

Fig. 3-6 CH_4 and H_2 production rate from 0.1vol% acetic acid reforming in dark condition, without photocatalyst and 0.1vol% acetic acid reforming over pure TiO_2 and 0.4%Pt0/TiO_2.

In this experiment, under xenon lamp photoirradiation, except H_2 and CH_4, no other kinds of gas products, such as CO, C_2H_6 and so on, were detected by using Micro-GC. As can be seen in the Fig. 3-7, after photoirradiation for 3h, no other liquid products except acetic acid was detected, indicating high selectivity for acetic acid by using Pt - loaded brookite TiO_2. BET results of pure brookite TiO_2 and as-prepared Pt0/TiO_2 samples are summarized in the Table 3-2. The specific surface area of pure brookite TiO_2 is 40.55 m^2/g. After metallic Pt0 modification, the BET of 0.1%Pt0/TiO_2,

0.2%Pt0/TiO_2, 0.4%Pt/TiO_2 and 0.6%Pt0/TiO_2 is 49.08 m^2/g, 49.01 m^2/g, 46.95 m^2/g, and 46.39 m^2/g, respectively. No obvious change of specific surface area was found, indicating that the BET change is not the impact factor for the difference of photocatalytic activity. Fig. 3-8 shows the production rate of CH_4 from 0.1vol% acetic acid reforming over different amount of Pt loaded TiO_2 in Ar atmosphere. With increasing the loaded Pt, the production rate of CH4 increases. When the loaded Pt is 0.4wt% (: TiO_2), the production rate of CH_4 is 189.6 μmol $g^{-1}h^{-1}$ and faster than that produced over other amount of Pt loaded TiO_2.

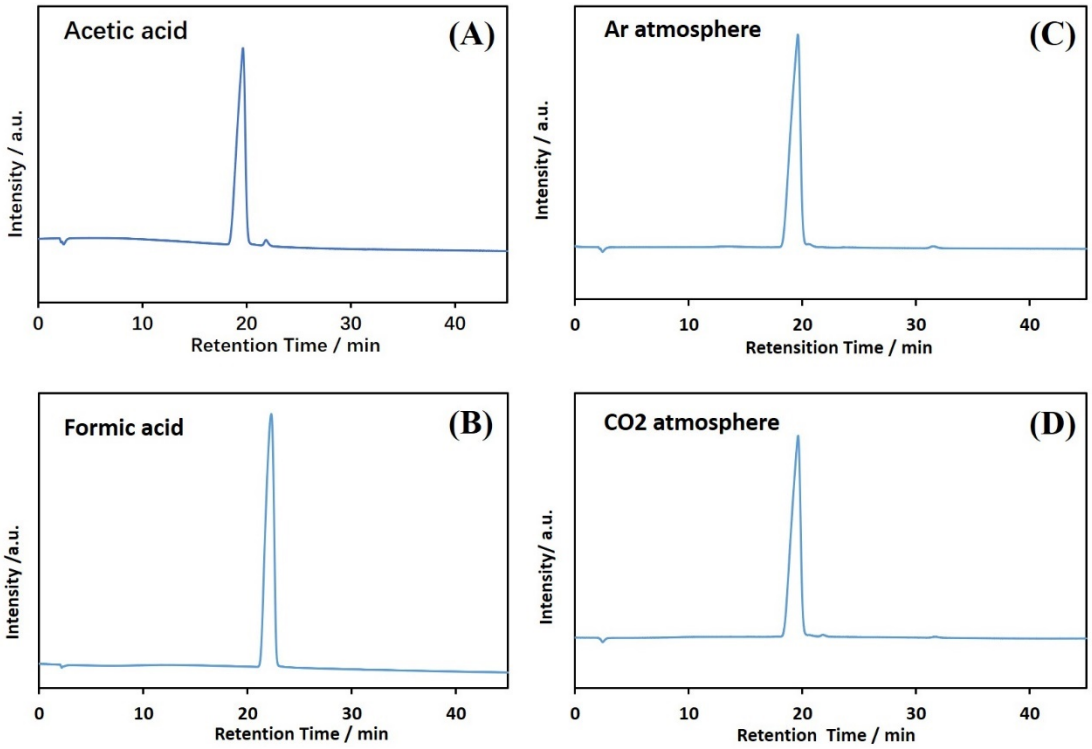

Fig. 3-7 The liquid chromatogram of (A)0.1vol% acetic acid, (B) 0.1vol% formic acid, (C) 0.1vol% acetic acid degraded over 0.4%Pt0/TiO_2 in Ar atmosphere after photoirradiation for 3h and (D) 0.1vol% acetic acid degraded over 0.4%Pt0/TiO_2 in CO_2 atmosphere after photoirradiation for 3h.

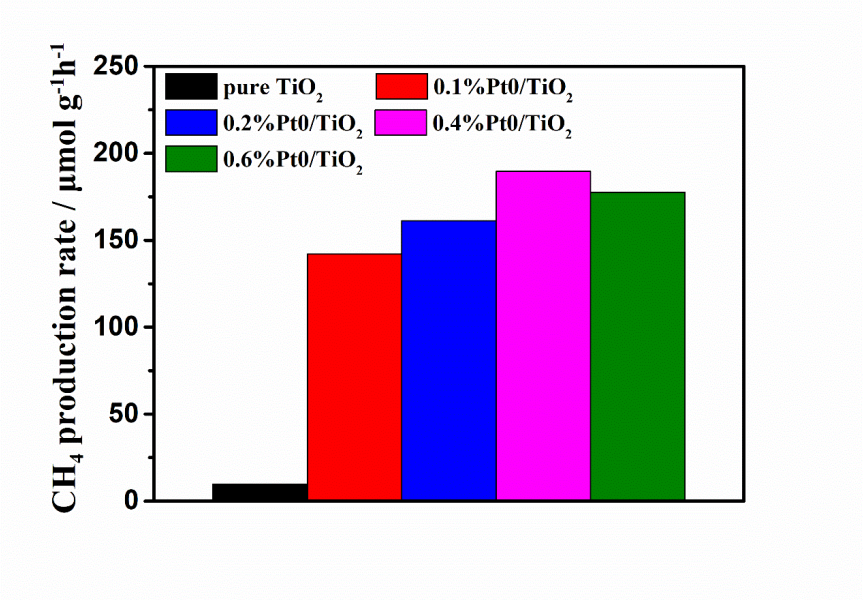

Fig. 3-8 CH_4 production rate from 0.1vol% acetic acid transformation over brookite TiO2 loaded with different amount of metallic Pt.

Table 3-2. BET of pure brookite TiO_2 and $Pt0/TiO_2$

Sample name	BET (m^2 / g)
Pure brookite	44.55
0.1%Pt0/brookite TiO_2	49.08
0.2%Pt0/brookite TiO_2	49.01
0.4%Pt0/brookite TiO_2	46.95
0.6%Pt0/brookite TiO_2	46.39
0.4%Pt0/anatase TiO_2	56.97
0.4%Pt0/anatase TiO_2	32.43

The comparison of CH_4 and H_2 production rate between pure brookite TiO_2 and 0.4%Pt0/TiO_2 is shown in the Fig. 3-6. After photoirradiation for 3h, The average rate of CH_4 and H_2 production over pure brookite is about 9.7 μmol $g^{-1}h^{-1}$ and 10.7 μmol $g^{-1}h^{-1}$, respectively. The average rate of CH_4 and H_2 production over 0.4%Pt0/TiO_2 is 189.6 μmol $g^{-1}h^{-1}$ and 485.0 μmol $g^{-1}h^{-1}$, respectively. The production rate of CH_4 and

H_2 over 0.4%Pt0/TiO_2 is much faster than pure brookite TiO_2. It is well known that Pt can act as a kind of co-catalyst to capture the electrons and promote electron-hole pairs separation, which is proved by PL spectra and shown in the Fig. 3-5.

We also compared the different valence states of Pt. As can be seen in the Fig. 3-9, the Pt0 loaded TiO_2 shows the highest photocatalytic activity for H_2 and CH_4 production produced from 0.1vol% acetic acid reforming.[30] As the valence of platinum ions increases, the production of hydrogen and methane also decreases gradually. It could be because the Pt^{4+} (or Pt^{2+}) ions capture the electrons and are reduced to Pt0. The CH_4 and H_2 production reaction by photocatalytic acetic acid reforming is shown in the following equation:

$$\boldsymbol{Photocatalyst} \xrightarrow{h\nu} \mathbf{h^+ + e^-} \quad \textbf{(1)}$$

$$\mathbf{h^+ + H_2O \rightarrow \bullet OH + H^+} \quad \textbf{(2)}$$

$$\mathbf{\bullet OH + CH3COO^- \rightarrow \bullet CH3 + OH^- + CO_2} \quad \textbf{(3)}$$

$$\mathbf{H^+ + e^- \rightarrow \bullet H} \quad \textbf{(4)}$$

$$\mathbf{\bullet CH_3 + \bullet H \rightarrow CH_4} \quad \textbf{(5)}$$

$$\mathbf{\bullet H + \bullet H \rightarrow H_2} \quad \textbf{(6)}$$

Under photoirradiation, photogenerated holes and electrons are excited and assemble at the valence band and conduction band, respectively. Photogenerated holes react with water to form •OH radical. The •OH radical then oxidizes the acetic acid to form • CH_3 radical and CO_2. Proton (H^+) gets one electron to form •H radical. A •CH_3 radical and an •H radical react with each other to form a CH_4 molecule. At the same time, two •CH_3 radicals can also react with each other to produce C_2H_6. And the two •H radicals react with each other to produce H_2.

The Fig. 3-10 shows the XPS spectra of Pt0/TiO_2, Pt^{2+}/TiO_2 and Pt^{4+}/TiO_2 before and after photoirradiation in aqueous acetic acid solution. From Fig. 3-10 A, the existence of +2 and +4 of Pt could be caused by incomplete reduction in the preparation process. After photoirradiation, the +4 of Pt disappeared and continue to be reduced. In general, the composition of Pt0 and Pt^{2+} does not change much, showing a certain stability. As

can be seen in the Fig. 3-10C, before photoirradiation, the XPS spectra of Pt4f of Pt^{2+}-loaded TiO_2 mainly consists of +2. From Fig. 3-10E, the valence state of Pt in Pt^{4+}-loaded TiO_2 is mainly consists of +4. No other elements were detected. From Fig.3 D, after photoirradiation for 3h, the part of Pt in Pt^{2+}/TiO_2 was reduced to Pt0. For Pt^{4+}/TiO_2, after photoirradiation for 3h, Pt4+ was reduced to be both +2 and 0 of Pt.[31-33] The reduction of Pt^{2+} (and Pt^{4+} ion) will capture and consume the electrons, which will compete with proton reduction for electrons. This could be the reason why the production of H_2 and CH_4 over Pt^{2+} and Pt^{4+} ion loaded TiO_2 is much less than that over Pt0-loaded TiO_2.

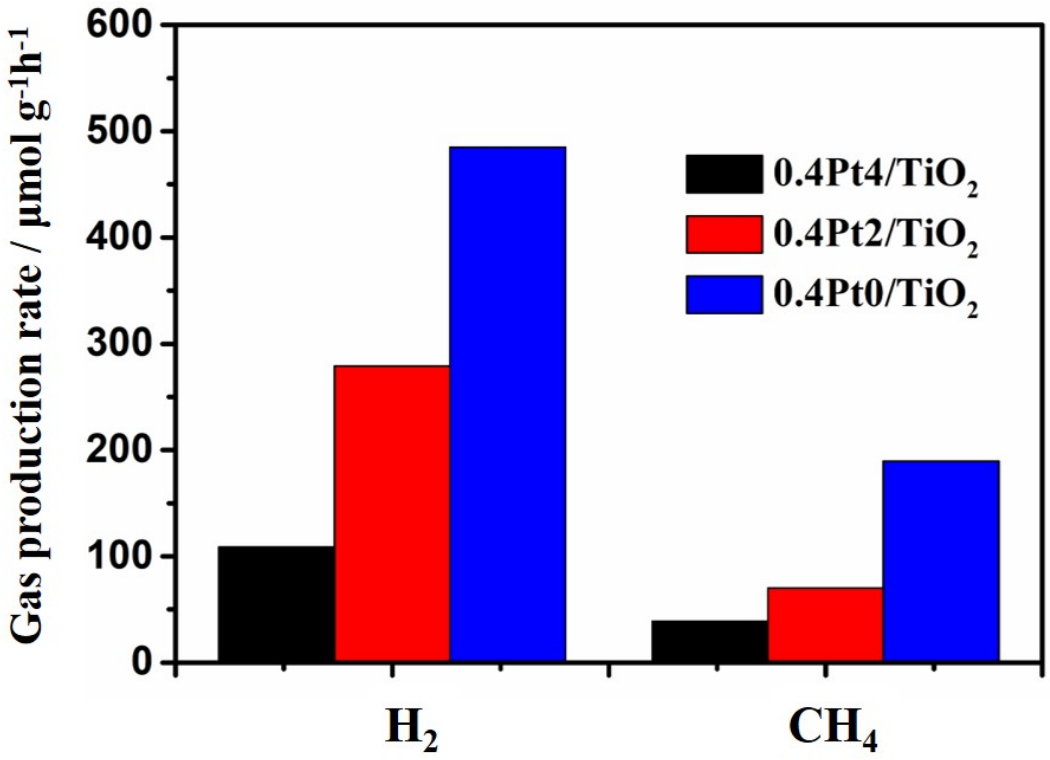

Fig. 3-9 CH_4 and H_2 production rate from 0.1vol% acetic acid reforming over brookite TiO_2 loaded with 0.4wt% Pt^{4+} ion, 0.4wt% Pt^{2+} ion and 0.4wt% Pt0.

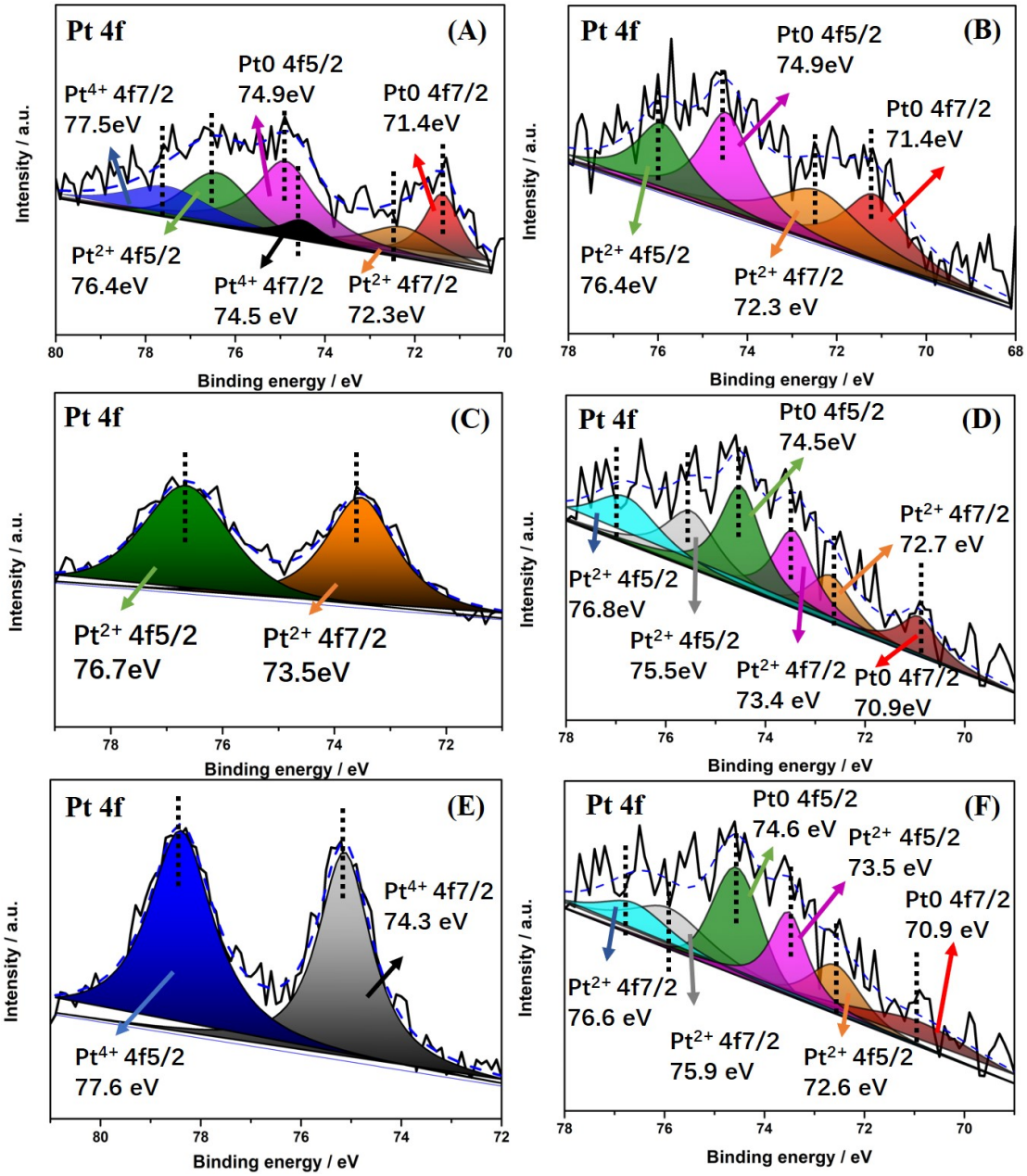

Fig. 3-10 XPS spectra of Pt4f of 0.4%Pt0/TiO_2: (A) before photoirradiation and (B) after photoirradiation. 0.4%Pt^{2+}/TiO_2: (C) before photoirradiation and (D) after photoirradiation, 0.4%Pt^{4+}/TiO_2: (E) before photoirradiation and (F) after photoirradiation.

The other kinds of metal on the surface of brookite TiO_2. The photocatalytic activity was evaluated by detecting the production rate of CH_4 and H_2 from 0.1vol% reforming in Ar atmosphere. As can be seen in the Fig. 3-11, the Au-loaded TiO_2 shows the higher selectivity of H_2 production, which could be because of the promotion of •OH radical

production and •CH_3 radical oxidation.[34] Even though the production of CH4 over Cu-loaded TiO2 is lower than Pt-loaded TiO_2, the Cu-loaded TiO_2 shows the high selectivity of CH_4 production. The Cu was reported to be the active sites of •CH_3 radical and H^+ reduction for CO_2 reduction reaction, which could be the reason for high selectivity of CH_4 production from acetic acid reforming over Cu-loaded brookite TiO_2.[35] The photocatalytic activity of Ag and Ni loaded TiO_2 is pretty low and almost has no efficiency for acetic acid reforming. Compared with other metal loaded TiO_2, Pt0-loaded TiO_2 shows much faster rate for the production of CH_4 and H_2, indicating the better photocatalytic activity for acetic acid reforming.

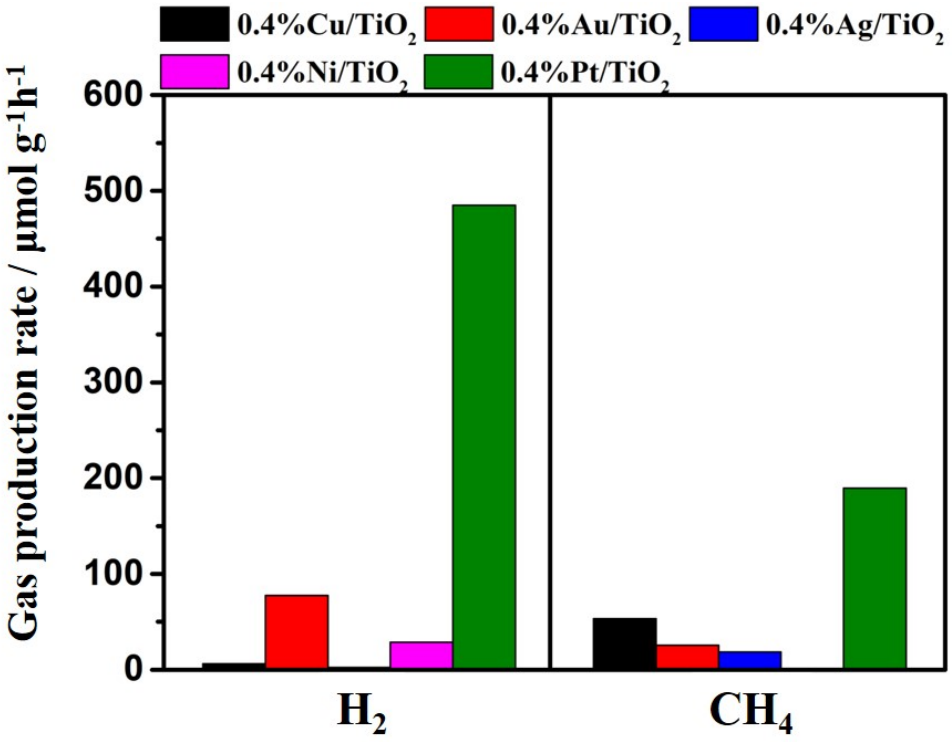

Fig. 3-11. CH_4 and H_2 production rate from 0.1vol% acetic acid transformation over brookite TiO_2 respectively loaded with Cu, Au, Ag, Ni and Pt.

Furthermore, we also loaded 0.4wt% Pt on different phases of TiO_2 (rutile, anatase and brookite), respectively. The BET of Pt0/TiO_2 is shown in the Table. 3-2. The specific surface area of Pt0-loaded anatase TiO_2 is 56.97 m^2/g and bigger than Pt0-

loaded brookite TiO_2(46.95 m^2/g). And specific surface area of Pt0-loaded rutile TiO_2 is 32.43 m^2/g and smaller than Pt0-loaded brookite TiO_2 (46.95 m^2/g). Fig. 3-12 shows the production rate of CH_4 and H_2 over 0.4wt% Pt loaded rutile, anatase and brookite TiO_2. The production rate of CH_4 and H_2 over anatase TiO_2 sample is 81.9 μmol $g^{-1}h^{-1}$ and 161.6 μmol $g^{-1}h^{-1}$, respectively. The production rate is much slower than that over brookite TiO_2 sample. For Pt0/rutile sample, no CH_4 or H_2 was detected, indicating that rutile TiO_2 cannot promote the decomposition of acetic acid. Besides, unlike some reference, only H_2 and CH_4 was detected by 0.4Pt0/brookite TiO_2, suggesting high selectivity.[36-38] Fig. 3-13 shows the concentration of acetic acid after stirring with different phases of TiO_2 for 24 hours. The remaining amount of acetic acid in anatase, brookite and rutile TiO_2 mixed solution is 8.7%, 1.6% and 1.5%, respectively. The relatively poor adsorption capacity for anatase TiO_2 could be reason for worse performance of acetic acid reforming. For rutile TiO_2, the deeper electron capture layer is not conducive to hot electrons participating in the reduction reaction of protons (generating •H).[22] As a result, no H_2 and CH_4 was detected in this experiment.

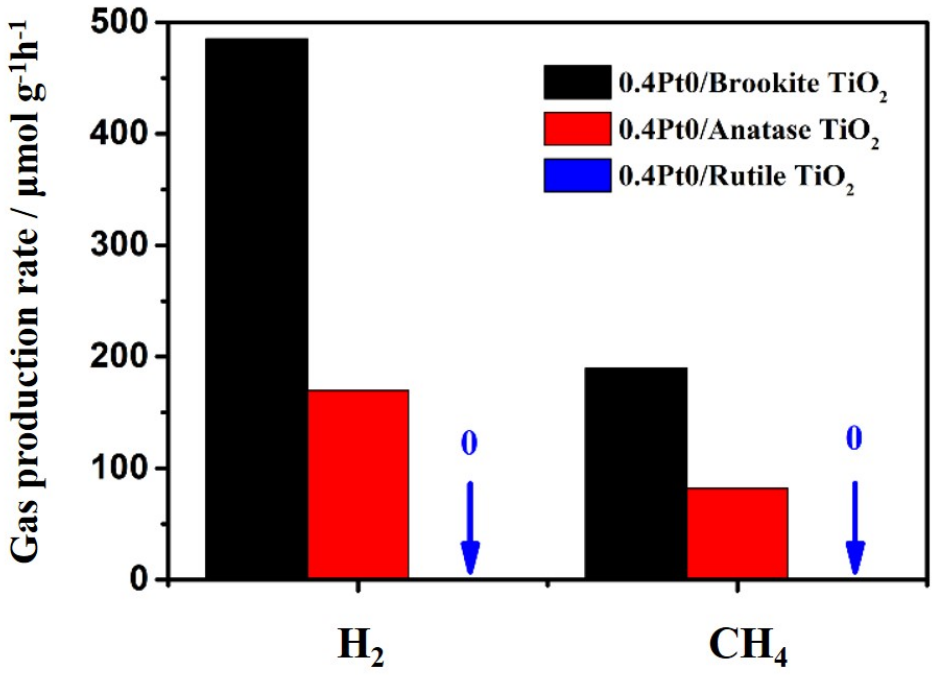

Fig. 3-12 Production rate of CH_4 and H_2 from 0.1vol% acetic acid transformation over 0.4%Pt0-loading different kinds of TiO_2 in Ar atmosphere.

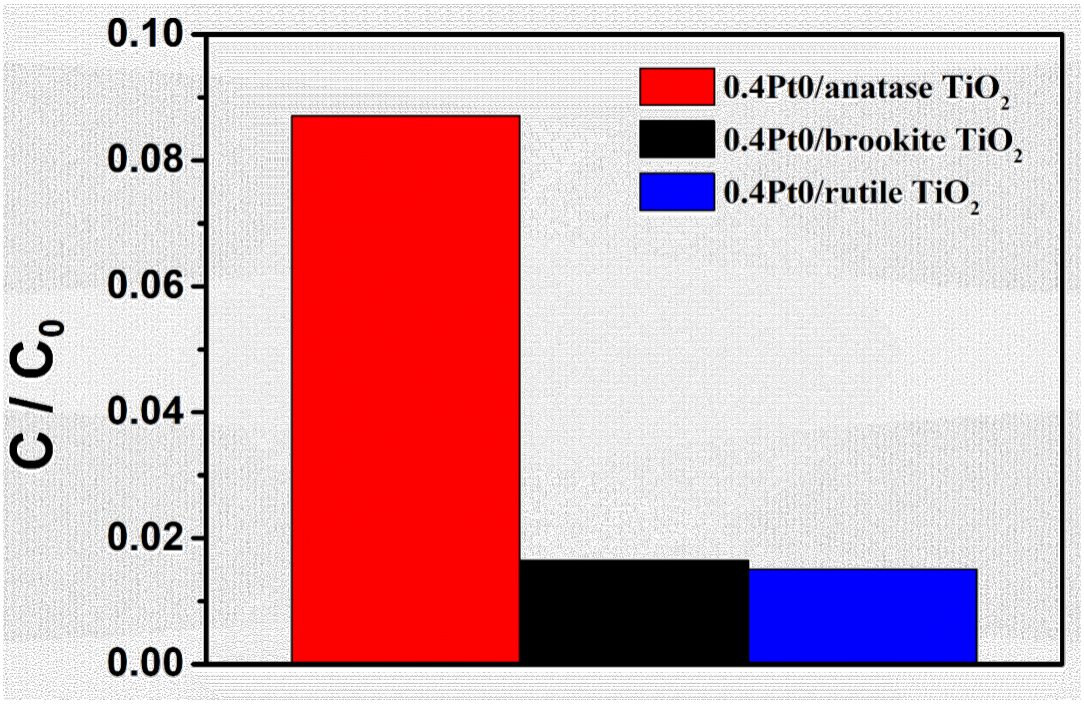

Fig. 3-13 Concentration of acetic acid after stirring with different phases of TiO_2 for 24 hours.

3.4 Conclusion

In conclusion, Pt is proved to be more suitable than some normal metal (Au, Ag, Cu and Ni) for degrading acetic acid to CH_4 and H_2 owing to its high efficiency of promoting charge separation. In the 3 valence states of Pt, Pt0 was proved to be the best valence state for the production of CH_4 and H_2. Although brookite has a smaller specific surface area than anatase (similar with rutile), brookite phase has higher activity for H_2 and CH_4 production and acetic acid reforming.

Reference

[1] L. Petersen, M. Heynen, F. Pellicciotti, Freshwater Resources: Past, Present, Future, International Encyclopedia of Geography2019, pp. 1-12.

[2] M.J. Gomez, S. Herrera, D. Sole, E. Garcia-Calvo, A.R. Fernandez-Alba, Spatio-temporal evaluation of organic contaminants and their transformation products along a

river basin affected by urban, agricultural and industrial pollution, Sci Total Environ, 420 (2012) 134-145.
[3] P. Rajasulochana, V. Preethy, Comparison on efficiency of various techniques in treatment of waste and sewage water - A comprehensive review, Resource-Efficient Technologies, 2 (2016) 175-184.
[4] R. Kishor, D. Purchase, G.D. Saratale, R.G. Saratale, L.F.R. Ferreira, M. Bilal, R. Chandra, R.N. Bharagava, Ecotoxicological and health concerns of persistent coloring pollutants of textile industry wastewater and treatment approaches for environmental safety, Journal of Environmental Chemical Engineering, 9 (2021).
[5] E.A. Noman, A.A.S. Al-Gheethi, B.A. Talip, R.M.S. Radin Mohamed, H. Nagao, A.H. Mohd Kassim, Xenobiotic Organic Compounds in Greywater and Environmental Health Impacts, Management of Greywater in Developing Countries2019, pp. 89-108.
[6] H. Bylinski, J. Gebicki, J. Namiesnik, Evaluation of Health Hazard Due to Emission of Volatile Organic Compounds from Various Processing Units of Wastewater Treatment Plant, Int J Environ Res Public Health, 16 (2019).
[7] Y.-h. Li, F.-m. Chang, B. Huang, Y.-p. Song, H.-y. Zhao, K.-j. Wang, Activated carbon preparation from pyrolysis char of sewage sludge and its adsorption performance for organic compounds in sewage, Fuel, 266 (2020).
[8] J. Quiroz Torres, S. Royer, J.P. Bellat, J.M. Giraudon, J.F. Lamonier, Formaldehyde: catalytic oxidation as a promising soft way of elimination, ChemSusChem, 6 (2013) 578-592.
[9] Z. Liang, J. Wang, Y. Zhang, C. Han, S. Ma, J. Chen, G. Li, T. An, Removal of volatile organic compounds (VOCs) emitted from a textile dyeing wastewater treatment plant and the attenuation of respiratory health risks using a pilot-scale biofilter, Journal of Cleaner Production, 253 (2020).
[10] B Kraeutler, A. Bard, The photoassisted decarboxylation of acetate on n-type rutile electrodes the photo-Kolbe reaction, Nouv. J. Chim, 194 (1979) 1-25.
[11] Bernhard Kraeutler, A.J. Bard, Photoelectrosynthesis of ethane from acetate ion at an n-type titanium dioxide electrode. The photo-Kolbe reaction, J. Am. Chem. Soc., 99

(1977) 7729–7731.

[12] Bernhard Kraeutler, Calvin D. Jaeger, A.J. Bard, Direct observation of radical intermediates in the photo-Kolbe reaction - heterogeneous photocatalytic radical formation by electron spin resonance, J. Am. Chem. Soc., 100 (1978) 4903-4905.

[13] B. Kraeutler, A.J.B. , Heterogeneous photocatalytic decomposition of saturated carboxylic acids on titanium dioxide powder. Decarboxylative route to alkanes, J. Am. Chem. Soc., 100 (1978) 5985-5992.

[14] S. Sato, Photo-Kolbe reaction at gas-solid interfaces, J. Phys. Chem. , 87 (1983) 3531-3537.

[15] A. Amorós-Pérez, L. Cano-Casanova, M.Á. Lillo-Ródenas, M.C. Román-Martínez, Cu/TiO 2 photocatalysts for the conversion of acetic acid into biogas and hydrogen, Catalysis Today, 287 (2017) 78-84.

[16] S. Mozia, A. Heciak, A.W. Morawski, Photocatalytic acetic acid decomposition leading to the production of hydrocarbons and hydrogen on Fe-modified TiO2, Catalysis Today, 161 (2011) 189-195.

[17] S. Hamid, R. Dillert, D.W. Bahnemann, Photocatalytic Reforming of Aqueous Acetic Acid into Molecular Hydrogen and Hydrocarbons over Co-catalyst-Loaded TiO2: Shifting the Product Distribution, The Journal of Physical Chemistry C, 122 (2018) 12792-12809.

[18] A. Amoros-Perez, L. Cano-Casanova, A. Castillo-Deltell, M.A. Lillo-Rodenas, M.D.C. Roman-Martinez, TiO(2) Modification with Transition Metallic Species (Cr, Co, Ni, and Cu) for Photocatalytic Abatement of Acetic Acid in Liquid Phase and Propene in Gas Phase, Materials (Basel), 12 (2018).

[19] S. Hamid, I. Ivanova, T.H. Jeon, R. Dillert, W. Choi, D.W. Bahnemann, Photocatalytic conversion of acetate into molecular hydrogen and hydrocarbons over Pt/TiO 2 : pH dependent formation of Kolbe and Hofer-Moest products, Journal of Catalysis, 349 (2017) 128-135.

[20] D. Reyes-Coronado, G. Rodriguez-Gattorno, M.E. Espinosa-Pesqueira, C. Cab, R. de Coss, G. Oskam, Phase-pure TiO(2) nanoparticles: anatase, brookite and rutile,

Nanotechnology, 19 (2008) 145605.

[21] ZHENG YANQING, SHI ERWEI, CUI SUXIAN, LI WENJUN, H. XINGFANG, Hydrothermal preparation and characterization of brookite-type

TiO_2 nanocrystallites, JOURNAL OF MATERIALS SCIENCE LETTERS, 19 (2000) 1445.

[22] J.J.M. Vequizo, H. Matsunaga, T. Ishiku, S. Kamimura, T. Ohno, A. Yamakata, Trapping-Induced Enhancement of Photocatalytic Activity on Brookite TiO_2 Powders: Comparison with Anatase and Rutile TiO_2 Powders, ACS Catalysis, 7 (2017) 2644-2651.

[23] H.T.T. Tran, H. Kosslick, M.F. Ibad, C. Fischer, U. Bentrup, T.H. Vuong, L.Q. Nguyen, A. Schulz, Photocatalytic Performance of Highly Active Brookite in the Degradation of Hazardous Organic Compounds Compared to Anatase and Rutile, Applied Catalysis B: Environmental, 200 (2017) 647-658.

[24] M.M. Rodriguez, X. Peng, L. Liu, Y. Li, J.M. Andino, A Density Functional Theory and Experimental Study of CO_2 Interaction with Brookite TiO_2, The Journal of Physical Chemistry C, 116 (2012) 19755-19764.

[25] A. Mattsson, L.O. sterlund, Adsorption and Photoinduced Decomposition of Acetone and Acetic Acid on Anatase, Brookite, and Rutile TiO_2 Nanoparticles, J. Phys. Chem. C, 114 (2010) 14121-14132.

[26] M. Bellardita, A. Di Paola, B. Megna, L. Palmisano, Absolute crystallinity and photocatalytic activity of brookite TiO2 samples, Applied Catalysis B: Environmental, 201 (2017) 150-158.

[27] M. Zhao, H. Xu, H. Chen, S. Ouyang, N. Umezawa, D. Wang, J. Ye, Photocatalytic reactivity of {121} and {211} facets of brookite TiO2 crystals, Journal of Materials Chemistry A, 3 (2015) 2331-2337.

[28] H. Lin, L. Li, M. Zhao, X. Huang, X. Chen, G. Li, R. Yu, Synthesis of high-quality brookite TiO2 single-crystalline nanosheets with specific facets exposed: tuning catalysts from inert to highly reactive, J Am Chem Soc, 134 (2012) 8328-8331.

[29] S.H. Hsieh, W.J. Chen, C.T. Wu, Pt-TiO_2/graphene photocatalysts for degradation of AO7 dye under visible light, Applied Surface Science, 340 (2015) 9-17.

[30] S. Ngo, L.M. Betts, F. Dappozze, M. Ponczek, C. George, C. Guillard, Kinetics and mechanism of the photocatalytic degradation of acetic acid in absence or presence of O_2, Journal of Photochemistry and Photobiology A: Chemistry, 339 (2017) 80-88.

[31] Z. Wu, Z. Sheng, Y. Liu, H. Wang, J. Mo, Deactivation mechanism of PtOx/TiO_2 photocatalyst towards the oxidation of NO in gas phase, J Hazard Mater, 185 (2011) 1053-1058.

[32] E.I. Vovk, A.V. Kalinkin, M.Y. Smirnov, I.O. Klembovskii, V.I. Bukhtiyarov, XPS Study of Stability and Reactivity of Oxidized Pt Nanoparticles Supported on TiO2, The Journal of Physical Chemistry C, 121 (2017) 17297-17304.

[33] B.D. Mukri, U.V. Waghmare, M.S. Hegde, Platinum Ion-Doped TiO2: High Catalytic Activity of Pt2+ with Oxide Ion Vacancy in $Ti^{4+}{}_{1-x}Pt^{2+}{}_{x}O^{2-}{}_{x}$ Compared to Pt^{4+} without Oxide Ion Vacancy in Ti4+1–xPt4+xO2, Chemistry of Materials, 25 (2013) 3822-3833.

[34] M. Zhou, J. Zhang, B. Cheng, H. Yu, Enhancement of Visible-Light Photocatalytic Activity of Mesoporous Au-TiO2Nanocomposites by Surface Plasmon Resonance, International Journal of Photoenergy, 2012 (2012) 1-10.

[35] S. Ali, J. Lee, H. Kim, Y. Hwang, A. Razzaq, J.-W. Jung, C.-H. Cho, S.-I. In, Sustained, photocatalytic CO_2 reduction to CH_4 in a continuous flow reactor by earth-abundant materials: Reduced titania-Cu2O Z-scheme heterostructures, Applied Catalysis B: Environmental, 279 (2020).

[36] S. Mozia, A. Kulagowska, A.W. Morawski, Formation of combustible hydrocarbons and H_2 during photocatalytic decomposition of various organic compounds under aerated and deaerated conditions, Molecules, 19 (2014) 19633-19647.

[37] S. Mozia, Generation of Useful Hydrocarbons and Hydrogen during Photocatalytic Decomposition of Acetic Acid on CuO/Rutile Photocatalysts, International Journal of Photoenergy, 2009 (2009) 1-8.

[38] S. Mozia, A. Heciak, A.W. Morawski, The influence of physico-chemical

properties of TiO_2 on photocatalytic generation of C1-C3 hydrocarbons and hydrogen from aqueous solution of acetic acid, Applied Catalysis B: Environmental, 104 (2011) 21-29.

Section 4. Higher efficiency of Acetic acid reforming over $Pt0/TiO_2$ in the condition of CO_3^{2-} cations

Abstract

CO_3^{2-}cations was reported to be able to react with •OH radical and generates a $\bullet CO_3^-$ radical with a lower oxidation potential. In this work, photo-Kolbe reaction was researched over 0.4Pt0-laoded brookite-TiO_2 photocatalyst. Ar and CO_2 was used as the shielding gas for preventing acetic acid being oxidized by O_2. Compared with the Ar atmosphere, the more CH_4 and H_2 in CO_2 atmosphere was detected. More •CH_3 radical was produced in the CO_2 atmosphere and checked by ESR analysis. With introducing CO_3^{2-}(Na_2CO_3) into the solution, the yield of CH_4 was found to be increased compared to no addition of CO_3^{2-} in the solution. It suggests that $\bullet CO_3^-$ radicals produced from CO_3^{2-} oxidation during photoirradiation, played an important role in promoting the selective oxidation of acetic acid.

Keyword

Metallic Pt, brookite TiO_2, photo-Kolbe reaction, CO_3^{2-}cations

4.1 Introduction

In earth, 3% of earth water is fresh water. And only 0.07% of earth water is available.[1] Fresh water is a kind of importance and scarce source for human being. With the development of industrial manufacture, agricultural production and society, the problem of water pollution is becoming more and more serious. It was reported that 1 billion people all of the world live in the condition of unclean water.[2] The organic compounds in the waste water are thought to correspond with many kinds of diseases, such as cancer and so on.[3-6] Lots of effort was made to remove organic compounds in waste water, for example adsorption, condensation, catalyst, electrochemical oxidation, membrane separation, biodegradation and et al.[7-12] However, the disadvantages of these methods like high cost, high energy consumption, generation of secondary

pollutants and et al, restrict the wide use.

Under photoirradiation, O_2 in the air can get one electron to for superoxide ion and then react with water to be •OH radical, which is thought to be a strong oxidizing substance and can finally degrade organic compounds to CO_2 and water.[13-15] This process can efficiently remove the organic compounds in the waste water. However, the acetic acid degradation in O_2 atmosphere also results in a waste of resources.[16] Different from complete degradation under oxygen conditions, under inert atmosphere conditions, by the photo-Kolbe reaction, some organic compounds with complex species in water that are difficult to separate and purify can be converted into single, easily collected gaseous organic compounds. So as to realize the recycling of resources. [17, 18]

Kazuhiro et al found the addition of CO_3^{2-} (or HCO_3^-) cations could obviously promote the water splitting and production of H_2 and O_2. The CO_3^{2-} (or HCO_3^-) cations come from CO_2 dissolved in the water may affect the acetic acid reforming. Many studies have confirmed that CO_3^{2-} (or HCO_3^-) cations dissolved in water can be oxidized by cavities to generate $\bullet CO_3^{2-}$ (or $\bullet HCO_3$) radicals, which contribute to the water splitting reaction.[19]

Owing to the advantage of cheap, non-toxic, high stability and so on, TiO_2 has great potential and broad application prospects in the field of photocatalysis. TiO_2 has 3 kinds of crystal structures: rutile, anatase and brookite. Limited by high difficulty preparation of high purity sample, brookite TiO_2 is rarely studied compared with other 2 phases.[20] However, it was reported that brookite TiO_2 has stronger photocatalytic activity for organic compounds degradation and similar capability of CO_2 adsorption with anatase for CO_2 reduction (better than rutile phase).[21, 22] And brookite TiO_2 has better adsorption capability than anatase TiO_2. Therefore, brookite TiO_2 is worth continuing to be studied.

In this study, high purity brookite TiO_2 was used as the photocatalyst. The photocatalytic activity of photo-Kolbe reaction (acetic acid) was evaluated upon

different phases of TiO_2 photocatalysts. Ar gas and CO_2 was used to remove the O_2, respectively. Evaluation of photocatalytic activity was estimated by the production of H_2, CH_4 and other gas from acetic acid transformation. Unlike in Ar atmosphere, a significant increase in yield and stability of CH_4 was observed in the condition of CO_2 atmosphere, suggesting that CO_2 could promote the efficiency and stability of photocatalytic activity of CH_4 production.

4.2 Experiment

4.2.1 Preparation of metal loaded TiO_2

Metal loaded brookite TiO_2 was prepared by the method of photo-deposition. 0.3g of commercial brookite TiO_2 powder (KOJUNDO CHEMICAL LABORATORY CO), chloroplatinic acid (10mmM, Wako), 80mL of Mill-q water and 20mL ethanol (Wako, Extra Pure, 95%) was mixed in a flask. After N_2 bubbling for 1h, the mixture solution was irradiated under a mercury lamp for 6h. The light intensity was 100 mW cm^{-2}. After photoirradiation, the resultant powder was gotten by filtration and washed by ultrapure water until conductivity below than 10 μS cm^{-1}.

4.2.2 Characterization

X-ray photoelectron spectra (XPS) of as-prepared samples were obtained by a Thermo ESCALAB 250Xi system at room temperature using Al Kα with monochromatic radiation. PL (Photoluminescence spectroscopy) spectra of different amount of Pt-loaded TiO_2 was analyzed by using with excitation light of 420nm. The isotopic analysis was performed by using GC-MS (GCMS-QP2010 ultra, SHIMAZU, column: 15m MS5A, carrier gas:He). ESR was analyzed and recorded on a standard X-band spectrometer (JOEL, JES-RE2X) in room temperature. Sample (0.4%Pt0/TiO_2, 6g/L) was put into a quartz capillary. DMPO (5,5-dimethyl-1-pyrroline N-oxide, Wako, Japan, 0.01M) was used as the radical trapping reagent. ESR spectra was measured in two kinds of gas atmosphere after 30min photoirradiation (Xenon lamp, 100mW cm^{-1}).

4.2.3 Photocatalytic activity tests

The photocatalytic activity tests of photocatalyst were evaluated by CH_4 and H_2 production from acetic acid reforming. First, 40mg TiO_2, 20 μL (0.1vol% (1.75×10^{-2}mol/L), 1vol%, 10vol% and 25vol% (: H_2O)) aqueous acetic acid was mixed together in a quartz container. Then ultrapure water was added to adjust the volume of the mixed solution to 20mL. After Ar or CO_2 gas bubbling for 30min, the mixed solution was irradiated under Xenon lamp for 3h. Micro-GC (Agilent Technologies 490 Micro GC with column: 10m MS5A) was used to detected the concentration of produced gas, for example H_2, CH_4, C_2H_6 and et al. The components and concentration of acetic acid water solution was evaluated by the liquid chromatography before and after experiment.

4.3 Results and Discussion

4.3.1 Acetic acid reforming in Ar and CO_2 atmosphere

In this section, the acetic acid photocatalytic reforming is on the base of 0.4%Pt0/brookite TiO_2, which has been discussed in the Section 3. The characteristic of photocatalyst is shown in the Section 3.

To evaluate the influence of different kinds of gas, photocatalytic activity of 0.4Pt0/TiO_2 was estimated in the condition of Ar and CO_2 bubbling. The result was shown in the Fig. 4-1(A). In the condition of Ar bubbling, after photoirradiation for 3h, the production rate of H_2 and CH_4 is 485.0 μmol $g^{-1}h^{-1}$ and 189.6 μmol $g^{-1}h^{-1}$, respectively. The average rate of CH_4 production in the condition of CO_2 is almost 1.5 times faster than the CH_4 production in the condition of Ar bubbling. At the same time, the reason for the slightly lower production of H_2 in the condition of CO_2 bubbling may be that more •H radicals combine with •CH_3 to generate more CH_4 than that in the condition of Ar bubbling. The production rate of CH_4 and H_2 production over different

amount of Pt-loaded TiO_2 is shown in the Fig. 4-2. The production rate of CH_4 over pure TiO_2 and all amount of the Pt-loaded TiO_2 in CO_2 atmosphere is more than that in Ar atmosphere, indicating that this result is universal. The situation in different concentration of acetic acid was also detected. From the Fig. 4-3, the production rate of CH_4 from 0.1vol%, 1vol%, 10vol% and 25vol% acetic acid over 0.4%Pt0/TiO_2 in CO_2 atmosphere is 47%, 53%, 69% and 19% faster than that in Ar atmosphere. Furthermore, in the Ar atmosphere, with the concentration of acetic acid increasing, the production rate of H_2 will decrease, which could be due to the increasing of $\bullet CH_3$ concentration. However, production rate of H_2 did not obviously decrease with increasing the concentration of added acetic acid. It suggests that CO_2 atmosphere can promote acetic acid reforming and produce more amount of •H radical. The concentration of acetic acid in both Ar and CO_2 atmosphere after 24h photoirradiation was shown in the Fig. 4-4. In the CO_2 atmosphere, the concentration of acetic acid is 72% (C/C_0) and lower than that in the Ar atmosphere (76% (C/C_0)), indicating faster reforming rate in CO_2 atmosphere. The pH of 0.1vol%, 1vol% and 10vol% acetic acid solution in Ar and CO_2 atmosphere before and after photoirradiation was shown in the Table 4-1. Nether Ar or CO_2 bubbling did not change the pH of the solution. It could be because the acidity of acetic acid is smaller than carbonate acid. Besides, the similar pH in both Ar and CO_2 atmosphere means the production of CH_4 and H_2 is not influenced by the difference of pH of solution. From Fig. 4-1(A), in the condition of O_2 atmosphere, no CH_4 or H_2 was detected. It means that both Ar and CO_2 can act as shielding gas to prevent direct oxidation of acetic acid.

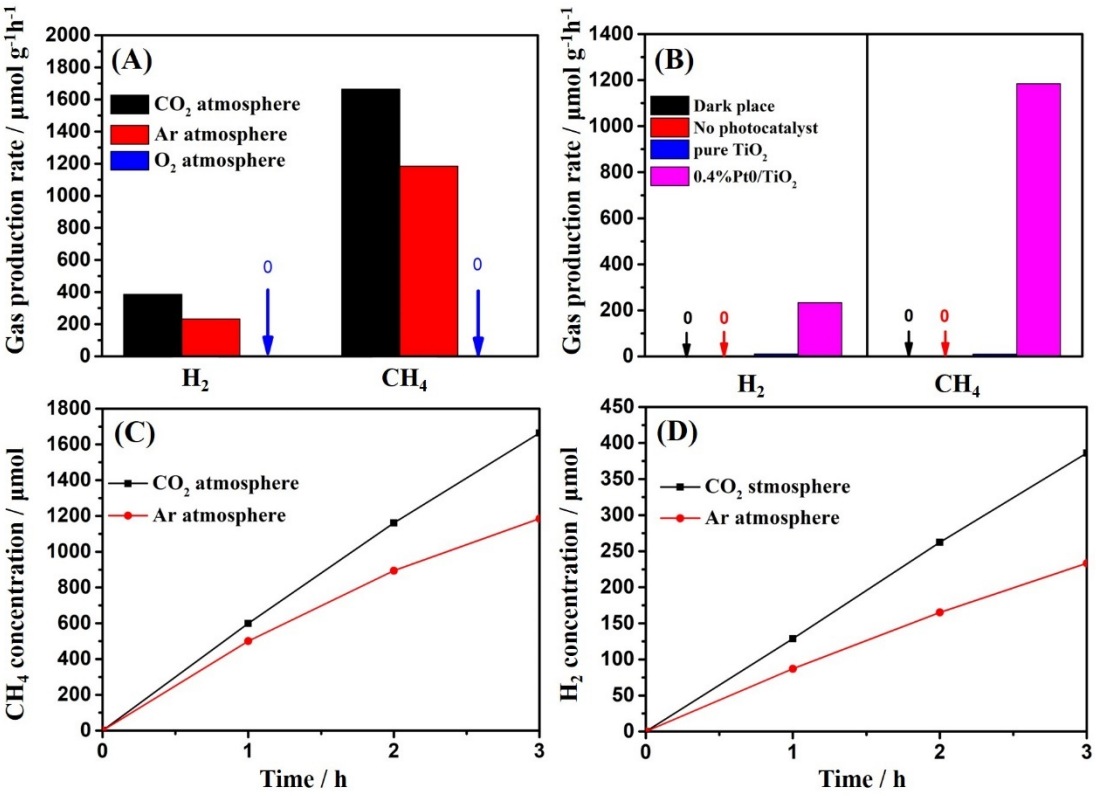

Fig. 4-1 (A) production rater of H_2 and CH_4 over 0.4%Pt0/TiO_2 in the condition of Ar, CO_2 and O_2 atmosphere, **(B)** production rate of CH_4 over pure brookite TiO_2 and 0.4%Pt0/TiO_2 in the condition of Ar bubbling, the amount of produced CH_4 **(C)** and H_2 **(D)** over 0.4%Pt0/TiO_2 in the condition of Ar and CO_2 bubbling and photoirradiation for 3h.

The stability of photocatalytic activity of 0.4%Pt0/TiO_2 in CO_2 and Ar stmosphere was estimated and shown in. Fig. 4-1(C) and (D). In the condition of Ar atmosphere, the production rate of CH_4 decrease gradually. Furthermore, a slight decrease of production rate of H_2 was found in the condition of Ar atmosphere. In the condition of CO_2 atmosphere, the production rate of CH_4 and H_2 is almost same for per hour, indicating good stability. The XPS spectra of Pt0/TiO_2 photo-irradiated in Ar and CO_2 atmosphere are shown in the Fig. 4-6 and 4-7, respectively. The XPS spectra of 0.4Pt0/TiO_2 before experiment is shown in the Fig. 4-5. The peak of O at 532.7eV, 531.6eV and 530.7eV belongs to Ti-O-C, Ti-O-H and Ti-O-Ti, respectively.[23, 24] According to Fig. S7(B), the element of Ti mainly consists of Ti^{4+}. Minute amount of

Ti^{3+} is from the oxygen vacancy of TiO_2.[25] Pt mainly consists of Pt0 and contains part of Pt^{2+} and Pt^{4+} ion component, which may cause by incomplete reduction during the process of photodeposition.[26-28] Compared with Pt0/TiO_2 before photoirradiation, no change was shown in the the XPS of Ti and O of Pt0/TiO_2 in the condition of Ar and CO_2. However, in the condition of Ar atmosphere, the part of Pt was reduced to Pt0. And in the condition of CO_2 atmosphere, the element of Pt show good stability, which match the result of photocatalytic activity.

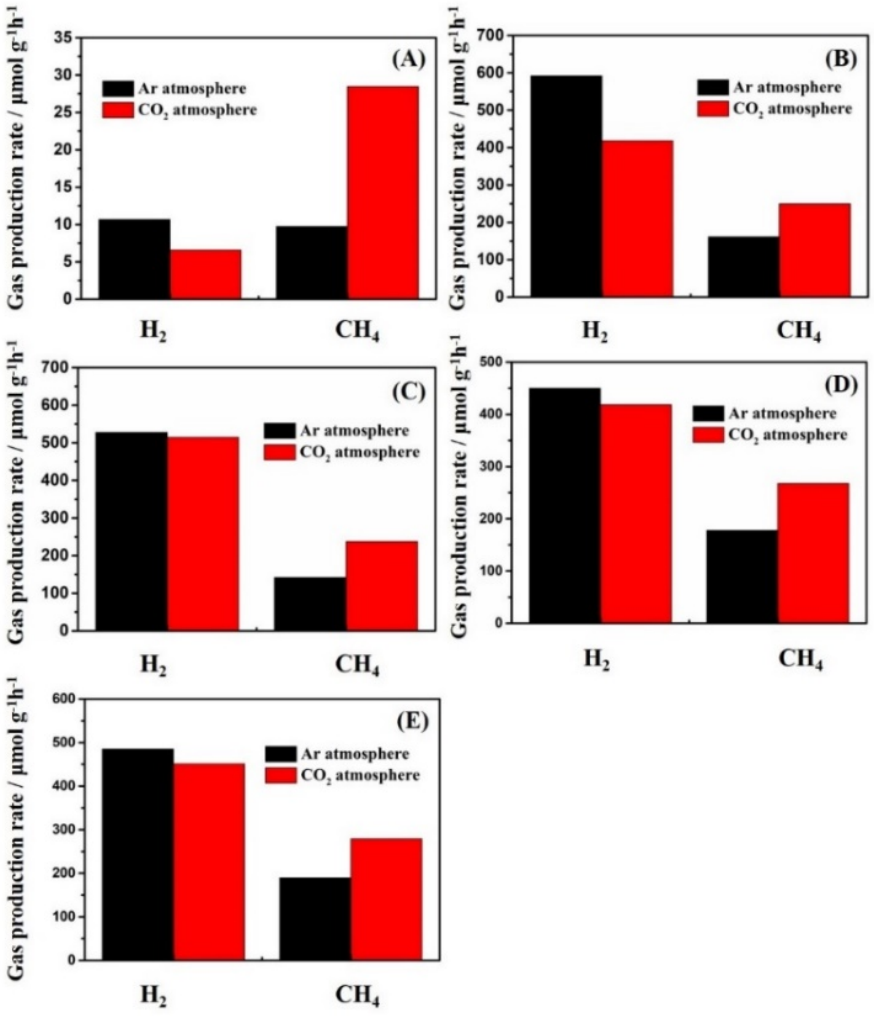

Fig. 4-2 Production rate of CH_4 and H_2 from 0.1vol% acetic acid transformation over (A) pure TiO2, (B) 0.1%Pt/ TiO_2, (C) 0.2%Pt/ TiO_2, (D) 0.4%Pt/ TiO_2 and (E) 0.6%Pt/ TiO_2.

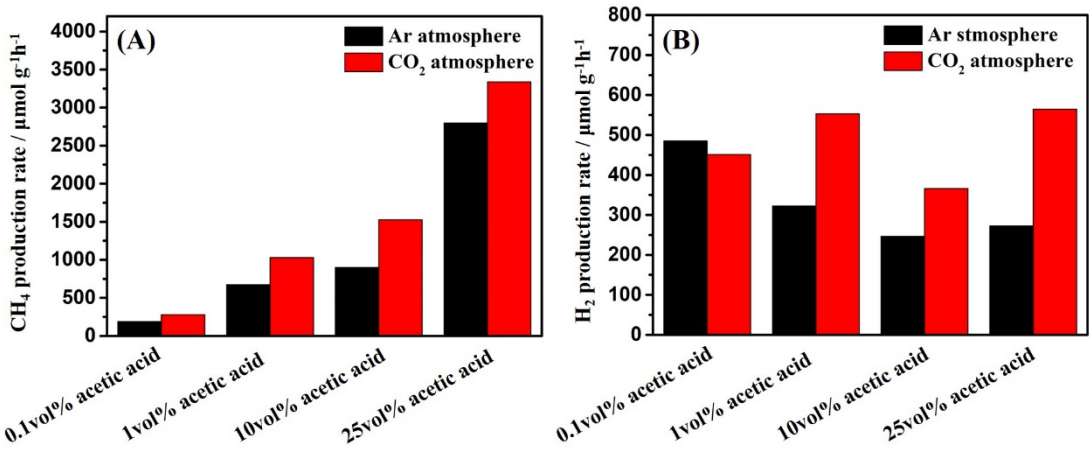

Fig. 4-3 Production rate of (A) CH_4 and H_2 from 0.1vol%, 1vol%, 10vol% and 25vol% acetic acid transformation over 0.4%Pt/ TiO2.

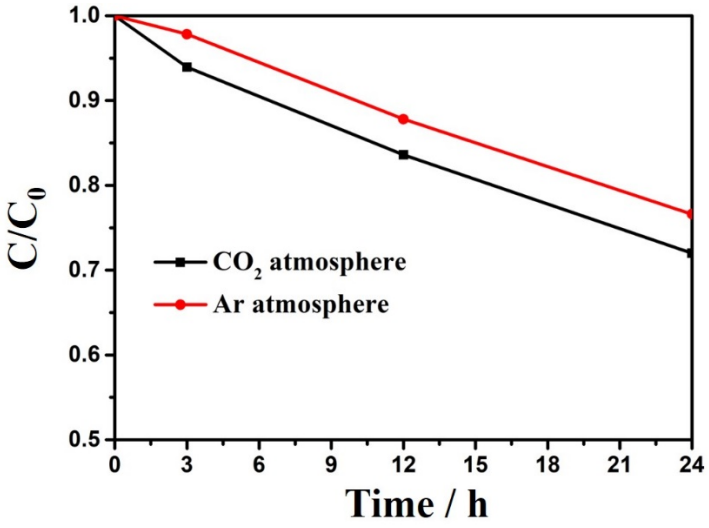

Fig. 4-4 Concentration of acetic acid in the solution after 24 h photoirradiation.

Table 4-1. Evaluation of pH after different kinds of gas bubbling

Sample name	pH
0.1vol% acetic acid + Ar	3.29
0.1vol% acetic acid + Ar after 3h photoirradiation	3.35
0.1vol%acetic acid+CO_2	3.33
0.1vol% acetic acid + CO_2 after 3h photoirradiation	3.37

Sample name	pH
1 vol% acetic acid + Ar after 3h photoirradiation	2.75
1 vol% acetic acid+CO_2	2.67
1 vol% acetic acid + CO_2 after 3h photoirradiation	2.70
10 vol% acetic acid + Ar	2.13
10 vol% acetic acid + Ar after 3h photoirradiation	2.15
1 vol% acetic acid + Ar	2.73
10 vol% acetic acid+CO_2	2.12
10 vol% acetic acid + CO_2 after 3h photoirradiation	2.15
10 vol% acetic acid + 0.1M Na_2CO_3	3.88
10 vol% acetic acid + 0.2M Na_2CO_3	4.08
10 vol% acetic acid + 0.5M Na_2CO_3	4.64

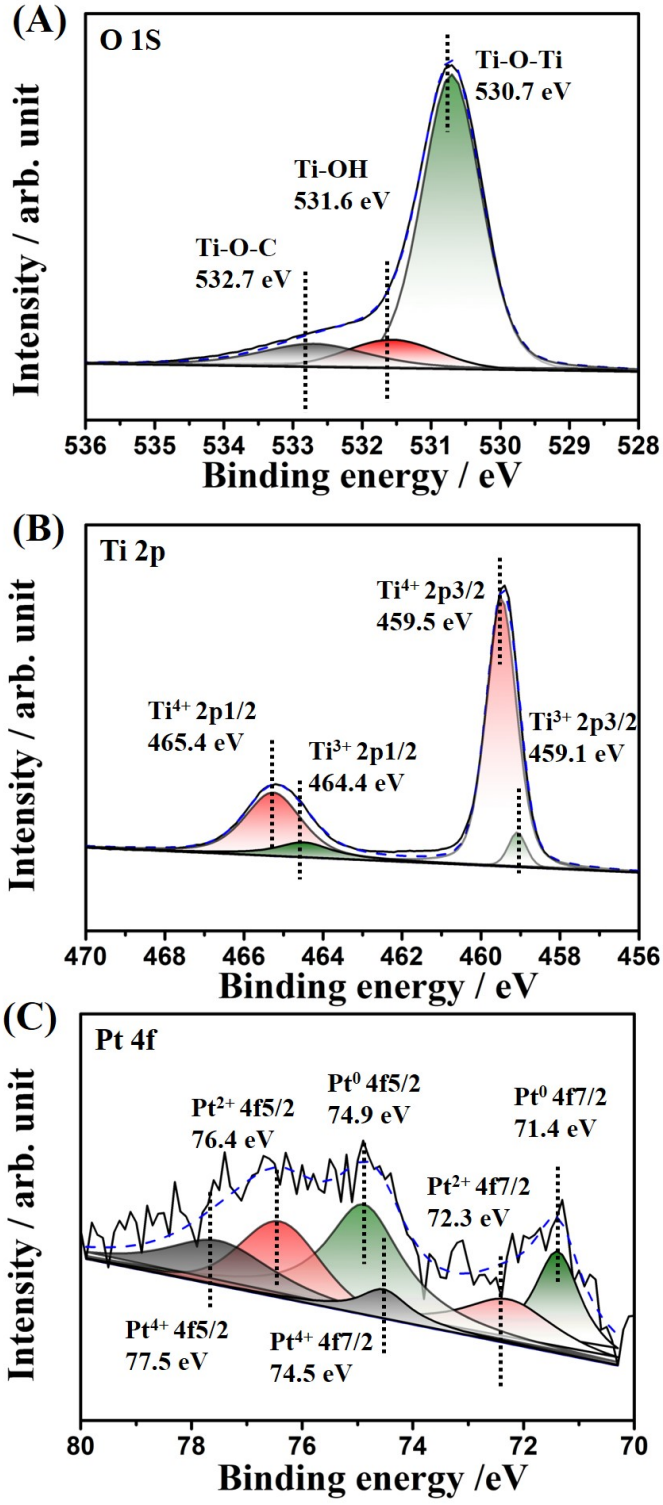

Fig. 4-5. XPS spectra of 0.4%Pt0/TiO_2: (A)O 1s, (B) Ti 2p, (C) Pt4f.

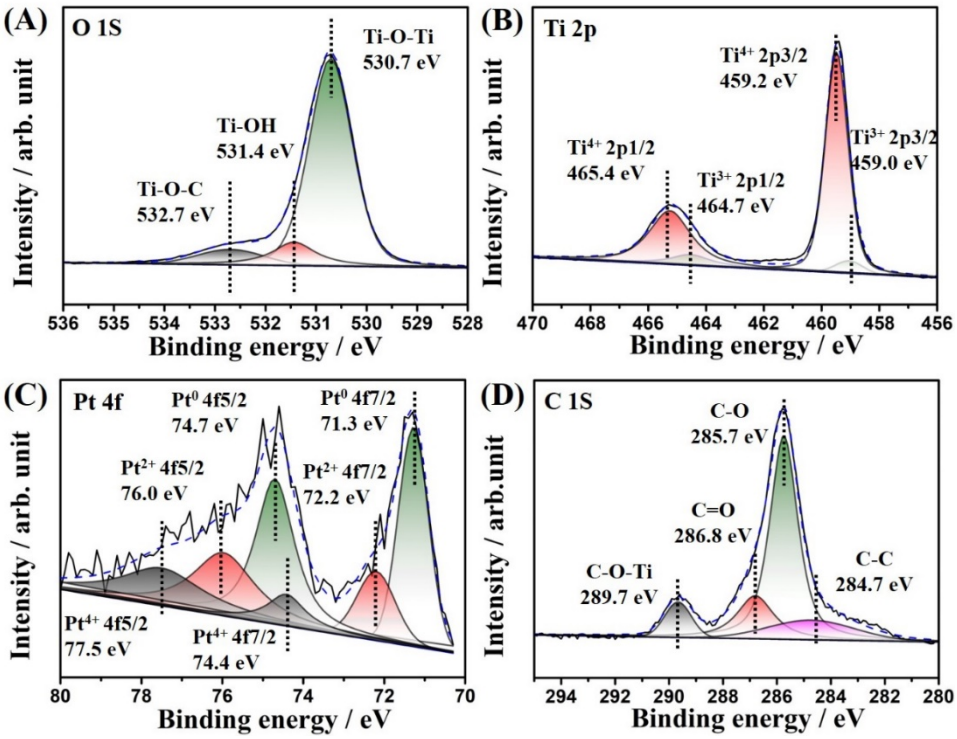

Fig. 4-6 XPS spectra of Pt0/TiO_2 photo-irradiated in the condition of Ar: (A) O 1s, (B) Ti 2p, (C)Pt 4f, (D) C 1s.

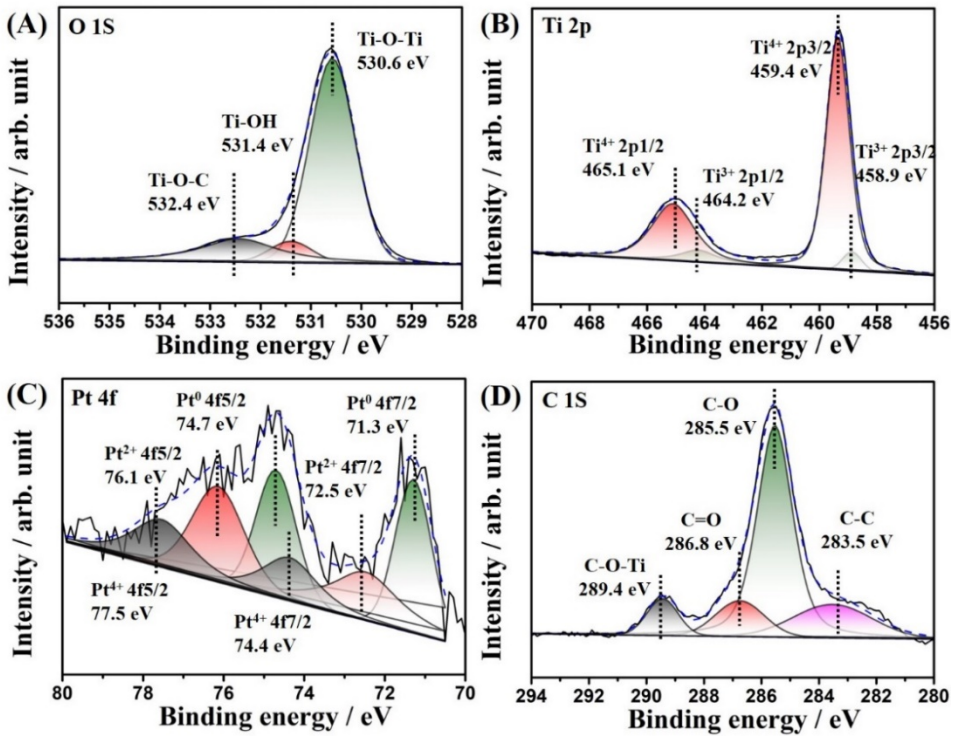

Fig. 4-7 XPS spectra of Pt0/TiO_2 photo-irradiated in the condition of CO_2: (A) O 1s, (B) Ti 2p, (C)Pt 4f, (D) C 1s.

4.3.2 Mechanism of acetic acid reforming in different gas atmosphere

The mechanism of H_2 and CH_4 produced from acetic acid photocatalytic reforming is shown in the equation (1), (2) and Scheme 1A. Under photoirradiation, holes (h^+) and electrons (e^-) were generated at the VB and CB of TiO_2 respectively. In the Ar atmosphere, holes react with H_2O to form •OH radical, which is a kind of strong oxidative species.[29] Then the •OH radical oxidizes CH_3COO^- cation. A proton (H^+) gets one electron and is reduced to a •H radical. Two •H radical combine with each other to form a H_2. Besides, one •H radical react with methyl radical ($\bullet CH_3$) to get CH_4.[30-32]

$$TiO_2 \xrightarrow{h\nu} h^+ + e^- \quad (1)$$

$$h^+ + H_2O \rightarrow \bullet OH + H^+ \quad (2)$$

$$\bullet OH + CH3COO^- \rightarrow \bullet CH_3 + CO_2 + OH^- \quad (3)$$

$$H^+ + e^- \rightarrow \bullet H \quad (4)$$

$$\bullet CH_3 + \bullet H \rightarrow CH_4 \quad (5)$$

$$\bullet H + \bullet H \rightarrow H_2 \quad (6)$$

Hole scavenger (EDTA) and electron scavenger ($K_2Cr_2O_7$) was respectively used to detect the factors influencing the reaction of acetic acid transformation to CH_4. The results are shown in the Fig. 4-8. In the presence of electron scavenger, the photogenerated electrons will be consumed by electron scavenger. No H_2 (and CH_4) was detected. It suggests that the formation of •H radical from proton(H^+) in the water reduction is one of the impact factors for H_2 and CH_4 production. The production rate of •H radical will influence the production of H_2 and CH_4.In the presence of hole scavenger, photogenerated holes will be consumed. Except H_2, no other gas was detected. The formation of CH_4 is from the combination of $\bullet CH_3$ radical and •H radical. It means that the process that the CH_3COO^- is decomposed by oxidative species (like holes, •OH and so on) is necessary for production of CH_4.

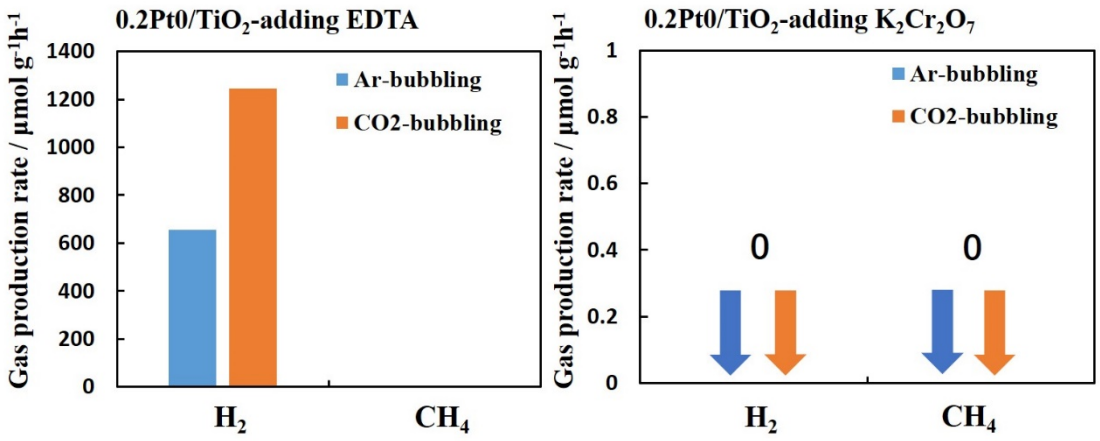

Fig. 4-8 Production rate of H_2 and CH_4 over $Pt0/TiO_2$ from acetic acid transformation in the presence of **(A)** EDTA and **(B)** $K_2Cr_2O_7$

Fig. 4-9 shows the gas chromatography- mass spectrometry (GC-MS) evaluation of CH_4 from acetic acid transformation. As can be seen in the Fig. 3(A), isotopic CO_2 ($^{13}CO_2$) was used to replace the normal CO_2 ($^{12}CO_2$). And normal acetic acid ($^{12}CH_3COOH$) was used as the source of acetic acid. Relative abundance of the nucleo plasmic relation at 16 m/z is 100%, indicating that all of produced CH_4 was $^{12}CH_4$. In the Fig. 3(B), isotopic acetic acid ($^{13}CH_3COOH$) was replaced the normal acetic acid. $^{12}CO_2$ was used as the gas atmosphere. The nucleo plasmic relation from 13 to 17 belong to ^{13}C,^{13}CH, $^{13}CH_2$,$^{13}CH_3$ and $^{13}CH_4$, respectively. No peak was found at 12 m/z and the relative abundance of nucleo plasmic relation at 17 m/z is 100%, indicating all of produced CH_4 is isotopic CH_4 ($^{13}CH_4$).[33, 34] In conclusion, CH_4 is not produced from CO_2 reduction in this experiment. According to the Fig. 4-9C, isotopic water (D_2O) was used to replace normal water. The nucleo plasmic relation of 17 m/z corresponds to CH_3D, indicating the •H is also from H^+ of water rection.

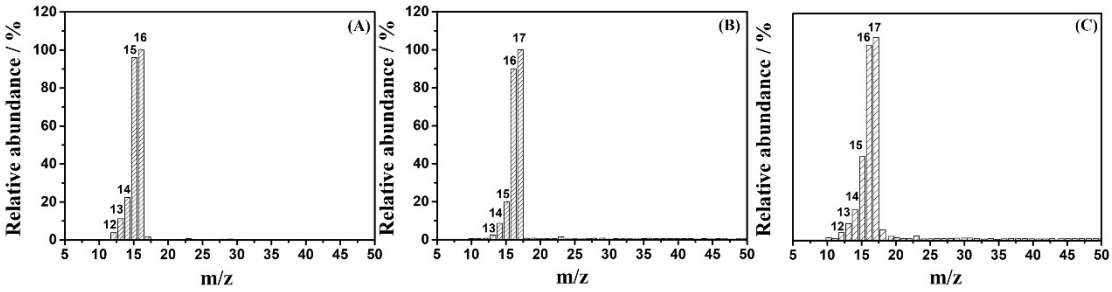

Fig. 4-9 Gas chromatography- mass spectrometry (GC-MS) evaluation of CH_4 from acetic acid transformation: (A) $^{12}CH_3COOH+^{13}CO_2+H_2O$, (B) $^{13}CH_3COOH+^{12}CO_2+H_2O$, (C) $^{12}CH_3COOH+^{12}CO_2+D_2O$.

The possible mechanism of CO_2 promoting the acetic acid reforming in the saturated CO_2 atmosphere is shown in the equation (7) ~ (10) and Scheme 1B. CO_2 firstly dissolved into the water and formed CO_3^{2-} (or HCO_3^-) cations.[35] The CO_3^{2-} (or HCO_3^-) cations then adsorb on the surface of TiO_2 and react with photogenerated holes to be an oxidation state, $\bullet CO_3^-$ (or $\bullet HCO_3$). The $\bullet CO_3^-$ (or $\bullet HCO_3$) radical, a kind of oxidative species, then oxidized CH_3COO^- to CO_2 and $\bullet CH_3$ radical. And the $\bullet CO_3^-$ (or $\bullet HCO_3$) radical finally recover to CO_3^{2-}(or HCO_3^-).[36-40] The H^+ get one electron to be •H radical, which then combine with $\bullet CH_3$ radical to form CH_4. The relative lower overpotential of $\bullet CO_3^-$ (1.77 V) than •OH radical (1.99 V) may be the reason for higher efficiency of acetic acid reforming. [41]

$$H_2O + CO_2 \rightarrow 2H^+ + CO_3^{2-} \quad (7)$$

$$\bullet OH + CO_3^{2-} \rightarrow \bullet CO_3^- + OH^- \quad (8)$$

$$h^+ + CO_3^{2-} \rightarrow \bullet CO_3^- \quad (9)$$

$$\bullet CO_3^- + CH_3COO^- \rightarrow CO_3^{2-} + \bullet CH_3 + CO_2 \quad (10)$$

The $\bullet CH_3$ radical produced from 10vol% acetic acid under Xenon lamp photoirradiation was detected by ESR analysis. Fig. 4-10 shows the spectra performed in the room temperature and different gas atmosphere. When DMPO was added into the solution, the $\bullet CH_3$ radical was trapped to be DMPO-CH_3•.[42] After photoirradiation for 30min, an increasing of ESR signal for CO_2 atmosphere was found compared with Ar atmosphere, indicating more $\bullet CH_3$ radical produced in CO_2 atmosphere.

For further evaluating the importance of CO_3^{2-}cation, on the basis of 10 vol% acetic

acid in Ar and CO_2 atmosphere, Na_2CO_3 was added into the solution to detect the importance of CO_3^{2-} cation for acetic acid reforming. As can be seen in the Fig. 4-11, without adding Na_2CO_3, the production rate of CH_4 from 10vol% acetic acid reforming in CO_2 atmosphere is 1524.9 μmol g^{-1} h^{-1} and 69% faster than that in Ar atmosphere. With adding 0.1M and 0.2M Na_2CO_3, the production rate of CH_4 in both Ar and CO_2 atmosphere increases (0.1M: 1595.2 μmol g^{-1} h^{-1} (CO_2) and 1225.9 μmol g^{-1} h^{-1} (Ar), 0.2M: 1766.5 μmol g^{-1} h^{-1} (CO_2) and 1389.1 μmol g^{-1} h^{-1} (Ar)). Besides, when 0.1M and 0.2M sodium carbonate was added, the CH_4 generation rate difference in the Ar atmosphere reduced to only 30% and 27% smaller than that in CO_2 atmosphere (before the difference is 69.7%), respectively. The pH of the solution after adding 0.1M, 0.2M and 0.5M Na_2CO_3 is shown in the Table. 4-1. When the amount of Na_2CO_3 added reaches 0.5M, the amount of CH_4 production is greatly reduced. It could be because too high pH caused by adding more Na_2CO_3 will affect the production of methane.[43] These results proved that CO_3^{2-} (or HCO_3^-) can promote acetic acid degraded to CH_4. When the concentration of Na_2CO_3 added was 0.2M, the production rate of H_2 increased, which could be due to the promoting effect of Na_2CO_3 on water splitting.[19]

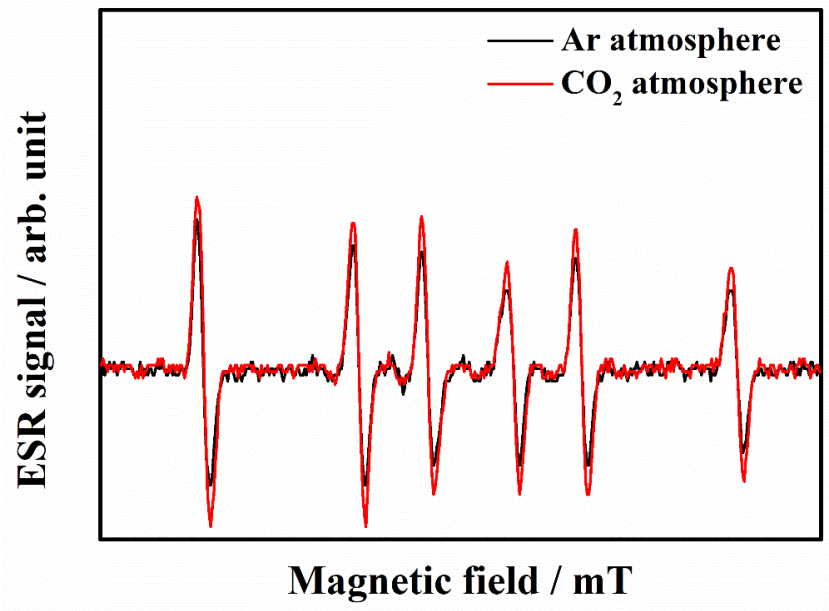

Fig. 4-10 ESR spectra obtained upon irradiation (Xenon lamp, light intensity: 100mW cm^{-1}, exposure: 15 min) in the presence of spin trapping agent (DMPO, 0.01M) from 10 vol% acetic acid reforming in the condition of (A) CO_2 and (B) Ar atmosphere.

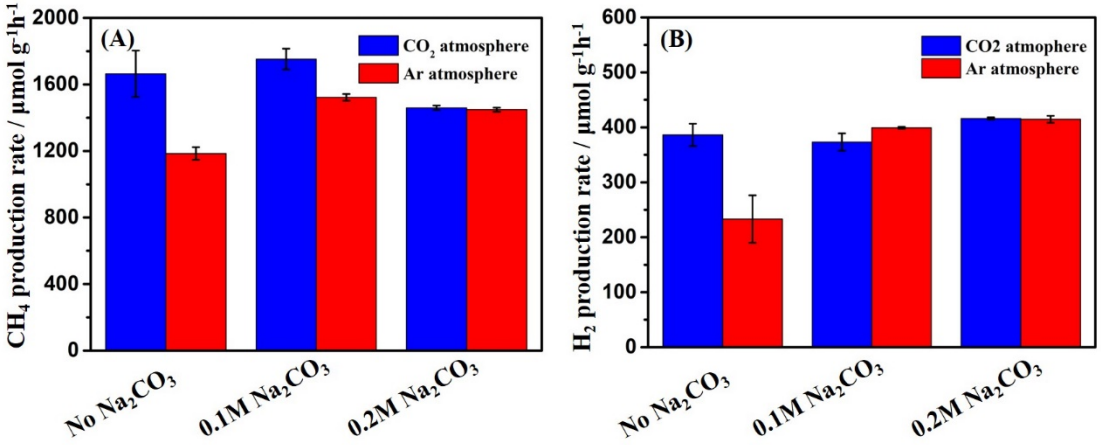

Fig. 4-11. Production rate of **(A)** CH_4 and **(B)** H_2 over 0.4%Pt0/TiO_2 from acetic acid reforming in the presence of Na_2CO_3.

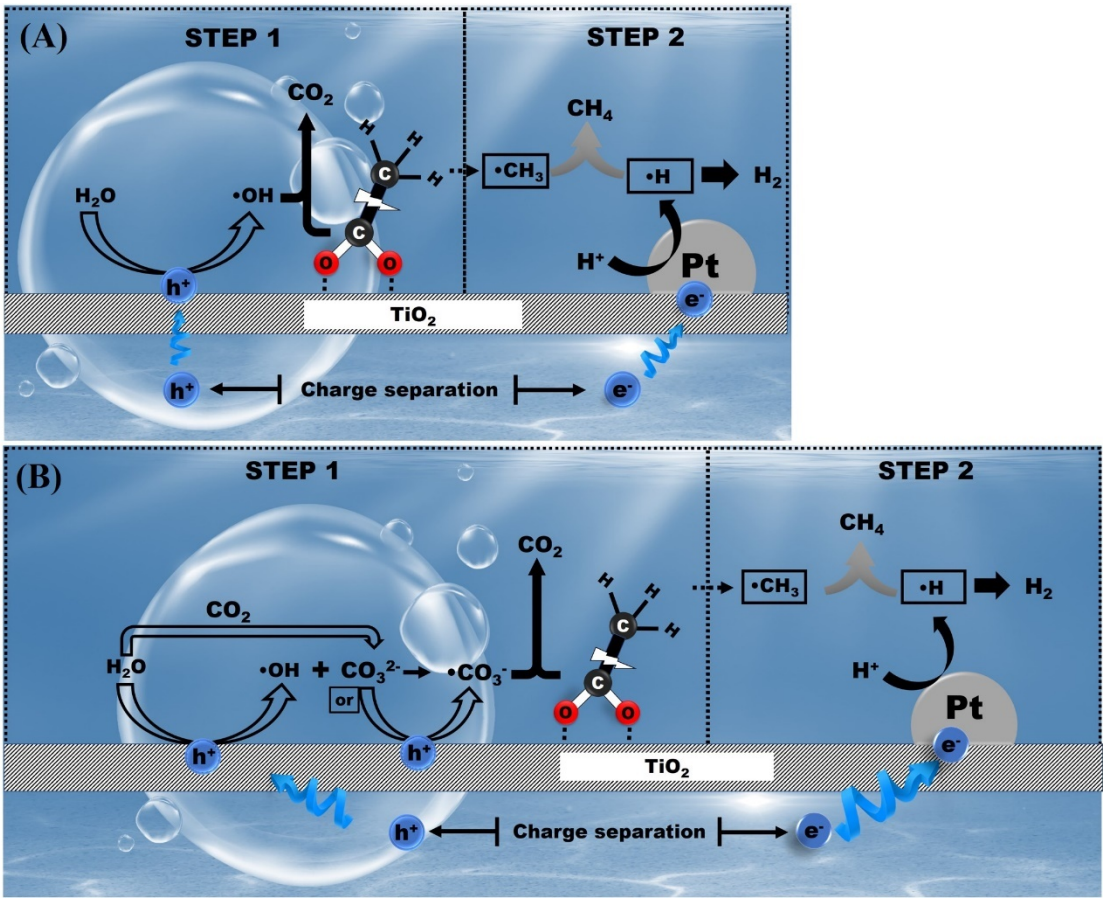

Scheme 1. Mechanism of transformation of acetic acid forming CH_4 and H_2 in the condition of (A) Ar atmosphere, (B) CO_2 atmosphere.

4.4 Conclusion

In conclusion, Compared with Ar atmosphere, CO_2 atmosphere can better promote acetic acid reforming. The CO_3^{2-} (or HCO_3^-) cations from CO_2 dissolved in the water, have lower redox potential than •OH radical and can more easily promote the photo-Kolbe reaction.

Reference

[1] L. Petersen, M. Heynen, F. Pellicciotti, Freshwater Resources: Past, Present, Future, International Encyclopedia of Geography2019, pp. 1-12.

[2] P. Rajasulochana, V. Preethy, Comparison on efficiency of various techniques in treatment of waste and sewage water – A comprehensive review, Resource-Efficient Technologies, 2 (2016) 175-184.

[3] R. Kishor, D. Purchase, G.D. Saratale, R.G. Saratale, L.F.R. Ferreira, M. Bilal, R. Chandra, R.N. Bharagava, Ecotoxicological and health concerns of persistent coloring pollutants of textile industry wastewater and treatment approaches for environmental safety, Journal of Environmental Chemical Engineering, 9 (2021).

[4] E.A. Noman, A.A.S. Al-Gheethi, B.A. Talip, R.M.S. Radin Mohamed, H. Nagao, A.H. Mohd Kassim, Xenobiotic Organic Compounds in Greywater and Environmental Health Impacts, Management of Greywater in Developing Countries2019, pp. 89-108.

[5] H. Bylinski, J. Gebicki, J. Namiesnik, Evaluation of Health Hazard Due to Emission of Volatile Organic Compounds from Various Processing Units of Wastewater Treatment Plant, Int J Environ Res Public Health, 16 (2019).

[6] M.J. Gomez, S. Herrera, D. Sole, E. Garcia-Calvo, A.R. Fernandez-Alba, Spatio-temporal evaluation of organic contaminants and their transformation products along a river basin affected by urban, agricultural and industrial pollution, Sci Total Environ, 420 (2012) 134-145.

[7] Z. Liang, J. Wang, Y. Zhang, C. Han, S. Ma, J. Chen, G. Li, T. An, Removal of volatile organic compounds (VOCs) emitted from a textile dyeing wastewater treatment plant and the attenuation of respiratory health risks using a pilot-scale biofilter, Journal of Cleaner Production, 253 (2020).

[8] B. Kakavandi, A. Takdastan, S. Pourfadakari, M. Ahmadmoazzam, S. Jorfi, Heterogeneous catalytic degradation of organic compounds using nanoscale zero-valent iron supported on kaolinite: Mechanism, kinetic and feasibility studies, Journal of the Taiwan Institute of Chemical Engineers, 96 (2019) 329-340.

[9] J. Quiroz Torres, S. Royer, J.P. Bellat, J.M. Giraudon, J.F. Lamonier, Formaldehyde: catalytic oxidation as a promising soft way of elimination, ChemSusChem, 6 (2013) 578-592.

[10] W. Raza, J. Lee, N. Raza, Y. Luo, K.-H. Kim, J. Yang, Removal of phenolic compounds from industrial waste water based on membrane-based technologies, Journal of Industrial and Engineering Chemistry, 71 (2019) 1-18.

[11] J. Hu, A. Aarts, R. Shang, B. Heijman, L. Rietveld, Integrating powdered activated carbon into wastewater tertiary filter for micro-pollutant removal, J Environ Manage, 177 (2016) 45-52.

[12] K.J. Lee, J. Miyawaki, N. Shiratori, S.H. Yoon, J. Jang, Toward an effective adsorbent for polar pollutants: formaldehyde adsorption by activated carbon, J Hazard Mater, 260 (2013) 82-88.

[13] S. Weon, W. Choi, TiO2 Nanotubes with Open Channels as Deactivation-Resistant Photocatalyst for the Degradation of Volatile Organic Compounds, Environ Sci Technol, 50 (2016) 2556-2563.

[14] H. Zhan, Q. Zhou, M. Li, R. Zhou, Y. Mao, P. Wang, Photocatalytic O2 activation and reactive oxygen species evolution by surface B-N bond for organic pollutants degradation, Applied Catalysis B: Environmental, 310 (2022).

[15] Y. Qian, J. Shi, X. Yang, Y. Yuan, L. Liu, G. Zhou, J. Yi, X. Wang, S. Wang, Integration of biochar into Ag3PO4/alpha-Fe2O3 heterojunction for enhanced reactive oxygen species generation towards organic pollutants removal, Environ Pollut, 303

(2022) 119131.
[16] S. Ngo, L.M. Betts, F. Dappozze, M. Ponczek, C. George, C. Guillard, Kinetics and mechanism of the photocatalytic degradation of acetic acid in absence or presence of O 2, Journal of Photochemistry and Photobiology A: Chemistry, 339 (2017) 80-88.
[17] Tadayoshi Sakata, Tomoji Kawai, a.K. Hashimoto, Heterogeneous photocatalytic reactions of organic acids and water. New reaction paths besides the photo-Kolbe reaction, J. Phys. Chem., 88 (1984) 2344-2350.
[18] D. Yang, X. Ni, W. Chen, Z. Weng, The observation of photo-Kolbe reaction as a novel pathway to initiate photocatalytic polymerization over oxide semiconductor nanoparticles, Journal of Photochemistry and Photobiology A: Chemistry, 195 (2008) 323-329.
[19] Kazuhiro Sayama, H. Arakawa, Effect of carbonate salt addition on the photocatalytic decomposition of liquid water over Pt–TiO2 catalyst, Journal of the Chemical Society, Faraday Transactions, 93 (1997) 1647-1654.
[20] ZHENG YANQING, SHI ERWEI, CUI SUXIAN, LI WENJUN, H. XINGFANG, Hydrothermal preparation and characterization of brookite-type

TiO2 nanocrystallites, JOURNAL OF MATERIALS SCIENCE LETTERS, 19 (2000) 1445.
[21] H.T.T. Tran, H. Kosslick, M.F. Ibad, C. Fischer, U. Bentrup, T.H. Vuong, L.Q. Nguyen, A. Schulz, Photocatalytic Performance of Highly Active Brookite in the Degradation of Hazardous Organic Compounds Compared to Anatase and Rutile, Applied Catalysis B: Environmental, 200 (2017) 647-658.
[22] M.M. Rodriguez, X. Peng, L. Liu, Y. Li, J.M. Andino, A Density Functional Theory and Experimental Study of CO2 Interaction with Brookite TiO2, The Journal of Physical Chemistry C, 116 (2012) 19755-19764.
[23] U. Naknikham, G. Magnacca, A. Qiao, P.K. Kristensen, V. Boffa, Y. Yue, Phenol Abatement by Titanium Dioxide Photocatalysts: Effect of The Graphene Oxide Loading, Nanomaterials (Basel), 9 (2019).

[24] P. Fu, Y. Luan, X. Dai, Preparation of activated carbon fibers supported TiO2 photocatalyst and evaluation of its photocatalytic reactivity, Journal of Molecular Catalysis A: Chemical, 221 (2004) 81-88.

[25] Q. Han, C. Wu, H. Jiao, R. Xu, Y. Wang, J. Xie, Q. Guo, J. Tang, Rational Design of High-Concentration Ti(3+) in Porous Carbon-Doped TiO2 Nanosheets for Efficient Photocatalytic Ammonia Synthesis, Adv Mater, 33 (2021) e2008180.

[26] Z. Wu, Z. Sheng, Y. Liu, H. Wang, J. Mo, Deactivation mechanism of PtOx/TiO(2) photocatalyst towards the oxidation of NO in gas phase, J Hazard Mater, 185 (2011) 1053-1058.

[27] B.D. Mukri, U.V. Waghmare, M.S. Hegde, Platinum Ion-Doped TiO2: High Catalytic Activity of Pt2+ with Oxide Ion Vacancy in Ti4+1–xPt2+xO2–x Compared to Pt4+ without Oxide Ion Vacancy in Ti4+1–xPt4+xO2, Chemistry of Materials, 25 (2013) 3822-3833.

[28] E.I. Vovk, A.V. Kalinkin, M.Y. Smirnov, I.O. Klembovskii, V.I. Bukhtiyarov, XPS Study of Stability and Reactivity of Oxidized Pt Nanoparticles Supported on TiO2, The Journal of Physical Chemistry C, 121 (2017) 17297-17304.

[29] Y. Nosaka, A. Nosaka, Understanding Hydroxyl Radical (•OH) Generation Processes in Photocatalysis, ACS Energy Letters, 1 (2016) 356-359.

[30] S. Mozia, A. Heciak, A.W. Morawski, Preparation of Fe-modified photocatalysts and their application for generation of useful hydrocarbons during photocatalytic decomposition of acetic acid, Journal of Photochemistry and Photobiology A: Chemistry, 216 (2010) 275-282.

[31] GUN D A E L E E , V U A . T U A N , J.O.H.N.L.F.A.L.C.O.N.E. R, Photocatalytic Oxidation and Decomposition of Acetic Acid on Titanium Silicalite, 35 (2001) 1252-1258.

[32] L.M. Betts, F. Dappozze, C. Guillard, Understanding the photocatalytic degradation by P25 TiO 2 of acetic acid and propionic acid in the pursuit of alkane production, Applied Catalysis A: General, 554 (2018) 35-43.

[33] N. Li, R. Jiang, Y. Li, J. Zhou, Q. Ma, S. Shen, M. Liu, Plasma-Assisted

Photocatalysis of CH4 and CO2 into Ethylene, ACS Sustainable Chemistry & Engineering, 7 (2019) 11455-11463.
[34] H. Song, X. Meng, S. Wang, W. Zhou, X. Wang, T. Kako, J. Ye, Direct and Selective Photocatalytic Oxidation of CH4 to Oxygenates with O2 on Cocatalysts/ZnO at Room Temperature in Water, J Am Chem Soc, 141 (2019) 20507-20515.
[35] E. Illes, A. Mizrahi, V. Marks, D. Meyerstein, Carbonate-radical-anions, and not hydroxyl radicals, are the products of the Fenton reaction in neutral solutions containing bicarbonate, Free Radic Biol Med, 131 (2019) 1-6.
[36] V. Shafirovich, A. Dourandin, W. Huang, N.E. Geacintov, The carbonate radical is a site-selective oxidizing agent of guanine in double-stranded oligonucleotides, J Biol Chem, 276 (2001) 24621-24626.
[37] Y. Lai, X. Liu, H. Ye, G. Ke, B. Lui, F. Dong, H. He, Objective Observations of the Electrochemical Production of H2O2 in KHCO3 Aqueous Electrolyte and Related Application Inspirations, The Journal of Physical Chemistry C, 125 (2021) 19831-19838.
[38] A. Aleboyeh, M.B. Kasiri, H. Aleboyeh, Influence of dyeing auxiliaries on AB74 dye degradation by UV/H2O2 process, J Environ Manage, 113 (2012) 426-431.
[39] J. Gao, X. Duan, K. O'Shea, D.D. Dionysiou, Degradation and transformation of bisphenol A in UV/Sodium percarbonate: Dual role of carbonate radical anion, Water Res, 171 (2020) 115394.
[40] K. Fuku, K. Sayama, Efficient oxidative hydrogen peroxide production and accumulation in photoelectrochemical water splitting using a tungsten trioxide/bismuth vanadate photoanode, Chem Commun (Camb), 52 (2016) 5406-5409.
[41] I. Popivker, D. Meyerstein, D. Gitin, E.N. Avraham, E. Maimon, T. Zidki, H. Cohen, G. Yardeni, P. Moisy, S. Pevzner, I. Zilbermann, Redox Properties of Ce(IV)DOTA in Carbonated Aqueous Solutions. A Radiolytic and an Electrochemical Study, J Phys Chem A, 125 (2021) 1436-1446.
[42] D. Dvoranova, Z. Barbierikova, V. Brezova, Radical intermediates in photoinduced reactions on TiO2 (an EPR spin trapping study), Molecules, 19 (2014)

17279-17304.

[43] S. Hamid, I. Ivanova, T.H. Jeon, R. Dillert, W. Choi, D.W. Bahnemann, Photocatalytic conversion of acetate into molecular hydrogen and hydrocarbons over Pt/TiO 2 : pH dependent formation of Kolbe and Hofer-Moest products, Journal of Catalysis, 349 (2017) 128-135.

Section 5. Outlook for the future of work

In this experiment, we used the Pt as the co-catalyst. Pt has high-efficiency for promoting the photocatalytic activity. However, as a precious metal, the high cost of Pt will also be a limiting factor for widespread use. Therefore, the development of non-precious metal cocatalyst-supported brookite TiO_2 is a future goal.

In the part of organic compounds removing in water, the photocatalytic reforming of acetic acid is performed under full spectrum of light. According to the UV-vis spectra, Pt0-loaded brookite TiO_2 cannot response to the visible light. In further, we need to continue to develop the visible light-induced brookite TiO_2 photocatalysts.

For photo-Kolbe reaction (acetic acid reforming in water), we need to develop new photocatalysts to promote the yield and selectivity of long chain alkanes.

Acknowledgements

Since my master's period, I have lived and studied in Kyushu Institute of Technology for more than 5 years. The research life is interesting and makes me feel very happy. This is because my research focus on the focus on the current hot issues of environmental pollution and energy shortage. However, my research life is also monotonous, stressful and challenging. Luckily, I met a lot of people who helped me a lot in my research. The person I am most grateful for is my supervisor, prof. Ohno, who provide the financial support of JSPS (Grant-in-Aid for Scientific Research (B) (20H02847)). Besides, it is also worth mentioning that prof. Ohno is always patient and give the greatest help to me when my research is stagnant. At the same time, in daily life, he is a positive person who often conveys an optimistic attitude to me. He also often introduced Japanese culture to me, which I couldn't learn from books. Besides, I also got lots of supporting from Dr. Zhang (Qitao Zhang) and Dr. LOU (SHI NEE LOU). They gave me a lot of useful advice during my experiments and helped me review my manuscript.

I also appreciate my parents who give me money and support my study. I stayed in Japan for three years without going back to China due to this pandemic. My family members always inspired me, when I was depressed. The most stressful period for me was during the graduation defense. I really appreciate Miss. Wang (Shanshan Wang), who always stay by my side and make me feel relaxed and happy. I hope our relationship can last forever. My friends, Dejian Zhang, Yihang Jiao, Yankun Yu, Xiaoyu Sun, Sicong Wang, Hengguang Xu, Rundong Zhang and so on, also, also give me so much support in the period.